

Clemson University

**TigerPrints**

---

All Dissertations

Dissertations

---

5-2024

## Loss of Tsc2 Results in Abnormal Postnatal Neurogenesis and Striatal Hamartomas

Victoria Riley  
vriley@g.clemson.edu

Follow this and additional works at: [https://tigerprints.clemson.edu/all\\_dissertations](https://tigerprints.clemson.edu/all_dissertations)



Part of the [Developmental Neuroscience Commons](#)

---

### Recommended Citation

Riley, Victoria, "Loss of Tsc2 Results in Abnormal Postnatal Neurogenesis and Striatal Hamartomas" (2024). *All Dissertations*. 3582.

[https://tigerprints.clemson.edu/all\\_dissertations/3582](https://tigerprints.clemson.edu/all_dissertations/3582)

This Dissertation is brought to you for free and open access by the Dissertations at TigerPrints. It has been accepted for inclusion in All Dissertations by an authorized administrator of TigerPrints. For more information, please contact [kokeefe@clemson.edu](mailto:kokeefe@clemson.edu).

LOSS OF *Tsc2* RESULTS IN ABNORMAL POSTNATAL  
NEUROGENESIS AND STRIATAL HAMARTOMAS

---

A Dissertation  
Presented to  
the Graduate School of  
Clemson University

---

In Partial Fulfillment  
of the Requirements for the Degree  
Doctor of Philosophy  
Biological Sciences

---

by  
Victoria Anne Riley  
May 2024

---

Accepted by:  
Dr. David M. Feliciano, Committee Chair  
Dr. Lisa Bain  
Dr. Julia George  
Dr. Kara Powder  
Dr. Emily Rosowski

## ABSTRACT

Billions of years of evolution have culminated in the most complex organ in all of biology: the brain. Its capacity to sense, store, and predict information uniquely bestows humans with the capability to generate art, music, language, and math and sets humans apart from other species. It is therefore prudent and worthwhile to study the brain and its development. A critical aspect of brain development is neurogenesis, or the production of neurons. Neurogenesis is facilitated by neural stem cells (NSCs) and is influenced by the mTORC1 signaling pathway. For NSCs to differentiate and become committed to a neuronal cell fate, mTORC1 signaling must decrease in amplitude. This is likely due to the role that mTORC1 signaling plays in regulating mRNA translation which are tightly controlled in NSCs.

Hyperactive mTORC1 signaling can result from the inactivation of either the *Tsc1* or *Tsc2* gene and is considered the main driver of symptoms in the developmental disorder Tuberous Sclerosis Complex (TSC). TSC is characterized by congenital growths that form in multiple organ systems, including the brain. In TSC, the brain has cellular abnormalities leading to three types of lesions: cortical tubers, subependymal nodules, and subependymal giant cell astrocytomas (SEGAs). TSC lesions are associated with neuropsychiatric symptoms including epilepsy, autism spectrum disorders, intellectual delay, and behavioral abnormalities. Given the role that mTORC1 signaling plays in NSC differentiation, NSCs were examined in a *Tsc2* null mouse model.

Briefly, genetic recombination was used to inactivate the *Tsc2* gene in NSCs of the ventricular-subventricular zone. *Tsc2* removal altered aspects of transcription and translation, including translational efficiency. Loss of *Tsc2* caused striatal growths reminiscent of SEGAs. The growths contained NSCs and differentiated progeny including neurons and glia, possibly indicating abnormal neurogenesis due to *Tsc2* loss in NSCs. There is evidence that *Tsc2* loss, subsequent upregulation of mTORC1 signaling, and translational dysregulation cause NSCs to retain aspects of stemness, which could potentially contribute to TSC growth formation.

DEDICATION

To my parents

So much of me is what I've learned from you.

## ACKNOWLEDGMENTS

I want to thank Dr. David Feliciano for guiding me and providing advice throughout my tenure at Clemson. You have always been unrelentingly understanding, patient, and kind. I will call on your shared wisdom for years to come. Thank you for giving me the armor that I wanted and the armor that I needed for the battles ahead. I am the scientist I am today because of your tutelage and effort.

Thank you to my committee members for your support and encouragement. Your insight has proven invaluable to me. I appreciate your time and dedication.

Thank you to Jennie Holmberg for answering all my questions, even the silly ones. Your presence has always guided how I do science and conduct myself in the lab. I appreciate your support.

To Sulagna Mukherjee, thank you for being there for me in every conceivable way. Your presence in my life has only made it better. I am grateful to you for your friendship. Thank you for always bringing me back down to earth. I can't wait to see the exciting things you do next.

To Prakrit Subba, thank you for all of your motivation and support. Your assiduous nature is both inspiring and meaningful. I know you are on the road to doing big, impactful things and I couldn't be happier for you.

To Leah DeLorenzo, thank you for being a constant presence at Clemson and a voice of support when I needed it. I am so excited for your new adventure!

To Victoria Neckles, thank you for always supporting and caring for me. You are one of the highlights of my graduate school experience.

To Varun Parthiban, thank you for always being yourself and reminding me not to take myself too seriously. Keep getting your hands dirty.

To Raven Moraney, thank you for always making me smile and reminding us to take breaks. Please never change.

To Saidat Adeniran-Obey, thank you for doing happy dances every time something good happened to me, no matter how insignificant. You are such a bright light in the world. I admire your resilience and authenticity in all that you do.

Lastly, to my wonderful family, thank you for always encouraging me. I could not be who I am today without your unceasing support. Thank you for pushing me and loving me with all that you have.

This thesis would not have been possible without the relentless compassion and support from my family, friends, and mentors. Because of you, I have had the pleasure and opportunity to go forward with my ambition and achieve my goals. Thank you.

## TABLE OF CONTENTS

	Page
TITLE PAGE .....	i
ABSTRACT.....	ii
DEDICATION.....	iii
ACKNOWLEDGMENTS .....	iv
LIST OF FIGURES.....	vii
CHAPTER	
I.    LITERATURE REVIEW.....	1
Embryonic neurogenesis .....	1
Postnatal neurogenesis .....	2
NSC activation.....	6
The role of mTORC1 in NSCs.....	8
Tuberous Sclerosis Complex .....	13
Neurological symptoms of TSC.....	16
Cortical Tubers.....	17
Subependymal Nodules .....	20
Subependymal Giant Cell Astrocytoma .....	24
Summary.....	28
II. <i>Tsc2</i> inactivation resulted in atypical translation in murine NSCs.....	31
Abstract.....	32
Introduction.....	33
Results .....	36
Discussion.....	51
Methods .....	54
III. <i>Tsc2</i> inactivation generates hamartomas .....	60
Abstract.....	61
Introduction.....	63
Results .....	66
Discussion.....	93
Methods .....	98

IV. <i>Tsc2</i> inactivation results in morphological abnormalities in the OB.....	103
Abstract.....	104
Introduction.....	105
Results .....	112
Discussion.....	126
Methods .....	129
V. CONCLUSION.....	136
Discussion.....	136
REFERENCES.....	142

## LIST OF FIGURES

### Figure

1.1 Neurogenesis in the murine brain.....	4
1.2 mTORC1 signaling plays a role in regulating translation.....	10
1.3 mTORC1 expression in neural stem cells.....	12
1.4 Types of hamartoma in the TSC brain.....	18
2.1 <i>Tsc2</i> inactivation was performed in Nestin-CRE-ER <sup>T2</sup> mice.....	38
2.2 bulk RNA sequencing resulted in differentially expressed transcripts .....	41
2.3 Top differentially expressed transcripts were associated with protein binding.....	40
2.4 Differential expression of mRNA transcripts in <i>Tsc2</i> null NSCs .....	42
2.5 Polysomal analysis resulted in differentially enriched mRNA transcripts .....	43
2.6 Differential expression of polysome-associated mRNA transcripts in <i>Tsc2</i> null NSCs .....	44
2.7 <i>Translational efficiency was altered between mutant</i> <i>and control conditions</i> .....	47
2.8 The transcriptome and translome differentially expressed ribosomal proteins expressed ribosomal proteins.....	48
2.9 Differentially translated transcripts were associated with translation and nervous system development.....	50
3.1 Postnatal electroporation of the V-SVZ resulted in <i>Tsc2</i> inactivation in NSCs .....	68
3.2 mTORC1 activity was increased in the mutant SVZ and striatum following <i>Tsc2</i> inactivation.....	70
3.3 <i>Tsc2</i> loss resulted in the formation of abnormalities similar to human TSC .....	72
3.4 <i>Tsc2</i> inactivation resulted in striatal hamartomas .....	73
3.5 Two categories of hamartomas were noted in the mutant striatum .....	74

## LIST OF FIGURES (continued)

Figure

3.6 Striatal hamartomas increased in size but not frequency with age .....	76
3.7 Striatal hamartomas expressed Sox2 .....	78
3.8 Striatal hamartomas expressed Nestin .....	79
3.9 Striatal hamartomas expressed Glutamine Synthetase .....	81
3.10 Striatal hamartomas expressed DCX .....	83
3.11 Striatal hamartomas expressed NeuN .....	84
3.12 The cellular composition of striatal hamartomas .....	86
3.13 <i>Tsc2</i> inactivation resulted in heterotopic neurons in the striatum .....	88
3.14 Neuronal morphology is aberrant in the <i>Tsc2</i> null striatum at P30 .....	91
3.15 Neurons are larger than wildtype in the mutant striatum at P60 .....	92
4.1 Olfactory bulb neurogenesis .....	110
4.2 Postnatal electroporation of the V-SVZ resulted in <i>Tsc2</i> inactivation in the OB .....	113
4.3 OB morphology and organization is disrupted following <i>Tsc2</i> inactivation .....	116
4.4 mTORC1 activity is increased in OB granule cells .....	117
4.5 <i>Tsc2</i> was inactivated in mature granule cell neurons of the OB .....	120
4.6 Bulk RNA sequencing of the <i>Tsc2</i> mutant OB .....	124

### **List of abbreviations**

NSC – neural stem cell; TAC – transit amplifying cell; IPC – intermediate progenitor cell; V-SVZ – ventricular-subventricular zone; OB – olfactory bulb; RMS – rostral migratory stream; SEN – subependymal nodule; SEGA – subependymal giant cell astrocytoma; TSC – Tuberous Sclerosis Complex; mTORC1 – mechanistic Target of Rapamycin Complex 1; TAND – TSC-associated neuropsychiatric disorder; ASD – autism spectrum disorder

## **CHAPTER ONE: Literature Review**

Stem cells are progenitor cells that are able to self-renew and have potency, which is the ability to generate other cell types (Singh et al., 2016). There are multiple types of stem cell potency which become more restrictive in terms of the types of cells that can be produced. The different types of potency are totipotency where stem cells can produce cells that can generate an entire organism at any developmental stage, pluripotency where stem cells only produce cells from a specific developmental stage but can generate cells that contribute to multiple tissue types, multipotency where stem cells can generate cells from a specific tissue, and unipotent where stem cells can only generate one specific cell type (Singh et al., 2016).

Neural stem cells (NSCs) are considered multipotent. NSCs produce diverse types of nervous system-specific daughter cells including neurons, astrocytes, oligodendrocytes, ependyma, and other NSCs at different developmental time points in the murine brain (Malatesta et al., 2000; Merkle et al., 2004; Noctor et al., 2001; Qian et al., 2000).

### **EMBRYONIC NEUROGENESIS**

The early neural tube is lined with stem cells called neuroepithelial cells during embryonic development, (Subramanian et al., 2017). Neuroepithelial cells give rise to the main dorsal cortical neural stem cell, the radial glia, which facilitates neurogenesis, or the production of neurons, in the cerebral cortex during early development (around embryonic day (E) 12) and cortical gliogenesis, or the production of glia, perinatally

(around E18) (Qian et al., 2000; Subramanian et al., 2017). Cortical neurogenesis begins around E12 with radial glia that produce intermediate progenitor cells (IPCs) which amplify neuroblast production (Figure 1.1.A) (Noctor et al., 2004; Qian et al., 2000). The IPC population is a highly mitotic progenitor population that rapidly produces neuroblasts that can divide, allowing for expansive neurogenesis (M. R. Costa et al., 2011; Doetsch et al., 1997). Neuroblasts are essentially immature neurons that are committed to neuronal cell fate. Neuroblasts migrate up the radial glia basal process to pattern the cortex as mature neurons. Following cortical neurogenesis, radial glia switch to producing astrocytes around E18, eventually turning into astrocytes and ependymal cells (Fame & Lehtinen, 2019; Ortiz-Álvarez et al., 2019; Spassky et al., 2005). They also produce the adult NSCs which take over neurogenesis and gliogenesis in the postnatal brain (Fumental et al., 2015; Furutachi et al., 2015; Merkle et al., 2004; Qian et al., 2000; Redmond et al., 2019).

## **POSTNATAL NEUROGENESIS**

Mice have ongoing postnatal neurogenesis in two primary niches: the ventricular zone-subventricular zone (V-SVZ) of the lateral ventricle and the dentate gyrus of the hippocampus (Kempermann et al., 2015; Lim & Alvarez-Buylla, 2016). This dissertation examines V-SVZ neurogenesis; hippocampal neurogenesis is described elsewhere (see Kempermann, Song, and Gage 2015). Murine postnatal V-SVZ neurogenesis begins with adult NSCs that line the lateral ventricle (Lim & Alvarez-Buylla, 2016). In the V-SVZ of the lateral ventricle, there are two general types of NSCs, the B1 and B2 cells (Doetsch et

al., 1997). The two types of stem cells can be differentiated by their location in the brain as well as their points of contact. B1 NSCs have two main processes: one that contacts the ventricle and one that contacts blood vessels; this is thought to facilitate environmental signals from circulation and the cerebrospinal fluid, which could contribute to stem cell activation, quiescence, or differentiation (Doetsch et al., 1997). B2 stem cells, on the other hand, are more lateral from the ventricle than B1 stem cells and only interface with blood vessels (Doetsch et al., 1997).

Postnatal neurogenesis in the murine V-SVZ proceeds as follows (Figure 1.1.B). Adult NSCs (B1 cells) are generated during embryonic development between gestational days 13.5 and 15.5 from radial glia but remain quiescent (non-dividing) until they are reactivated postnatally (Fuentelba et al., 2015; Furutachi et al., 2015; Merkle et al., 2004). During postnatal neurogenesis, a subset of adult NSCs of the SVZ divide symmetrically to produce transit amplifying cells (TACs) (M. R. Costa et al., 2011; Doetsch et al., 1999; Obernier et al., 2018). Unlike in cortical neurogenesis where neuroblasts migrate up a radial glial scaffold, postnatal neuroblasts migrate closely together potentially using blood vessels as a scaffold (Whitman et al., 2009). The migratory neuroblasts are ensheathed in the processes of B cells as they move through the rostral migratory stream (RMS) toward the olfactory bulb (OB) (Doetsch et al., 1997; Doetsch & Alvarez-Buylla, 1996; Platel et al., 2019). Upon reaching the OB, neuroblasts mature into functional subtypes of granular and periglomerular neurons, with the vast majority residing in the granule cell layer of the OB (Doetsch et al., 1999; Young et al., 2007).

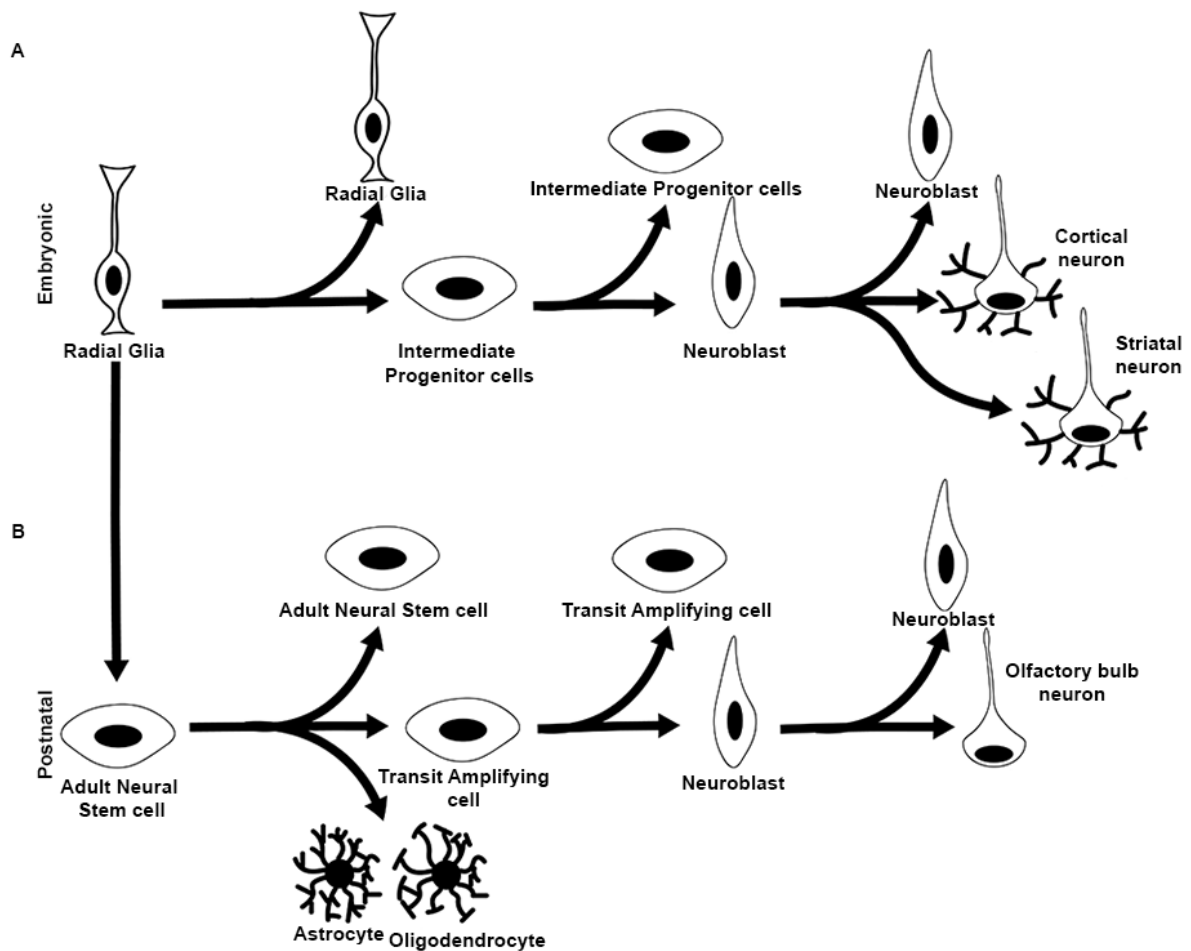


Figure 1.1 *Neurogenesis in the murine brain*

A. Embryonic neurogenesis: Cortical neurogenesis begins around E12 with radial glia that produce transit amplifying cells, which amplify neuroblast production, and neuroblasts. Neuroblasts migrate up the radial glia basal process as scaffolding to pattern the cortex as mature neurons. These radial glia also produce neurons that populate the striatum and adult NSCs that take over neurogenesis and gliogenesis in the postnatal brain. B. Postnatal neurogenesis: A subset of adult NSCs of the SVZ divide symmetrically to produce transit-amplifying cells and neuroblasts. Postnatal neuroblasts migrate through the rostral migratory stream toward the OB. Upon reaching the OB, the neuroblasts mature into functional subtypes of granule cells and periglomerular neurons, with the vast majority residing in the granule cell layer. Adult NSCs also produce astrocytes and oligodendrocytes that populate other brain regions during this period.

The neuronal subtypes that are produced postnatally in the OB are partially determined by the regionality and transcriptional profile of stem cells in the V-SVZ (Batista-Brito et al., 2008; Fuentealba et al., 2015; Merkle et al., 2007; Young et al., 2007). NSCs produce different transcription factors based on their location in the V-SVZ, leading to discrete compartments of NSCs in the V-SVZ that produce different cell subtypes (Mizrak et al., 2019).

This has been taken advantage of in a study by Young et.al., in which reporter mice under control of different regionally specific promoters were used to assess how different regions of stem cells in the V-SVZ contributed to neuronal diversity in the OB (Young et al., 2007). *Emx1* is a transcription factor primarily expressed in dorsal and septal NSCs. Using *Emx1*-Cre mice, cells that have an active *Emx1* promoter will undergo genomic recombination that causes the constitutive expression of GFP. In these mice, GFP fluorescent calretinin<sup>+</sup> neurons were found in the glomerular and granule cell layer of the OB, indicating that these neurons arose from *Emx1*-expressing progenitors. Similarly, calbindin neurons in the glomerular cell layer were produced in *Gsh2*-Cre promoter mice, which mark the NSCs in the lateral portion of the SVZ that is derived from the lateral ganglionic eminence. Both *Emx1*-Cre and *Gsh2*-Cre mice contributed GFP<sup>+</sup> tyrosine hydroxylase positive periglomerular cells in the glomerular cell layer of the OB (Young et al., 2007). This shows that different regional populations of NSCs produce different subsets of neurons in the OB (Young et al., 2007). However, this study does not differentiate whether it is the region of the V-SVZ that is important to neuronal

subtype production (i.e., environmental cues), the expressed transcription factor, such as *Emx1* or *Gsh2* (i.e., intrinsic cues), or a combination of factors.

To elucidate if the regional specificity of NSCs was due to environmental factors or intrinsic NSC cues, Merkle et. al., performed a study wherein NSCs from one region of the V-SVZ were transplanted into another region of the V-SVZ (Merkle et al., 2007). Cells that were transplanted continued to generate neuronal subtypes typical of their region of origin rather than the currently occupied transplanted region, indicating that NSCs express a pre-set profile of transcription factors that result in specific subtypes of neurons regardless of their location (Merkle et al., 2007). This indicates that NSCs of the V-SVZ have an intrinsic identity even before differentiation and neuron production. Therefore, different subsets of NSCs exist in the regions of the V-SVZ which contribute neurons to the OB. These studies underscore the heterogeneity of NSCs, the V-SVZ neurogenic niche, and the coordinated, synchronized regulation that controls neurogenesis and brain patterning.

## **NSC ACTIVATION**

Before postnatal neurogenesis occurs, adult NSCs must leave quiescence and become activated. The direct molecular mechanisms that facilitate the transition of NSCs are unknown. Still, studies have shown that numerous environmental signals from the vasculature and the choroid plexus can play a role in the regulation and production of adult NSCs and their progeny (Lepko et al., 2019; Silva-Vargas et al., 2016; M. Tavazoie et al., 2008).

Single cell sequencing of the adult NSC niche has identified some molecular underpinnings of NSC activation. Adult NSCs of the V-SVZ exist along a gradient of activation and quiescence but can be separated into stages based on gene profiling and protein expression (Shin et al., 2015). Using injury models, it has been shown that NSCs can move through activation stages and revert to earlier stages of quiescence, making the neural stem cell state a fluid mechanism (Basak et al., 2018). Neural stem cell activation can be grouped into four main stages. The first is the quiescent/dormant stage. Quiescent/inactive NSCs are not actively dividing and retain glial characteristics (Dulken et al., 2017; Llorens-Bobadilla et al., 2015). As these cells move to the second stage, toward activation, they become “primed”. Primed quiescent (or early active in some studies), begin to lose their glial characteristics but are not proliferative (Baser et al., 2017). The move from quiescence to activation is marked by increased ribosome biogenesis and subsequent protein production (Baser et al., 2019). Once NSCs are in the third stage they are considered activated and lose their glial markers completely and begin to express markers of proliferation and the cell cycle (Dulken et al., 2017; Llorens-Bobadilla et al., 2015). This state is most likely representative of self-renewing cycling NSCs. At the fourth late-stage of neural stem cell activation, just before differentiation, cells remain proliferative but also begin to take on early markers of neuronal differentiation, such as *Dlx2*, in a phenomenon called differentiation priming (Dulken et al., 2017; Llorens-Bobadilla et al., 2015).

## **THE ROLE OF MTORC1 IN NSCS**

The activation of adult NSCs is marked by a large increase in ribosome biogenesis and subsequent mRNA translation (Blair et al., 2017; Dulken et al., 2017; Llorens-Bobadilla et al., 2015; Sampath et al., 2008). This is partly due to the mTOR signaling pathway, specifically mTORC1, which influences translation (Figure 1.2.A) (Beretta et al., 1996; A. C. Gingras et al., 2001; Svitkin et al., 2001). mTORC1 plays many roles in the regulation of translation initiation, but its influence on the substrates 4EBP and 70S6K is the most well-studied (Choo et al., 2008; Tee & Blenis, 2005). Sensitive to growth factors, mitogens, amino acids, insulin levels, and other factors, mTORC1 is activated when there are sufficient resources for protein production, as mRNA translation is the most energy-intensive phenomenon in the cell (Baser et al., 2017). When mTORC1 is activated, one substrate it phosphorylates is 4EBP (Figure 1.2.C) (A. Gingras et al., 1999; Mader et al., 1995; Thoreen et al., 2012). The phosphorylation of 4EBP prevents binding to the translation initiator, eIF4E. When eIF4E is released from 4EBP, it directly binds to cap-dependent mRNA to facilitate the beginning of translation (A. Gingras et al., 1999). mTORC1's phosphorylation of 4EBP therefore increases mRNA translation by regulating mRNA transcripts, specifically those with a 5' terminal oligo pyrimidine motif, which are known to be associated with the translational machinery and ribosome biogenesis (Gandin et al., 2016; Jefferies et al., 1997a; Thoreen et al., 2012). mTORC1 also phosphorylates the protein 70 S6 Kinase (p70S6K) (Holz et al., 2005; Jefferies et al., 1997a). P70S6K is complexed with the

eukaryotic initiation factor eIF3 and, upon phosphorylation, dissociates and allows translation to proceed (Holz et al., 2005). In addition, upon phosphorylation, P70S6K will phosphorylate translation initiation factor eIF4B and ribosomal protein S6, which further facilitate the translation of mRNA transcripts (Figure 1.2.B) (Holz et al., 2005). mTORC1 is, therefore, crucial for the regulation of mRNA translation and plays a significant role in determining the level of neural stem cell activation.

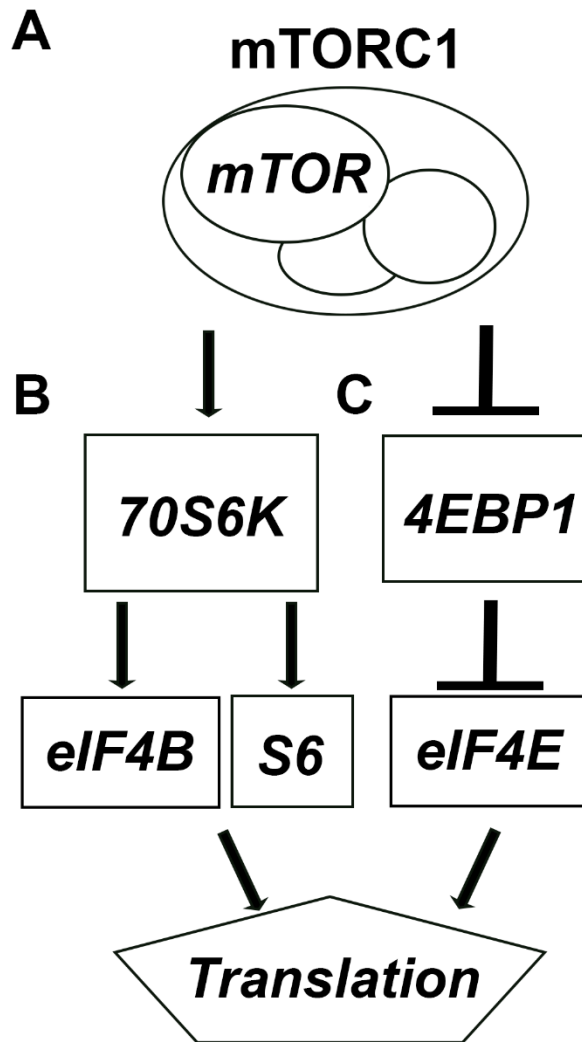


Figure 1. 2 *mTORC1* signaling plays a role in regulating translation

A. The mTORC1 signaling complex phosphorylates 70S6K (B) and 4EBP1 (C), B. Following phosphorylation by mTORC1, p70S6K phosphorylates eIF4B and S6, C. Following phosphorylation by mTORC1, p4EBP phosphorylates eIF4E to influence translation

In contrast to NSC activation, when NSCs begin to differentiate, there is a dramatic decrease in mTORC1 activity (Figure 1.3) (Baser et al., 2019; Blair et al., 2017, 2018; V. Costa et al., 2016; Paliouras et al., 2012). One study determined this by isolating actively translating mRNA at different maturation stages, including adult NSCs, early neuroblasts, late neuroblasts, early neurons, and late neurons (Baser et al., 2019). Bioinformatic analysis determined that the majority of genes that were downregulated during the transition of adult NSCs to neuroblasts (during differentiation) were those with a 5' terminal oligopyrimidine motif, which are mainly regulated by mTORC1 signaling (Baser et al., 2019). When examined further, it was found that when stem cells began to divide there was a decrease in mTORC1 activity that subsequently caused a reduction in *Sox2* transcript and protein expression. The reduction of *Sox2* activity contributes to differentiation (Baser et al., 2019). Additionally, when mTORC1 levels were increased, *Sox2* activity did not decrease, and stemness was retained (Baser et al., 2019).

This phenomenon is further corroborated by the fact that in organoids, mTORC1 signaling decreases as human embryonic stem cells move from a proliferative state to a differentiated state (Blair et al., 2018). However, it has also been shown that the inhibition of mTOR by the mTOR inhibitors rapamycin and KU0063794, in the absence of EGF can also cause a delay in differentiation and the retention of stem cell markers (V. Costa et al., 2016; Hartman et al., 2013; Paliouras et al., 2012). Given that these two studies seemingly have opposing results, it implies that mTORC1 activity is tightly controlled in NSCs, directly regulates differentiation, and is likely cell type specific.

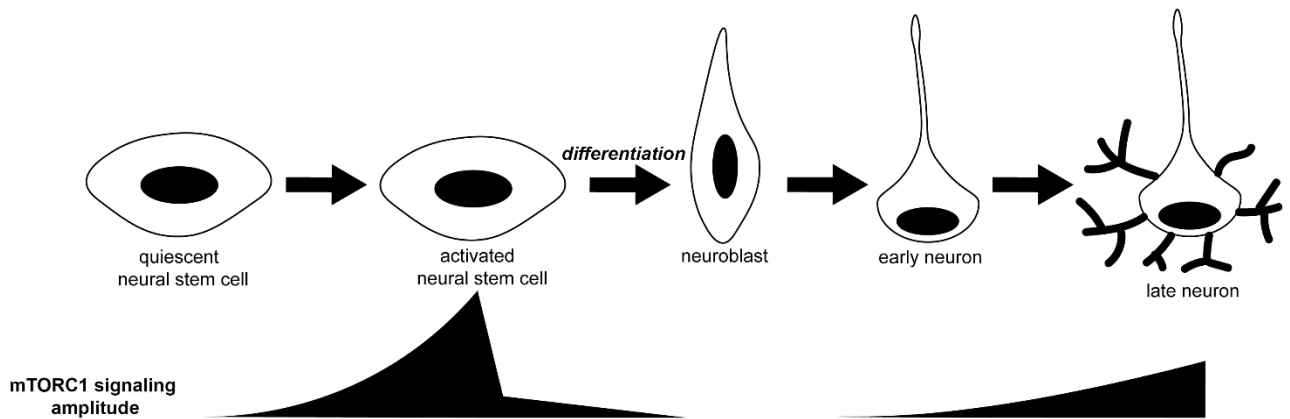


Figure 1.3 *mTORC1* expression in neural stem cells

mTORC1 signaling amplitude is low in quiescent NSCs and rises throughout activation. Prior to differentiation, there is a sharp decrease in mTORC1 signaling and it remains low throughout early neuronal development. mTORC1 signaling amplitude begins to rise slightly once neurons reach maturity.

Given that mTORC1 plays a key role in neurogenesis and stem cell fate, it follows that aberrations in this pathway can lead to neurodevelopmental disorders. Disorders characterized by altered mTOR pathway activity are called mTORopathies (Crino, 2020). By studying the mTORopathies, underpinnings of neurogenesis and stem cell development can be elucidated which can then be used to treat said disorders.

## **TUBEROUS SCLEROSIS COMPLEX**

Tuberous Sclerosis Complex (TSC, OMIM #613254) is the prototypical mTORopathy. TSC is a neurodevelopmental genetic disorder that affects multiple body organ systems including the heart, kidney, liver, lungs, skin, and brain (Feliciano, 2020). TSC is caused by inactivating mutations in either the TSC1 or TSC2 genes (European Tuberous Sclerosis Consortium, 1993; Feliciano, 2020; van Slegtenhorst et al., 1997). TSC1 on chromosome 9 and TSC2 on chromosome 16 encode the proteins hamartin and tuberlin, respectively (European Tuberous Sclerosis Consortium, 1993; van Slegtenhorst et al., 1997).

Hamartin and tuberlin act in a heterotrimeric complex along with a small protein termed TBC1D7 (Dibble et al., 2012). Importantly for TSC, if one of the subunits is missing from the heterotrimeric complex, the other members are subsequently ubiquitinated and degraded, leading to similar, though not identical, disease presentation (Benvenuto et al., 2000; S. Jozwiak et al., 2004). In this complex, TBC1D7 stabilizes hamartin and together they bind and stabilize tuberlin (Dibble et al., 2012). Tuberlin contains the active site of the complex, a GAP moiety that stimulates the GTPase activity

of Rheb, causing its conversion from GTP-bound Rheb to GDP-bound Rheb (Tee et al., 2003). GTP-bound Rheb, in the presence of the Rag-Ragulator complex, binds to the lysosomal surface and activates the mTORC1 complex (Sancak et al., 2010). In the absence of the heterotrimeric *Tsc1/Tsc2/Tbc1d7* complex, Rheb remains in its GTP-bound form, resulting in constant activation of mTORC1 signaling and subsequent TSC phenotypes (Tee et al., 2003).

Mutations in the TSC genes usually occur in one allele of the affected gene and, upon loss of heterozygosity (LOH) and depending on the timing of LOH, more severe symptoms can occur (European Tuberous Sclerosis Consortium, 2001; Gelot & Represa, 2020; Magri et al., 2013). LOH makes TSC a disorder that displays somatic mosaicism wherein only a portion of cells lose functionality in both TSC alleles and contribute to the severe pathology of the disorder. Interestingly, cells that have mutations in *TSC1* result in less severe symptoms than those caused by mutations in *TSC2* in both patients and mouse models of the disease (L. H. Zeng et al., 2011). This is theorized to be because *TSC2* contains the functional GAP domain whereas *TSC1* acts as a stabilizer for the complex, meaning that *TSC2* has a more significant effect on mTORC1 activation (European Tuberous Sclerosis Consortium, 2001; Huang & Manning, 2008; L. H. Zeng et al., 2011). *TSC2* mutations are more common than *TSC1* mutations and are disproportionately observed in growths that have undergone LOH (European Tuberous Sclerosis Consortium, 2001; Kingswood et al., 2017). However, this may be due to decreased symptoms and less likelihood of diagnosis in patients with *TSC1* mutations. Mutation of *TSC1/TSC2* usually occurs either from familial inheritance or spontaneously (60%)

(DiMario Jr, 2004; Han et al., 2004; Tyburczy et al., 2015). Mutations in the TSC genes are variable and numerous. In one longitudinal study, it was found that the majority of mutations that cause TSC are “small” mutations with 38% of their cohort of 224 patients having small deletions or insertions and a further 50% with nonsense, splice-site, or missense point mutations in either TSC1 or TSC2 (European Tuberous Sclerosis Consortium, 2001). However, “large” mutations were also found where 12% of mutations were genomic deletion or rearrangement (European Tuberous Sclerosis Consortium, 2001). Interestingly, the large mutations in this study only occurred in patients with mutations in TSC2, possibly indicating a predisposition to this mutation type in this gene (European Tuberous Sclerosis Consortium, 2001). It should be noted that due to the somatic mosaicism seen in TSC, it can be difficult to identify mutations and could bias these results. That being said, the various mutations and somatic mosaicism that occur in TSC contribute to the vast heterogeneity in symptom presentation seen within the disorder.

Due to the role that the mTOR signaling pathway plays in cell growth, maturation, metabolism, and protein translation, hyperactivation of this pathway results in the primary histopathology of TSC in multiple organ systems of the body. This includes gross malformations including cardiac rhabdomyoma, renal angiomyolipoma, periungual fibromas, hypomelanotic macules, facial angiofibroma, shagreen patches, retinal hamartomas olfactory hamartomas cortical tubers, subependymal nodules (SEN) and subependymal giant cell astrocytoma (SEGA) (Northrup et al., 2013). When examined more closely, TSC brains also have syndromic cellular phenotypes including

enlarged dysmorphic neurons, increased cortical thickness, errors in the lamination of the cortex, increased astrogliosis, and hypomyelination. In addition to these manifestations, TSC brain lesions can contribute to the generation of neuropsychiatric anomalies referred to as TSC-associated neuropsychiatric disorders (TANDs) which include behavioral abnormalities, intellectual delay, autism, and intractable epilepsy (Northrup et al., 2013).

### **NEUROLOGICAL SYMPTOMS OF TSC**

The most common neurological symptom in TSC is epilepsy. Epilepsy occurs in around 88% of TSC patients and usually presents during the first few months after birth as infantile spasms (Specchio et al., 2020; Weiner et al., 2006). Epilepsy associated with TSC is variable and often intractable (F. E. Jansen et al., 2007, 2008; Jensen, 2009; Specchio et al., 2020). Epilepsy is thought to contribute to the progression of symptoms in TSC and has been associated with the presence of other neurological disorders, such as autism, and physical brain manifestations such as cortical tubers, especially in cases where seizures are intractable (Jensen, 2009; Specchio et al., 2020). It has been noted in TSC that the earlier the onset of seizures, the worse the associated neurological symptoms become, implying that seizure activity is partly responsible for these manifestations (McMahon et al., 2015). However, other symptoms of TSC such as cortical malformations and abnormal brain patterning can contribute to increased seizure activity or the likelihood of increased seizure activity (Feliciano et al., 2011). Given this duality, a current area of debate is whether TSC-associated epilepsy is causal or

consequential to the other symptoms of TSC or if it is a devastating feedback loop (Jensen, 2009; Moavero et al., 2020; Specchio et al., 2020).

In addition to seizures, TSC patients are often afflicted with TANDs. TANDs can include many different disorders but the most common are autism spectrum disorders (ASD) (25-50% of TSC patients), ADHD (30-50% of TSC patients), cognitive impairment (50% of TSC patients have an IQ of less than 70), and behavioral issues, such as depression and anxiety (30-60% of TSC patients) (De Vries et al., 2015). While the percentage of TSC patients with these specific TANDs can be variable it has been found that most TSC patients experience some type of TAND at some point in their lifetime and that TANDs are often combinatorial (Leclezio et al., 2015).

## **CORTICAL TUBERS**

Growths that occur in TSC are often called hamartomas. Hamartomas are groups of abnormal cells that are often ectopic, meaning they are in the incorrect anatomical position in the brain. The three main types of brain hamartomas that form in the TSC brain are the cortical tuber, subependymal nodule (SEN), and subependymal giant cell astrocytoma (SEGA). These lesions can be differentiated by the frequency at which they occur in patients, their location in the brain, and cellular characteristics.

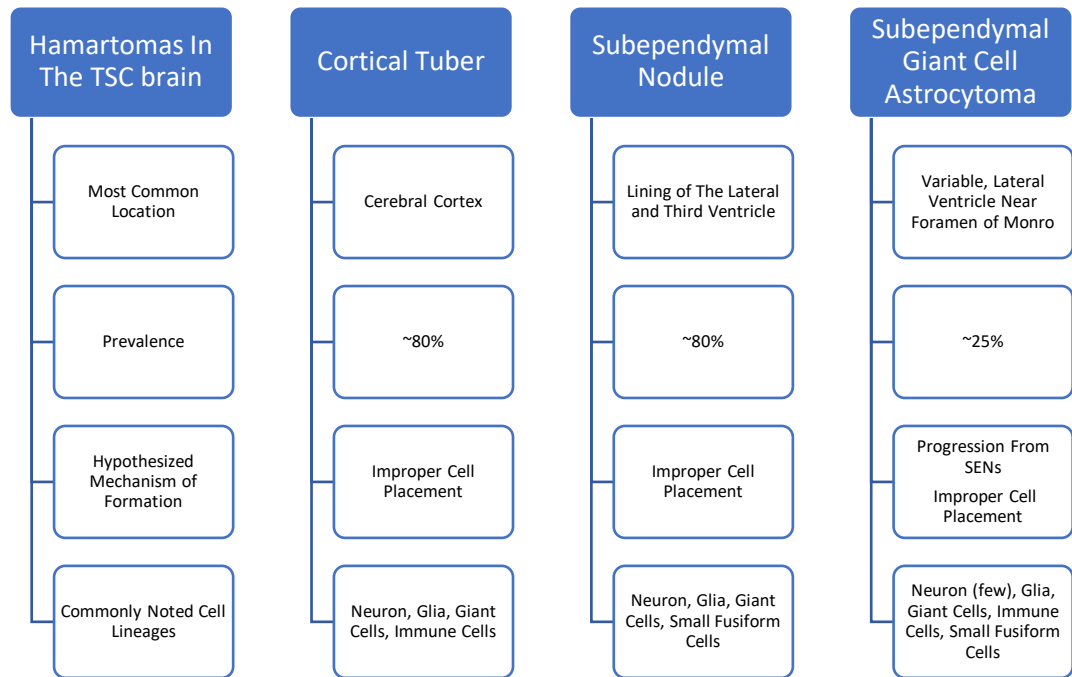


Figure 1. 4 *Types of Hamartoma in the TSC brain*

The three main types of hamartoma in the TSC brain: cortical tuber, subependymal nodule, and subependymal giant cell astrocytoma. Their prevalence, hypothesized mechanism of formation, and commonly noted cell lineages are given. It should be noted that hamartoma presentation in TSC is variable and not all hamartomas are represented by these categories.

The first type of hamartoma is the cortical tuber which occurs in 82.2% of patients (Kingswood et al., 2017). Cortical tubers are a cause of TSC-associated epilepsy and other TSC-associated neuropsychiatric disorders as an increase in the number of cortical tubers is concurrent with an increase in epileptic severity and in most cases, upon surgical resection, there is a decrease in seizure severity (Weiner et al., 2006).

Cortical tubers form within the cerebral cortex and are believed to contribute to many of the neuropsychiatric manifestations of TSC. In humans, they can initiate as early as 19 gestational weeks and are believed to develop from aberrantly migrating neuroepithelial cells (Gelot & Represa, 2020; Park et al., 1997; Prabowo et al., 2013). They are large groups of dysplastic cells located in the cortex that contain neurons, astrocytes, and giant cells (Talós et al., 2008). Giant cells are unique cells that are commonly found in TSC brain lesions. They measure approximately 5-10 times larger than other neurons and have a mixed astrocyte-neuronal phenotype (Yamanouchi et al., 1997). Giant cells have a diverse presentation where some express only neuronal markers, some express only astrocytic markers, some express both types of markers, and still others defy categorization (Yamanouchi et al., 1997). It has been postulated that giant cells arise due to abnormal differentiation of NSCs given giant cell's proclivity to stain positively for stem cell and immature markers (Eichmüller et al., 2022; Gelot & Represa, 2020; Yamanouchi et al., 1997).

The formation of cortical tubers is progressive throughout fetal development, beginning as disorganized astrocytes and taking on the more neuronal and Giant cell phenotype later in development (Eichmüller et al., 2022; Gelot & Represa, 2020; Park et

al., 1997). Cortical tubers are immunoreactive for inhibitory and excitatory neuronal markers (Eichmüller et al., 2022). They also have decreased neurotransmitter uptake, GABA and glutamate receptor subunits, and voltage-gated potassium ion channels compared to control tissue from the same brain (Boer et al., 2010). This could likely contribute to E/I imbalance, a driver of seizures and seizure activity. Cortical tubers also have a marked increase in inflammatory and immune response pathways and cell adhesion-related genes compared to control tissue from the same brain (Boer et al., 2010; Prabowo et al., 2013). Immune activation could either be causative of cortical tubers or a consequence of them.

Cortical tubers have been previously modeled in mice (Feliciano et al., 2011). The first model to do this deleted *Tsc1* at E15/16 via *in utero* electroporation in a small subset of radial glia lining the lateral ventricle. This resulted in cerebral lesions predominantly comprised of cytomegalic NeuN<sup>+</sup> neurons with elevated pS6 (Feliciano et al., 2011). Additionally, and importantly, around 10% of ectopic cytomegalic neurons were also multinucleated (Feliciano et al., 2011). This was highly reminiscent of resected TSC patient cortical tubers (Crino, 2010). This model has since become a standard model for focal cortical dysplasia with ties to mTOR and cortical tubers (Feliciano, 2023).

## **SUBEPENDYMAL NODULES**

Another benign growth commonly found in TSC patients' brains is the subependymal nodule (SEN). SENs are small disruptions of the V-SVZ that form within the lateral ventricles in 78.2% of patients (European Tuberous Sclerosis Consortium,

2001; Gelot & Represa, 2020; Kingswood et al., 2017). They are comprised of multiple cell types including giant cells, dysmorphic astrocytes and neurons, and small fusiform cells (Gelot & Represa, 2020). These cell types have also been shown to express immature and mature cell markers and occasional immune cell markers (Gelot & Represa, 2020; Zordan et al., 2018). Molecularly, SENs have evidence of activation of the mTORC1 signaling pathway and AKT phosphorylation (Zordan et al., 2018). In one study, a collection of human SEN samples at different stages of development were utilized to study possible mechanisms of SEN development (Gelot & Represa, 2020). It should be noted that, due to the heterogenous nature of TSC, the stages of SEN development observed used separate human samples that may not reflect natural SEN development but rather the differences seen between TSC patients or SEN location. However, dysmorphic astrocytes appeared first in early SEN samples, followed by the generation of giant cells on the periphery and small fusiform cells that formed the core of the nodule (Gelot & Represa, 2020). As development proceeded, DCX+ neuroblasts circumscribed SENs, and cytomegalic dysmorphic neurons with inhibitory markers began to appear (Gelot & Represa, 2020). This developmental progression could indicate the presence of dysplastic astrocytic NSCs which begin to produce neuroblasts and eventually neurons to cause hamartoma formation. SENs usually arise early in development and, therefore, might result from aberrations in early progenitor cells.

Mouse models have subsequently been developed to look at SEN development. Some of these mouse models use mechanisms that cause biallelic inactivation of the TSC genes to generate large growths within the lateral ventricle (Zhou et al., 2011; Zordan et

al., 2018). Other mouse models used germline heterozygous mutations and caused loss of functionality in the other allele at a different point in development to mimic second-hit mutations (Magri et al., 2011, 2013). The germline heterozygous/conditional model resulted in an expanded accumulation of cells in the dorsal SVZ that could be interpreted as an SEN (Magri et al., 2011). This region had DCX+, Tuj1+, and PSA-NCAM+ cells, indicating the presence of neuroblasts and neurons (Magri et al., 2011). There were also many GFAP+ cells and peripheral Tbr2+ cells which suggests the expansion had glial or progenitor components (Magri et al., 2011). The expansion also contained cells that express markers that are typically found in human SENs, including GPNMB and PTGDS (Magri et al., 2011). While this model generated a SEN-like region, the biallelic inactivation models resulted in a more severe human-like phenotype.

One such model of SENs results due to biallelic inactivation of *Tsc1* in postnatal NSCs (Zhou et al., 2011). Generated SENs had hyperchromatic nuclei and scant cytoplasm, spindle-like cells, and differentiated cells (Zhou et al., 2011). Growths contained cells that expressed glial markers (S100b and GFAP) or neuronal markers (MAP2 and NeuN) (Zhou et al., 2011). Some cells also had a mixed glioneuronal phenotype and were co-labeled with GFAP and MAP2 (Zhou et al., 2011). In addition to these cells, there were few Nestin+ and Ki67+ cells in the growths, indicating a small proportion of progenitor cells (Zhou et al., 2011). The growths also had giant cells and a glial-fibrillary matrix generated by the GFAP cells (Zhou et al., 2011). These growths were found to form due to disrupted OB neurogenesis. In normal OB neurogenesis, postnatal NSCs will produce transit-amplifying cells and neuroblasts that migrate down

the rostral migratory stream to populate the granule cell layer (Lim & Alvarez-Buylla, 2016). In the mice that had lost *Tsc1* in postnatal NSCs, the cell density of the granule cell layer of the OB was significantly reduced, indicating that cells were not reaching the OB from the V-SVZ (Zhou et al., 2011). It was further hypothesized that DCX+ neuroblasts were failing to migrate properly, leading to the buildup of cells in the V-SVZ and caused SENs (Zhou et al., 2011). This indicates that SENs may arise due to migration errors and an inability to leave the neurogenic niche. This migratory disruption was confirmed in another mouse model where the inactivation of *Tsc1* in V-SVZ NSCs resulted in rostral migratory stream (RMS) and olfactory hamartomas (Feliciano et al., 2012). Hamartomas were small clumps of cells found throughout the TSC brain that contained cells with increased mTORC1 activity and cytomegaly. Cells of the V-SVZ that had lost *Tsc1* and were migrating to the OB were found to be 33% slower than wildtype cells as they traversed the RMS, confirming that migration may play a role in growth formation (Feliciano et al., 2012).

SENs/SEGAs have been shown to have increased AKT phosphorylation (J. Jozwiak et al., 2007; Siedlecka et al., 2015a; Zordan et al., 2018). To model this phenotype more closely, mice that have biallelic inactivation of *Tsc1* and *Pten* in postnatal NSCs have been generated. *Pten* deletion results in increased AKT phosphorylation, mimicking TSC SEGA. This model resulted in an expansion of dorsal SVZ as seen in models with heterozygous/conditional mutations and nodular structures along the V-SVZ that resembled SENs (Zordan et al., 2018). The nodules were

heterogeneous in terms of cellular composition and had markers of both immaturity and maturity as well as immune activation.

Taken together, human and mouse SENs appear to have a heterogeneous cellular composition including neurons, neuroblasts, and glia. In the mouse, they potentially form due to disrupted OB neurogenesis wherein cells cannot migrate properly to the OB. This could possibly explain why SEN formation is a developmental phenomenon, as neurogenesis in humans becomes extremely protracted postnatally as opposed to mice.

#### SUBEPENDYMAL GIANT CELL ASTROCYTOMA

In mouse models of SENs, it has often been found that the lesions progress throughout life. This supports the idea that SENs occasionally progress into a third type of central nervous system TSC growth, SEGA (Kim et al., 2001; Morimoto & Mogami, 1986; Siedlecka et al., 2015b). Typically, SENs are not distinguished from SEGAs histopathologically but rather due to their size in humans. SENs are less than one centimeter in circumference whereas SEGAs are larger than one centimeter in humans (Kim et al., 2001; Northrup et al., 2013). It is, therefore, hard to distinguish between SENs and SEGAs by size in mice.

SEGAs are growths that form in 24.4% of TSC patients in various brain regions, including the striatum but are most commonly found near the lateral ventricles of the brain (Adriaensen et al., 2009; Kingswood et al., 2017; Yeung et al., 1997). They occur primarily in children but can occur in adults (A. C. Jansen et al., 2019; Kingswood et al., 2017). The lesions cause generally minor symptoms but can grow to block the flow of

cerebrospinal fluid and cause life-threatening hydrocephalus and brain hemorrhage (Kingswood et al., 2017; Tsai et al., 2016). In one study of 2223 patients, it was found that 422 patients had SEGA at the time of study. Of these 422 patients, 36.7% of SEGAs showed signs of growth (Kingswood et al., 2017). This growth was most common between ages five and eighteen but occasionally persisted into adulthood (A. C. Jansen et al., 2019; Kingswood et al., 2017). In addition to hydrocephalus, those afflicted with SEGA can also experience increased seizure frequency, behavioral disturbances, headache, vomiting, and intellectual decline (Kim et al., 2001; Kingswood et al., 2017). SEGAs are traditionally surgically resected when they become detrimental to the patient's health, but more recently, mTOR inhibitors have proven to be effective in causing hamartoma regression (Franz et al., 2006; Kingswood et al., 2017). Interestingly, when mTOR inhibitors are stopped, it results in regrowth, meaning that TSC patients with SEGA must maintain a medicinal course in perpetuity (Franz et al., 2006).

Histologically, SEGAs are similar to SENs. They have a glial-fibrillary matrix and are comprised of glial and neuronal cells, multinucleated giant cells, microglia, and other immune cells (Bongaarts et al., 2017; Kim et al., 2001; Martin et al., 2017). Despite their growth patterns, SEGAs generally have a low mitotic index (Kim et al., 2001). While progression is slow and growth could result from low level mitotic activity, SEGA growth could also result from immune cell infiltration, calcification, or migratory behavior.

Despite their growth, SEGAs are not readily distinguishable from SENs in mice. Therefore, differing expression profiles often equate murine growths to their human

counterparts. It has been shown in mouse models of SENs that either observing at later time points or causing recombination later in development leads to phenotypes similar to human SEGAs.

In one such murine model, SEGAs are derived when *Tsc1* and *Pten* were inactivated in NSCs were compared to human SEGAs samples and it was found that they both had similar cellular compositions, including the presence of cells expressing markers of immaturity and stemness including SOX2 and Vimentin (Zordan et al., 2018). Additionally, there was an increased immune response and inflammation in both human and murine SEGAs (Zordan et al., 2018). Molecularly, both lesions in mice and humans had increased Akt phosphorylation and increased activation of the mTORC1 and mTORC2 signaling pathways. Taken together, these comparisons show that SEGAs phenotypes can be recapitulated in mice.

Given the results in mouse models, multipotent neural progenitor cells are considered to be the cell of origin for TSC hamartomas (Feliciano et al., 2011; Fu et al., 2012; Magri et al., 2011; Rushing et al., 2019; Zhou et al., 2011; Zordan et al., 2018). However, due to their location, cellular characteristics, and gene expression profiles, the cell of origin for cortical tubers and SENs/SEGAs are considered to be different. However, it is also possible that one cell type is producing many aberrant cells that are destined for other brain regions (Eichmüller et al., 2022; Martin et al., 2017).

The majority of SEGAs arise from mutations in the *TSC2* gene and are caused by biallelic inactivation (Bongaarts et al., 2017, 2022; Carbonara et al., 1996; Crino et al., 2010; Ess et al., 2005; Kwiatkowski et al., 2004; Sinson et al., 1977). SEGAs are

primarily initiated according to Knudsen's two-hit hypothesis, wherein a patient will have a mutation in one allele of a gene, and it is only when the second allele becomes inactivated that hamartomas are generated (Crino et al., 2010; Green et al., 1994; Henske et al., 1996; S. Jozwiak et al., 2004; Knudson, 1971; Kwiatkowski et al., 2004; Niida et al., 2001; Sepp et al., 1996). Due to the high numbers of sporadic mutations that cause TSC, it might be reasonable to conclude that the causative genes of TSC are predisposed to mutation and likely to undergo loss of heterozygosity (LOH). LOH is one of the driving factors behind TSC growth formation and is found in other TSC hamartoma types besides SEGA (Au et al., 1999; Bongaarts et al., 2017; Giannikou et al., 2016; Green et al., 1994; Henske et al., 1996; Martin et al., 2017; Niida et al., 2001). For example, renal angiomyolipoma, cortical tubers, and cardiac rhabdomyoma have all shown LOH upon mutational analysis (Au et al., 1999; Crino et al., 2010; Henske et al., 1996; Martin et al., 2017). LOH has been shown only to affect hamartomatous tissue whereas surrounding tissue retains only monoallelic inactivation. In the TSC brain, most cells are heterozygous for one of the TSC genes. Monoallelic inactivation for the TSC genes has been shown to have very small or no effects on cellular morphology and TSC manifestation (Riley et al., 2022; S. F. Tavazoie et al., 2005; H. Zhang et al., 2003). It is upon LOH that more severe phenotypes manifest, including SEGA formation.

Recently, it has been postulated using cerebral organoids that LOH is required for hamartoma progression but not hamartoma initiation (Eichmüller et al., 2022). However, this study collected analyses at a time before the onset of TSC phenotypes (Eichmüller et al., 2022), which could preclude LOH events. Additionally, LOH is often measured by B

allele frequency analysis and whole exome sequencing studies (Eichmüller et al., 2022; Martin et al., 2017). These analyses can be challenging to assess due to the mosaic nature of SEGAs wherein there are contaminating wildtype alleles from normal cells within the growth which influence experimental outcomes.

## **SUMMARY**

Given that the growths in TSC contain cells that maintain immature characteristics as well as cells that have both glial and neuronal markers, it is tempting to hypothesize that each growth is a miniature neurogenic niche that contributes to its own hamartoma progression and severity.

TSC is caused by inactivating mutations in either the *Tsc1* or *Tsc2* gene (Crino, 2010). The inactivation of either of these genes results in the hyperactivation of the mTORC1 signaling pathway which regulates many aspects of mRNA translation and contributes to the symptoms of TSC (Crino, 2010; Feliciano, 2020; Kwiatkowski, 2003). One such symptom is SEGA which affects approximately 20% of TSC patients and is a cause of morbidity in patients. SEGAs are believed to form due to inactivating mutations occurring in NSCs (Feliciano, 2020). However, the role of *Tsc2* in regulating mTORC1 and its influence on translation in NSCs has not been fully investigated. Given this fact, it was hypothesized that loss of *Tsc2* would result in differential regulation of translation that could potentially contribute to SEGA formation. In order to assess this, *Tsc2* was inactivated in murine NSCs and the transcriptome and translome was examined. It was found that mRNA transcripts were differentially enriched in the mutant neural stem cells

that were associated with aspects of translation, metabolism, and nervous system development. In addition, the mRNA transcripts were found to be differentially regulated. Given that translation, protein production, and mTORC1 activity are implicated in the regulation of NSC differentiation, it was hypothesized that *Tsc2*'s effect on translation may result in the retention of mRNA transcripts that could potentially convey a stem-like identity. Cells that maintain these transcripts could contribute to growth formation *in vivo*. Congruently, the retention of stem cell transcripts, such as *Sox2* and *Nestin*, have previously been shown in models of TSC (Blair et al., 2018; Zordan et al., 2018).

In order to examine the consequences *Tsc2* loss in NSCs *in vivo* and generate a model of SEGA, *Tsc2* was inactivated in the V-SVZ of the lateral ventricle in mice. This resulted in the formation of striatal hamartomas that were reminiscent of SEGA. Striatal hamartomas were heterogeneous and had similar cellular compositions to human SEGAs, including a NSC component, both glial and neuronal cells, and cells along various developmental stages. As stated previously, the presence of these cell types could indicate that each striatal hamartoma is a minor neurogenic and gliogenic niche, wherein NSC-like cells are producing neurons and glia that contribute to hamartoma formation. In addition to striatal hamartomas, there were a greater proportion of neurons seen in the mutant striatum when compared to wildtype. This is similar to finding in patient samples where ectopic neurons contribute to the typical manifestations of TSC (Carson et al., 2012; Ehninger et al., 2008; Feliciano et al., 2011; Magri et al., 2011, 2013; Way et al., 2009).

In addition to the NSCs in the V-SVZ, their progeny was also examined to get a full picture of the effect of *Tsc2* loss in NSCs effect on neurogenesis. The progeny of *Tsc2* null NSCs in the V-SVZ are the granule cell interneurons of the olfactory bulb (OB) (Lim & Alvarez-Buylla, 2016). Previous studies of the OB have mostly focused on the effects of *Tsc1* loss on neuron morphology and function (Feliciano et al., 2012; Zhou et al., 2011). It has been shown that there are a smaller number of OB neurons produced in *Tsc1* null mice, a phenomenon that might be explained by migration deficits (Zhou et al., 2011). Additionally, *Tsc1* null OB neurons have been shown to be morphologically distinct, being disorganized and cytomegalic (Feliciano et al., 2012). Further olfactory micronodules were shown to occur both in the OB and rostral migratory stream, not unlike those previously seen in patient samples (de León et al., 1988; Feliciano et al., 2012). Taken together, these studies indicate that *Tsc1* plays a significant role in inhibitory granule cell morphology. However, the role of *Tsc2* in granule cells has not been established. In order to examine the consequences of *Tsc2* loss, *Tsc2* was inactivated in NSCs and the OB was examined. The mutant OB was found to have intense disorganization, cytomegalic neurons, and increased mTORC1 signaling. When transcriptomic profiling was performed, it was found that OB transcripts associated with the regulation of the synapse were upregulated in the *Tsc2* null condition. This could potentially have relevance for the neurological manifestations of TSC. Taken together, this shows that *Tsc2* plays a critical role in the morphology of OB granule cells.

## CHAPTER TWO

### ***Tsc2* inactivation resulted in atypical translation in murine NSCs.**

A version of this data is published in iScience:

Riley, V.A., Shankar, V., Holmberg, J.C., Sokolov, A.M., Neckles, V.N., Williams, K., Lyman, R., Mackay, T.F.C., and Feliciano, D.M. (2023). *Tsc2* coordinates neuroprogenitor differentiation. *iScience*. 10.1016/j.isci.2023.108442.

The experiments presented in Chapter II were performed as follows. Tamoxifen injections, cell culture, polysomal isolations, RNA isolations, and bioinformatic analyses were performed by Victoria Riley. Microdissections of the V-SVZ were performed by David Feliciano. Genotyping PCRs were performed by Victoria Riley, Sulagna Mukherjee, Melanie Garcia, Victoria Neckles, and Anthony Minerva. Library preparation, RNA quality assessment, and RNA sequencing were performed by Kaitlyn Williams.

## Abstract

mTORC1 signaling has been implicated in the regulation of neurogenesis and neural stem cell functionality. A large decrease in mTORC1 signaling has been observed in conjunction with neural stem cell differentiation. In the neurodevelopmental disorder TSC, mTORC1 signaling is hyperactive and cannot lessen prior to differentiation. To investigate the consequences of hyperactive mTORC1 signaling in neural stem cells (NSCs), the transcriptome of *Tsc2* null NSCs was examined. RNA sequencing showed that *Tsc2* loss resulted in the differential expression of mRNA transcripts associated with translation and ribosome biogenesis. Given this, polysomal profiling was performed to assess the translome of *Tsc2* null NSCs. Importantly, translational efficiency was altered in the mutant condition when compared to the wildtype. Thus, in *Tsc2* null NSCs the processes of transcription and translation were dysregulated and typical developmental processes may not proceed as normal. It was hypothesized that the dysregulation of transcription and translation causes the expression of unwanted transcripts at inappropriate times. Given that a lack of mTORC1 signaling is required for NSC differentiation and that mTORC1 signaling is not downregulated in TSC, it was further hypothesized that mutant NSCs potentially retain some stem cell associated transcripts which impacts neurogenesis and hamartoma formation.

## **Introduction**

Subependymal Giant Cell Astrocytomas (SEGAs) are a catastrophic symptom of TSC that can cause hydrocephalus and death in patients (Northrup et al., 2013). SEGAs are believed to originate with neural stem cells (NSCs) of the ventricular-subventricular zone (V-SVZ) of the lateral ventricle (Bongaarts et al., 2020; Ess et al., 2005; Feliciano, 2020; Kim et al., 2001; Raju et al., 2007). They are caused by inactivating mutations in one of the TSC genes followed by loss of heterozygosity (LOH) in the second allele (Bongaarts et al., 2017, 2020; Kwiatkowski et al., 2004). These mutations most commonly occur in the TSC2 gene, theoretically due to its larger effect on regulating mTORC1 signaling (Bongaarts et al., 2017). Losing functionality in both alleles of either of the TSC genes results in the hyperactivation of the mTORC1 signaling pathway (Giannikou et al., 2021; H. Zhang et al., 2003). Therefore, it is likely the hyperactivation of mTORC1 signaling that causes SEGA formation to occur.

mTORC1 plays a key role in the regulation of mRNA translation (Grabole et al., 2016; Thoreen et al., 2012). When nutrients and amino acids are freely available mTORC1 will be activated due to the presence of proper resources. When mTORC1 is activated, it regulates cap dependent translation by phosphorylating a protein called 4EBP (A. Gingras et al., 1999). When 4EBP is phosphorylated, it is unable to bind to the translation initiation factor eIF4E, one of the rate limiting proteins in translation (A. Gingras et al., 1999). Therefore, based on nutrient input, which must be considered as protein production is the most energy intensive process of the cell, mTORC1 can regulate

whether the cell has sufficient energy to undergo translation and protein production (Gandin et al., 2014).

mTORC1 signaling and its effect on translation is crucial to proper development and maturation (Liu & Sabatini, 2020). Therefore, it is unsurprising that mTORC1 activity is highly regulated in NSCs, the cell of origin of SEGA (Baser et al., 2019; Blair et al., 2017, 2018). During typical development, in quiescent adult NSCs, mTORC1 activity is generally low as translation and subsequent protein production are not immediately necessary nor energetically worthwhile (Baser, Skabkin, and Martin-Villalba 2017). As adult NSCs become more activated, the amplitude of mTORC1 signaling also increases before sharply decreasing upon differentiation (Baser et al. 2019; Blair, Hockemeyer, and Bateup 2018). While cells differentiate and mature, mTORC1 signaling remains low before rising slightly once more in mature cells (see Figure 1.3) (Blair et al. 2017). In congruence with this, organoid models have shown that the expression of mTORC1 substrates pS6 and p4EBP is decreased as organoids transition through differentiation in control and heterozygous organoids but not in TSC null mutants (Blair, Hockemeyer, and Bateup 2018). This indicates that when TSC genes are inactivated, mTORC1 signaling is not downregulated as it would typically be throughout NSC maturation. Therefore, the TSC genes are crucial to proper development. Indeed, the transcriptome of TSC2 null embryonic human stem cells has been examined previously and it was shown that there were altered proportions of cell lineages between mutant and wildtype cells, indicating that abnormal translation in the mutant is leading to improper brain patterning and development (Grabole et al., 2016). This phenomenon was believed

to be caused in part by translational changes in the absence of transcriptional changes, especially for 5' TOP mRNA transcripts which are primarily regulated by mTORC1 signaling (Grabole et al. 2016).

As mentioned above, SEGA are believed to originate from NSCs that lose functionality in either of the TSC genes, most commonly the TSC2 gene (European Tuberous Sclerosis Consortium, 2001). Given the regulatory role that mTORC1 signaling has on translation and the importance of this pathway in NSCs, it follows that aspects of translation may be aberrant in NSCs which could contribute to lesion formation. In this chapter, the translome and transcriptome were examined in *Tsc2* null murine NSCs in order to get a comprehensive look at the effects of *Tsc2* regulation on mTORC1 signaling, translation, and NSCs.

## Results

### *Tsc2* was inactivated in *Nestin-CRE-ERT2* mice

Mice having a conditional *Tsc2* allele ( $Tsc2^{tm1.1Mjg/J}$ ) containing LoxP sites flanking exons 2 - 4 were crossed to Ai9 mice (B6. Cg-Gt (ROSA) 26Sortm9 (CAG-tdTomato) Hze/J) that have a LoxP-flanked STOP cassette that prevents transcription of a CAG-promoter driven variant of red fluorescent protein (RFP). These mice were further crossed to *Nestin-CRE-ER<sup>T2</sup>* mice. *Nestin-CRE-ER<sup>T2</sup>* mice express a CRE recombinase fused to a mutant form of the estrogen receptor which does not bind the physiological ligand. Instead, 4-hydroxytamoxifen causes cytoplasmic-localized CRE to dimerize and enter the nuclear compartment where it subsequently excises regions of DNA flanked by LoxP sites. The *CRE-ER<sup>T2</sup>* fusion protein is downstream of the Nestin promoter and is therefore only expressed in cells in which the Nestin promoter is active (Figure 2.1.A). The Nestin promoter is active in NSCs and, upon activation, *CRE-ER<sup>T2</sup>* will remove the stop sequence to induce RFP expression and cause *Tsc2* recombination in NSCs along the lateral ventricle and their progeny (Figure 2.1.B) (Lendahl et al., 1990).

In order to investigate the transcriptional and translational effects that hyperactive mTORC1 signaling has on NSCs, 4-hydroxytamoxifen was administered twice via IP injection on postnatal day 2 and 3 mice to induce recombination of *Tsc2* in NSCs (Figure 2.1.C). Genotypes were verified for all mice via PCR specific for the wildtype and conditional *Tsc2* allele. Recombination was validated via long range PCR specific for recombined and non-recombined versions of the allele (Figure 2.1.D). It should be noted that both mutant and floxed alleles are present due to the presence of non-affected cells.

Recombination could be further validated macroscopically as the substantial number of affected cells in the OB colored them visibly red (Figure 2.1.E). Following recombination, mice were subsequently euthanized and the NSCs of the V-SVZ were microdissected to generate primary RFP+ neural stem cell cultures from both *Tsc2<sup>mut/mut</sup>* and *Tsc2<sup>wt/wt</sup>* mice (Figure 2.1.C). Primary cultures were RFP+ and appeared homogenous when kept in a self-renewing NSC media (Figure 2.1.F). Upon passage, adherent cells remained in the mutant NSC culture dishes. These adherent cells were cytomegalic and occasionally multinucleated (Figure 2.1.G). These were reminiscent of giant cells seen in patient samples (Gelot & Represa, 2020).

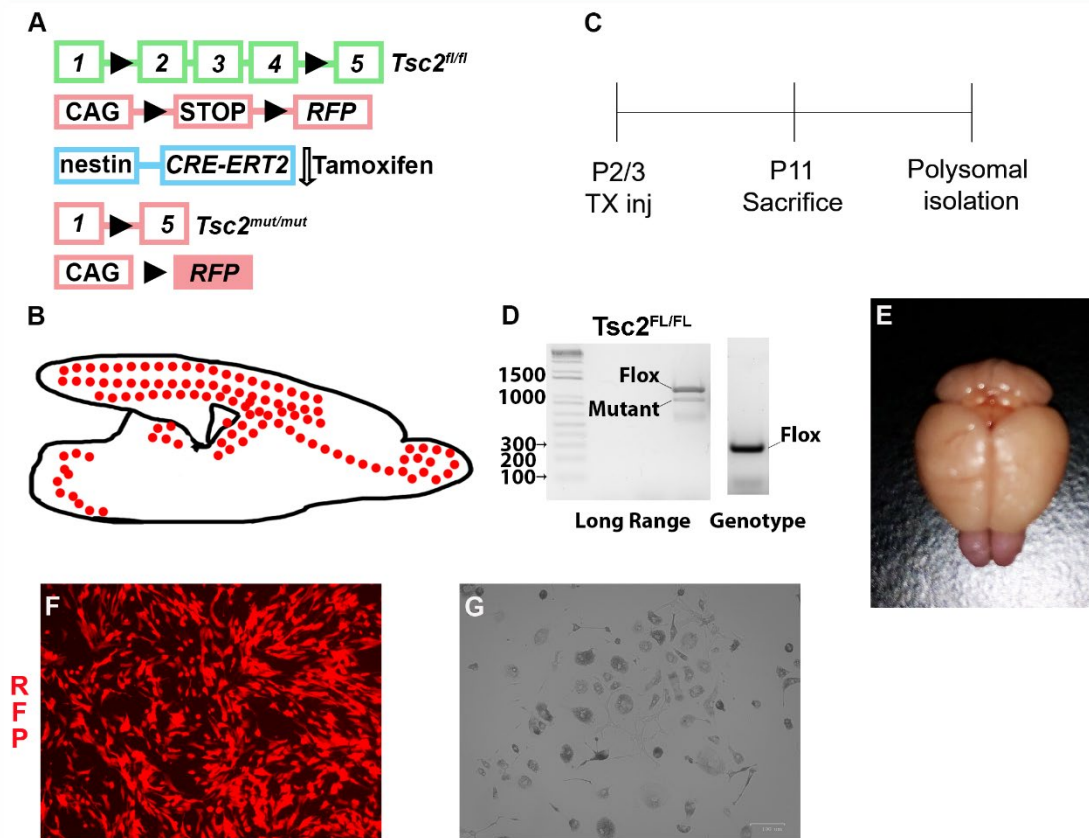


Figure 2.1 *Tsc2* inactivation was performed in *Nestin-CRE-ER<sup>T2</sup>* mice  
 A. Schematic diagram of conditional *Tsc2* and inducible *RFP* genes. *Tsc2* is mutated and *RFP* is expressed when CRE recombinase is present. Triangles denote LoxP sites, B. Recombination in NSCs results in red fluorescent *Tsc2* null cells in multiple brain regions, C. Schematic diagram of experimental set up, D. PCR showing recombination (long range) and genotype determination, E. Mouse brain with macroscopic evidence of recombination with pink OBs, F. Example of primary NSC culture that is RFP+ and homogeneous, G. Adherent cells after passage, note the large, multinucleated cells. scale bars = 100  $\mu$ m

*RNA sequencing of Tsc2 null NSCs revealed altered translation and ribosome biogenesis*

RNA from primary NSCs was isolated and bulk RNA sequencing was performed. RNA sequencing identified 4,035 differentially expressed mRNAs between the mutant and wildtype cells, 2254 which were downregulated (Figure 2.2.A, p adjusted value <0.01, mRNA transcripts with less than 100 counts were excluded from the Gene Ontology (GO) term analysis). gProfiler was used which reports filtered driver GO terms based on subontologies and connections (Raudvere et al., 2019). GO analysis of the topmost abundant transcripts revealed enrichment of terms such as structural component of the ribosome, mRNA binding, and translation regulator activity as well as terms involved with development (Figure 2.2.B). Further analysis of the topmost differentially expressed transcripts showed driver GO terms associated with and the regulation of cell signaling and homeostatic processes (Figure 2.3.A). Similarly, when terms were assessed based on fold change, it was found that transcripts that were upregulated in the mutant condition were associated with processes such as cell adhesion, the inflammatory response, the regulation of phosphorylation, metabolic processing, and the MAPK signaling cascade (Figure 2.4.A). Alternatively, transcripts that were downregulated in the mutant condition were associated with ribosome biogenesis and metabolic processes (Figure 2.4.B). These analyses underscore the important regulatory role that *Tsc2* has in ribosome biogenesis and translational regulation and that *Tsc2* has influences on translation and cellular communication at the transcriptomic level.

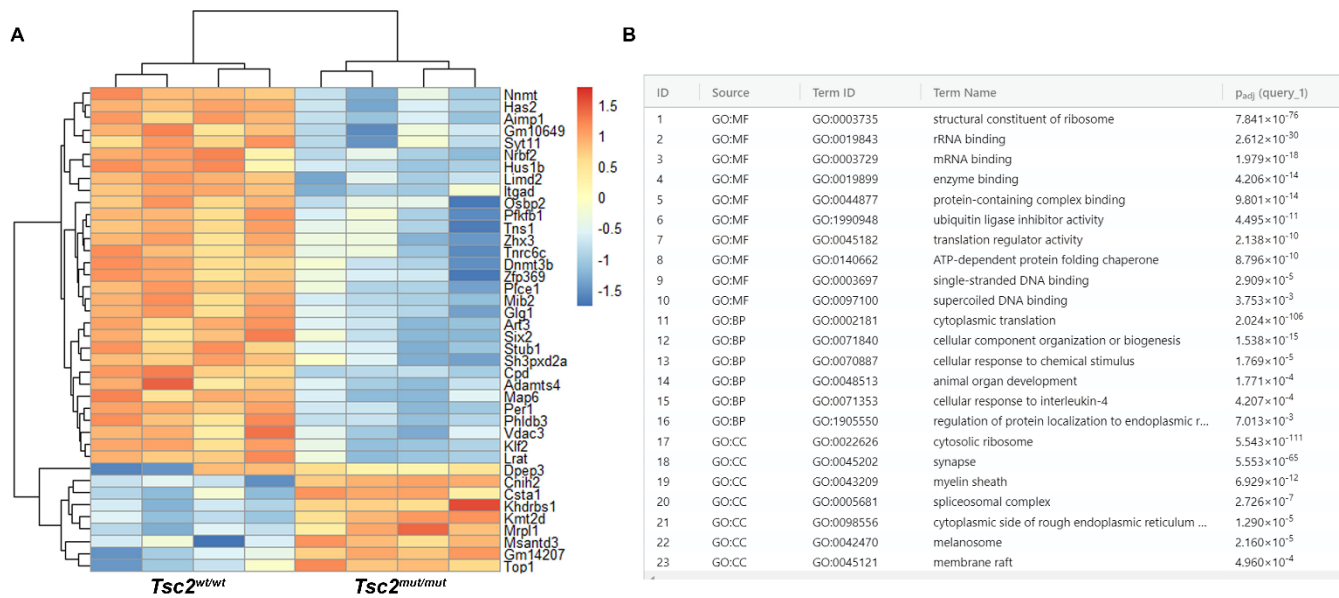


Figure 2.2 bulk RNA sequencing resulted in differentially expressed transcripts

A. Heatmap and hierarchical clustering of mRNA transcripts from primary *Tsc2<sup>wt/wt</sup>* and *Tsc2<sup>mut/mut</sup>* NSCs There were 4035 differentially expressed transcripts, 2254 which were downregulated, B. Driver GO term analysis of 200 most abundant transcripts, p adjusted value < 0.01, mRNA transcripts with less than 100 counts were excluded from the GO term analysis.

A

ID	Source	Term ID	Term Name	P <sub>adj</sub> (query_1)
1	GO:MF	GO:0005515	protein binding	$8.942 \times 10^{-22}$
2	GO:MF	GO:0005201	extracellular matrix structural constituent	$6.763 \times 10^{-5}$
3	GO:MF	GO:0005518	collagen binding	$9.531 \times 10^{-4}$
4	GO:BP	GO:0023051	regulation of signaling	$1.885 \times 10^{-14}$
5	GO:BP	GO:0007155	cell adhesion	$7.098 \times 10^{-14}$
6	GO:BP	GO:0051246	regulation of protein metabolic process	$5.827 \times 10^{-6}$
7	GO:BP	GO:0030198	extracellular matrix organization	$1.035 \times 10^{-5}$
8	GO:BP	GO:0006811	monoatomic ion transport	$2.713 \times 10^{-5}$
9	GO:BP	GO:0042592	homeostatic process	$1.507 \times 10^{-3}$
10	GO:BP	GO:0034616	response to laminar fluid shear stress	$3.030 \times 10^{-3}$
11	GO:BP	GO:1901564	organonitrogen compound metabolic process	$7.453 \times 10^{-3}$
12	GO:CC	GO:0071944	cell periphery	$4.132 \times 10^{-21}$
13	GO:CC	GO:0043235	receptor complex	$9.120 \times 10^{-3}$

Figure 2.3 *Top differentially expressed transcripts were associated with protein binding*

A. Driver GO term analysis of 200 most differentially expressed transcripts, p adjusted value < 0.01, mRNA transcripts with less than 100 counts were excluded from the GO term analysis.

### A Upregulated mRNA transcripts

ID	Source	Term ID	Term Name	P <sub>adj</sub> (query_1)
1	GO:MF	GO:0005515	protein binding	1.031×10 <sup>-18</sup>
2	GO:MF	GO:0005201	extracellular matrix structural constituent	5.928×10 <sup>-6</sup>
3	GO:MF	GO:0005518	collagen binding	1.003×10 <sup>-3</sup>
4	GO:BP	GO:0007155	cell adhesion	4.681×10 <sup>-17</sup>
5	GO:BP	GO:0051239	regulation of multicellular organismal process	2.129×10 <sup>-14</sup>
6	GO:BP	GO:0030198	extracellular matrix organization	1.289×10 <sup>-7</sup>
7	GO:BP	GO:0008015	blood circulation	4.397×10 <sup>-4</sup>
8	GO:BP	GO:0072086	specification of loop of Henle identity	2.468×10 <sup>-3</sup>
9	GO:BP	GO:0034616	response to laminar fluid shear stress	2.968×10 <sup>-3</sup>
10	GO:BP	GO:0006954	inflammatory response	2.996×10 <sup>-3</sup>
11	GO:BP	GO:0042325	regulation of phosphorylation	6.826×10 <sup>-3</sup>
12	GO:BP	GO:0030574	collagen catabolic process	9.624×10 <sup>-3</sup>
13	GO:BP	GO:0040007	growth	9.713×10 <sup>-3</sup>
14	GO:BP	GO:0000165	MAPK cascade	9.979×10 <sup>-3</sup>
15	GO:CC	GO:0071944	cell periphery	1.133×10 <sup>-22</sup>
16	GO:CC	GO:0098839	postsynaptic density membrane	8.431×10 <sup>-3</sup>
17	GO:CC	GO:0043235	receptor complex	8.783×10 <sup>-3</sup>

### B Downregulated mRNA transcripts

ID	Source	Term ID	Term Name	P <sub>adj</sub> (query_1)
1	GO:MF	GO:0030515	snoRNA binding	9.721×10 <sup>-8</sup>
2	GO:MF	GO:0140640	catalytic activity, acting on a nucleic acid	2.593×10 <sup>-7</sup>
3	GO:MF	GO:0043021	ribonucleoprotein complex binding	1.667×10 <sup>-6</sup>
4	GO:MF	GO:0005515	protein binding	2.692×10 <sup>-6</sup>
5	GO:MF	GO:0009982	pseudouridine synthase activity	1.562×10 <sup>-3</sup>
6	GO:MF	GO:0016462	pyrophosphatase activity	6.697×10 <sup>-3</sup>
7	GO:BP	GO:0042254	ribosome biogenesis	1.214×10 <sup>-22</sup>
8	GO:BP	GO:0034660	ncRNA metabolic process	3.382×10 <sup>-15</sup>
9	GO:BP	GO:0006259	DNA metabolic process	5.458×10 <sup>-13</sup>
10	GO:BP	GO:0009411	response to UV	2.628×10 <sup>-5</sup>
11	GO:CC	GO:0005654	nucleoplasm	1.759×10 <sup>-15</sup>
12	GO:CC	GO:0030684	preribosome	5.937×10 <sup>-12</sup>

Figure 2. 4 *Differential expression of mRNA transcripts in Tsc2 null NSCs*

A. Driver GO term analysis of 200 upregulated transcripts with the largest fold change, p adjusted value < 0.01, mRNA transcripts with less than 100 counts were excluded from the GO term analysis.

B. Driver GO term analysis of 200 downregulated transcripts with the smallest fold change, p adjusted value < 0.01, mRNA transcripts with less than 100 counts were excluded from the GO term analysis.

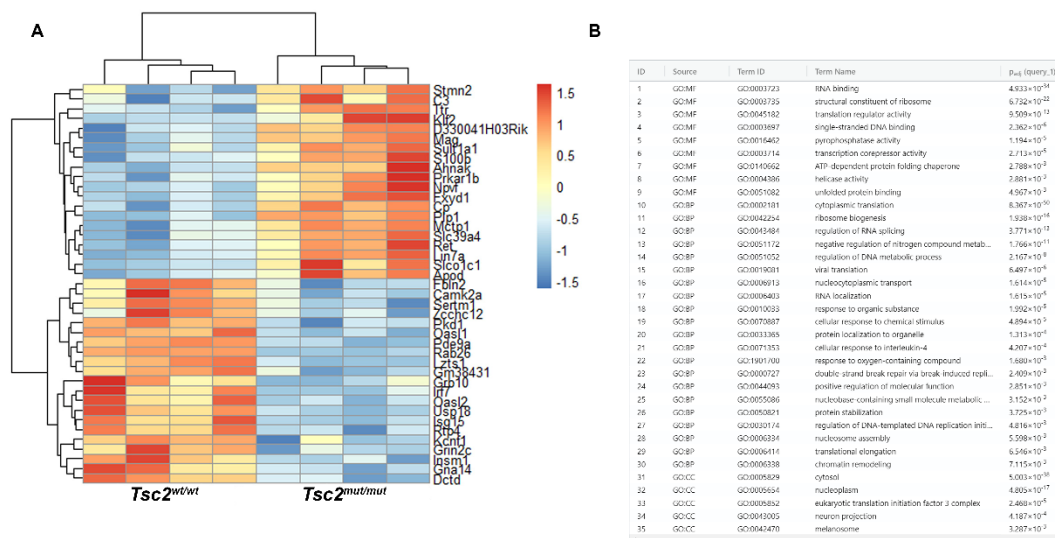


Figure 2.5 Polysomal analysis resulted in differentially enriched mRNA transcripts

A. Heatmap and hierarchical clustering of polysome associated mRNA transcripts from *Tsc2<sup>wt/wt</sup>* and *Tsc2<sup>mut/mut</sup>* NSCs. 628 transcripts were differentially enriched between *Tsc2<sup>wt/wt</sup>* and *Tsc2<sup>mut/mut</sup>* NSC polysomal isolations (p adjusted value<0.0001) B. Driver GO term analysis of 200 most abundant transcripts, p adjusted value < 0.01, mRNA transcripts with less than 100 counts were excluded from the GO term analysis.

**A** Upregulated polysome-associated mRNA transcripts

ID	Source	Term ID	Term Name	P <sub>adj</sub> (query_1)
1	GO:MF	GO:005515	protein binding	7.186×10 <sup>-13</sup>
2	GO:MF	GO:0043169	cation binding	8.306×10 <sup>-3</sup>
3	GO:BP	GO:0023051	regulation of signaling	3.006×10 <sup>-10</sup>
4	GO:BP	GO:0009056	catabolic process	2.993×10 <sup>-5</sup>
5	GO:BP	GO:0051246	regulation of protein metabolic process	2.914×10 <sup>-4</sup>
6	GO:BP	GO:0009636	response to toxic substance	4.751×10 <sup>-4</sup>
7	GO:BP	GO:0046688	response to copper ion	8.204×10 <sup>-3</sup>
8	GO:CC	GO:0030424	axon	2.954×10 <sup>-12</sup>
9	GO:CC	GO:0005576	extracellular region	3.013×10 <sup>-10</sup>
10	GO:CC	GO:0005764	lysosome	9.510×10 <sup>-3</sup>

**B** Downregulated polysome-associated mRNA transcripts

ID	Source	Term ID	Term Name	P <sub>adj</sub> (query_1)
1	GO:MF	GO:005488	binding	4.828×10 <sup>-10</sup>
2	GO:MF	GO:0016879	ligase activity, forming carbon-nitrogen bonds	8.236×10 <sup>-5</sup>
3	GO:MF	GO:003712	transcription coregulator activity	2.461×10 <sup>-5</sup>
4	GO:MF	GO:0016741	transferase activity, transferring one-carbon groups	4.820×10 <sup>-3</sup>
5	GO:BP	GO:0042254	ribosome biogenesis	2.370×10 <sup>-9</sup>
6	GO:BP	GO:1901362	organic cyclic compound biosynthetic process	1.951×10 <sup>-8</sup>
7	GO:BP	GO:0009987	cellular process	4.510×10 <sup>-7</sup>
8	GO:BP	GO:0006189	'de novo' IMP biosynthetic process	6.032×10 <sup>-5</sup>
9	GO:BP	GO:0044208	'de novo' AMP biosynthetic process	2.784×10 <sup>-4</sup>
10	GO:BP	GO:0097293	XMP biosynthetic process	2.784×10 <sup>-4</sup>
11	GO:BP	GO:0007275	multicellular organism development	3.819×10 <sup>-3</sup>
12	GO:BP	GO:0006177	GMP biosynthetic process	5.226×10 <sup>-3</sup>
13	GO:BP	GO:0051726	regulation of cell cycle	8.452×10 <sup>-3</sup>
14	GO:BP	GO:0048519	negative regulation of biological process	9.166×10 <sup>-3</sup>
15	GO:CC	GO:0005654	nucleoplasm	1.640×10 <sup>-10</sup>
16	GO:CC	GO:0030684	preribosome	1.875×10 <sup>-5</sup>
17	GO:CC	GO:0005732	sno(s)RNA-containing ribonucleoprotein complex	9.318×10 <sup>-4</sup>

Figure 2. 6 Differential expression of polysome-associated mRNA transcripts in Tsc2 null NSCs

A. Driver GO term analysis of 200 upregulated polysome-associated transcripts with the largest fold change, p adjusted value < 0.01, mRNA transcripts with less than 100 counts were excluded from the GO term analysis, B. Driver GO term analysis of 200 downregulated polysome associated transcripts with the smallest fold change, p adjusted value < 0.01, mRNA transcripts with less than 100 counts were excluded from the GO term analysis.

### *Actively translated mRNA transcripts are associated with translation*

*Tsc2* regulates mTORC1 signaling which in turn regulates many aspects of translation (Kwiatkowski et al., 2004). Therefore, when *Tsc2* is lost in NSCs, there are likely differences in translation that can affect neurogenesis and potentially contribute to TSC growth formation. In order to investigate the transcriptome of *Tsc2* null NSCs, actively translated mRNA transcripts were isolated from cultures via polysomal profiling. Polysomal profiling is a technique wherein cellular lysates are separated using sucrose density fractionation with the idea that mRNA transcripts that contain a higher number of polysomes will be denser than monosomal mRNA transcripts (Lou et al., 2014). In addition to total mRNA transcripts, polysomal mRNA was also isolated from primary NSC cultures in paired, matched samples. In the polysomal fraction, 628 transcripts were differentially expressed between the two conditions (p adjusted value < 0.0001), the majority of which were elevated in *Tsc2* null cells (Figure 2.5.A). Similar to bulk RNA sequencing, driver GO term analysis of the most abundant transcripts indicated an increase in terms related to the structural components of the ribosome, translation regulation, and ribosome biogenesis (Figure 2.5.B). In the polysomal fraction, some transcripts that were upregulated in the *Tsc2* mutant condition were associated with metabolic, catabolic, and cellular signaling (Figure 2.6.A). Whereas some transcripts that were downregulated in the mutant condition compared to wildtype were associated with ribosome biogenesis, biosynthetic processes, development, and the regulation of the cell cycle (Figure 2.6.B). GO terms associated with translation and ribosomal proteins were consistently downregulated in the mutant condition, however the specific transcripts

differed between the transcriptomic and translatomic analyses, indicating independent regulation by *Tsc2* and potential compensatory mechanisms regulating these processes. (Figure 2.7). Taken together, these analyses underscore the vital role that *Tsc2* plays in regulating translation and protein expression.

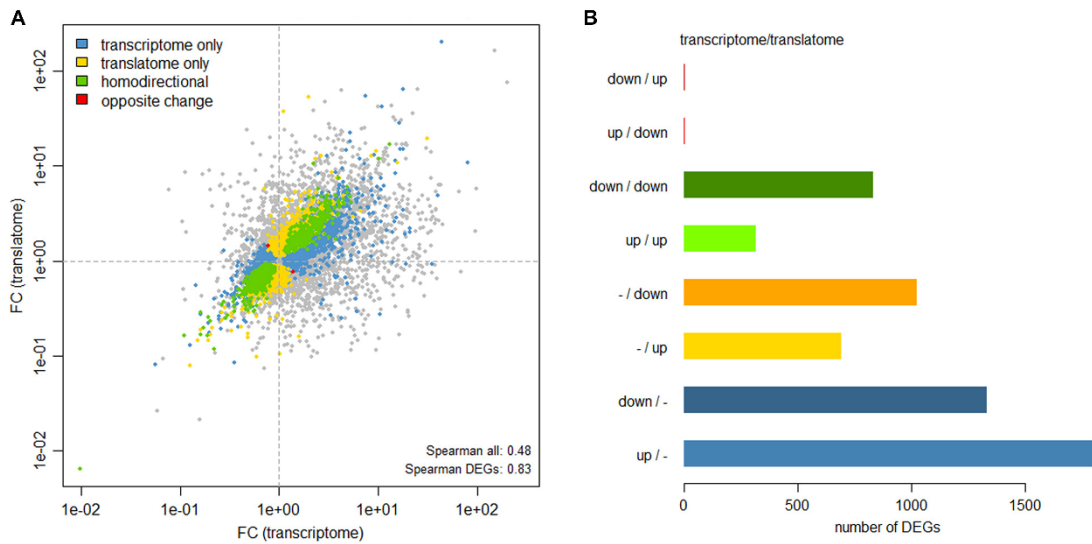


Figure 2.7 *Translational efficiency was altered between mutant and control conditions*

A. Scatterplot of mRNA transcript availability compared to translatoome abundance. Each diamond represents an mRNA transcript plotted on the x axis which represents the total mRNA abundance (transcriptome) and the y axis represents the polyribosome abundance (translatome). A gray diamond indicates there is no change between  $Tsc2^{wt/wt}$  and  $Tsc2^{mut/mut}$ . A blue diamond indicates changes to the total mRNA abundance only without translational changes. A yellow diamond indicates changes only to the translatoome. A green diamond denotes changes for both transcriptome and translatoome that occur in the same direction (i.e., more total mRNA correlates with more polyribosome mRNA = homodirectional). A red diamond reflects changes in the opposite direction (more total abundance but less polyribosome abundance) (Riley et al., 2023), B. Histogram of transcript and translatoome abundance and changes. FC=Fold change between  $Tsc2^{wt/wt}$  and  $Tsc2^{mut/mut}$ , DEG=Differentially expressed genes.



### *Polysomal analysis resulted in differentially enriched transcripts*

In order to ascertain if the trends seen in the translome were a direct consequence of the changes in the transcriptome, translational efficiency was measured. Translational efficiency is the measure of how likely and/or quickly a transcript is translated and is found by taking the ratio of the polysomal fraction (translatome) over the total mRNA (transcriptome) (Chassé et al., 2017). The translational efficiency was calculated for each transcript in the wildtype and mutant condition and then compared between conditions (Figure 2.7.A). It was found that some transcripts in the transcriptome correlated to the levels present in the translome (Figure 2.7.A, B). However, not all transcripts followed this trend, indicating that *Tsc2* variably regulates translation in NSCs (Figure 2.7.A, B).

A GO term analysis was performed on the top transcripts with altered transcript efficiency between mutant and wildtype conditions. It was found to be enriched in terms associated with mRNA translation and metabolism (Figure 2.8.A). Similarly, those transcripts with the highest translational efficiency, which are those that were enriched in the polysomal fraction and being more readily translated, had terms that were associated with telencephalon development, differentiation, morphogenesis, and central nervous system development (Figure 2.8.B). These GO term analyses underscore the important role that *Tsc2* plays in regulating translation and the role it plays in NSC and brain development.

**A Top differentially translated**

GO Biological Processes	Fold Enrichment	FDR
translation	1.56	7.64E-09
peptide biosynthetic process	1.66	1.02E-08
cytoplasmic translation	0.48	2.48E-08
peptide metabolic process	2.02	9.94E-08
amide biosynthetic process	2.12	1.63E-07
translation at synapse	0.21	2.14E-07
translation at postsynapse	0.21	2.50E-07
cellular biosynthetic process	8.33	3.02E-06
organonitrogen compound biosynthetic process	5.32	3.98E-06
amide metabolic process	3.16	4.29E-06
translation at presynapse	0.2	4.33E-06
cellular nitrogen compound biosynthetic process	6.08	6.56E-06
cellular metabolic process	23.39	6.84E-06
positive regulation of nitrogen... metabolic process	13.11	2.07E-05
cellular process	63.79	2.19E-05
metabolic process	34.31	3.36E-05
positive regulation of metabolic process	16.36	5.25E-05
organic substance biosynthetic process	9.94	6.76E-05
positive regulation of cellular process	24.34	6.84E-05
biosynthetic process	10.22	1.10E-04
organic substance metabolic process	32.71	1.19E-04
organonitrogen compound metabolic process	19.99	1.23E-04
primary metabolic process	29.61	1.94E-04
positive regulation of biological process	27.31	3.31E-04
positive regulation of macromolecule metabolic process	14.91	3.35E-04
cellular nitrogen compound metabolic process	13.08	4.36E-04
positive regulation of cellular metabolic process	12.61	6.16E-04

**B Increased translational efficiency**

GO Biological Processes	Fold Enrichment	FDR
mesodermal cell differentiation	32.07	4.42E-02
mesoderm morphogenesis	15.81	9.00E-03
telencephalon development	7.51	2.40E-03
forebrain development	4.92	3.38E-02
brain development	4.87	7.97E-04
head development	4.48	1.16E-03
positive regulation of transcription by RNA polymerase II	4.1	5.31E-05
central nervous system development	4.09	1.13E-03
tissue morphogenesis	3.85	4.47E-02
tube morphogenesis	3.57	4.49E-02
regulation of anatomical structure morphogenesis	3.55	9.29E-03
positive regulation of DNA-templated transcription	3.5	1.09E-04
positive regulation of nucleic acid-templated transcription	3.5	1.46E-04
positive regulation of RNA biosynthetic process	3.49	9.53E-05
tube development	3.41	1.36E-02
positive regulation of RNA metabolic process	3.34	8.10E-05
negative regulation of DNA-templated transcription	3.34	2.36E-03
negative regulation of nucleic acid-templated transcription	3.33	2.35E-03
negative regulation of RNA biosynthetic process	3.31	2.47E-03
epithelium development	3.19	9.18E-03
anatomical structure formation involved in morphogenesis	3.14	4.39E-02
negative regulation of transcription by RNA polymerase II	3.12	4.39E-02
positive regulation of macromolecule biosynthetic process	3.09	6.00E-04
negative regulation of RNA metabolic process	3.05	6.22E-03
positive regulation of nucleobase...metabolic process	2.99	5.40E-04
tissue development	2.96	1.08E-03
regulation of transcription by RNA polymerase II	2.96	9.09E-05

Figure 2.9 *Differentially translated transcripts were associated with translation and nervous system development*

A. GO term analysis of most abundant mRNAs with altered translation efficiency, B. GO term analysis of mRNAs having the most highly increased translational efficiency.

## Discussion

SEGAs are believed to form due to LOH of the TSC genes in NSCs of the V-SVZ (Bongaarts et al., 2017; Kwiatkowski et al., 2004). *Tsc2* is most well-known for its regulation of the mTORC1 signaling pathway which plays a significant role in regulating aspects of translation, including 5' cap-dependent translation and the generation of ribosomal proteins (A. C. Gingras et al., 2001; Jefferies et al., 1994, 1997b; Ma & Blenis, 2009; Richter & Sonenberg, 2005; Tee & Blenis, 2005; Thoreen et al., 2012). Additionally, mTORC1 signaling has been shown to play a role in NSC development and maintenance (Baser et al., 2017, 2019; Blair et al., 2017, 2018). When NSCs are activated and begin to differentiate, there is a sharp decrease in mTORC1 signaling that is likely regulated by the TSC genes (Baser et al., 2019). In TSC, the decrease in mTORC1 activity does not happen due to a lack of TSC gene expression and hyperactivation of mTORC1 signaling. This could possibly lead to abnormal differentiation and neurogenesis (Baser et al., 2019; Blair et al., 2018).

Given that mTORC1 signaling plays a crucial role in translation and in NSC development, the translome of NSCs was examined to provide mechanistic insight into SEGA formation. It was found that *Tsc2* regulated the translome independently of the transcriptome for some mRNA transcripts but not all transcripts (Figure 2.7). Given that there are variable changes in how *Tsc2* regulates mRNA transcripts, it was hypothesized that loss of *Tsc2* resulted in stochastic translation wherein mRNA transcripts are potentially translated at different times in the wrong quantities during development. Given that translation and protein production are crucial mechanisms regulating NSC

differentiation and development, it was postulated that stochastic translation in NSCs resulted in the retention of stem cell-like transcripts in some cells. These cells would maintain aspects of stemness rather than downregulating them upon differentiation. A similar phenomenon has previously been suggested in a SEN/SEGA organoid model wherein cells lacking *Tsc1* and *Pten* retained an NSC-specific neurofilament protein despite being prodded to differentiate and despite a concurrent reduction of the same protein in wildtype neurospheres (Zordan et al., 2018). Retention of stem cell transcripts throughout maturation would likely result in mature cells that retained aspects of immaturity including but not limited to stemness. Perhaps giving further credence to this hypothesis, TSC SEGAs and cortical tubers often contain both mature and immature cells as well as cells with both neuronal and glial expression markers (Adriaensen et al., 2009; Ahluwalia & Chandrasoma, 1993; Bongaarts et al., 2017; Eichmüller et al., 2022; Giannikou et al., 2021; A. C. Jansen et al., 2019; Kwiatkowski et al., 2004; Morimoto & Mogami, 1986; Raju et al., 2007; Shepherd et al., 1991). This could be indicative of cells that are retaining improper mRNA transcripts that could potentially contribute to SEN/SEGA formation.

In this same vein, when the topmost differentially enriched transcripts were probed for GO terms, it was found that the transcripts with the highest translational efficiency were associated with cellular differentiation, morphogenesis, and nervous system development, indicating that the genes involved with NSC development are the most aberrant in the *Tsc2* null condition (Figure 2.9). This underscores the fact that *Tsc2*

and its regulation of translation are crucial for the development of postnatal NSCs and the brain.

While neither neurogenesis nor differentiation were directly studied in this study, it has been shown previously that inactivation of the TSC genes and upregulation of the mTORC1 pathway have influence on these processes in models of TSC (Blair et al., 2017, 2018; Magri et al., 2011; Onda et al., 2002; Way et al., 2009). In order to verify that NSC-associated transcripts are being retained in NSCs throughout differentiation and maturation, further studies should be done to differentiate these cells and examine their transcriptional and translational milieu. Further, the *Tsc2* null NSCs should be examined *in vivo* and their ability to contribute to SEGA formation should also be assessed.

Taken altogether, the findings presented in this chapter point to the important regulatory role that *Tsc2* plays in the regulation of translation in postnatal NSCs and potential mechanisms that could contribute to SEGA formation.

## Methods

Animals. Clemson University Institutional Animal Care and Use Committee approved experiments, and all guidelines set forth by the Clemson University Institutional Animal Care and Use Committee and were compliant with the Animal Care and Use Review Office (ACURO), a component of the USAMRDC Office of Research Protections (ORP) within the Department of Defense (DoD). Red fluorescent protein (RFP<sup>+/-</sup>, <sup>+/+</sup>) (B6. CgGt (ROSA)26Sortm9 (CAG-tdTomato)<sup>Hze/J</sup> (Strain #007909), C57BL/6-Tg (Nes-Cre/ERT2)<sup>K<sup>Eisc</sup>/J</sup> (Strain #:016261), *Tsc2*<sup>tm1.1Mjg/J</sup> (Strain #027458) were acquired from Jackson Laboratories. Mice were housed under pathogen-free conditions with a 12-h light/dark cycle and fed ad libitum.

PCR. The tissue was incubated in 50 mM NaOH and 0.2 mM EDTA at 50°C overnight. An equal volume of 100 mM Tris-HCl was added to samples. Samples were subject to routine genotyping using Taq DNA Polymerase with the following conditions: Initial denaturation step at 98°C for 2 min, followed by 35 cycles of denaturation at 95°C for 30 s, an annealing step at 60°C for 30 s, and an extension at 72°C for 30 seconds followed by a final extension at 72°C for 3 min. Samples were loaded onto a 1.7% agarose gel with 1X Blue Juice and run at 100 V for 20– 30 mins. Mice having conditional *Tsc2* alleles are distinguished by endpoint genotyping PCR using the following primer sequences, 5'-ACAATGGGAGGCACATTACC-3' and 5-AAGCAGCAGGTCTGCAGTG-3'. Tomato (RFP) genes were identified for Stock #7914 using the following primer sequences, 5'-

AAGGGAGCTGCAGTGGAG TA-3' and 5'-CCGAAAATCTGTGGGAAG TC-3' and 5'-GGCATTAAAGCAGCGTATCC-3' and 5'CTGTTCTGTACGGCATGG-3'. *Nestin-CRE-ER<sup>T2</sup>* mice were genotyped with 5'ATGCAGGCAAATTTTGGTGT-3' and 5'-CGCCGCTACTTCTTTTCAAC-3' or 5'ATACCGGAGATCATGCAAGC-3' and 5'-GGCCAGGCTGTTCTTCTTAG-3' and 5' CTAGGCCACAGAATTGAAAGATCT-3' (Internal Positive Control) and 5' GTAGGTGGAAATTCTAGCATCATCC-3' (Internal Positive Control). Long-range PCR was performed as previously described.

Primary NSC Culture and Tamoxifen injection. *Nestin-CRE-ER<sup>T2</sup>* mouse pups were weighed and injected with approximately 20 µg/g (Z)-4-Hydroxytamoxifen (Sigma Aldrich, #H7904) and 2.2 µg/g EdU (Invitrogen, #C10337) at P2/3. At P11, brains were bisected into two sagittal hemispheres. The V-SVZ was micro-dissected in ice cold Neurobasal A (Gibco, #10888022) medium. Dr. David Feliciano performed the V-SVZ microdissections. 100 µl 0.25% Trypsin (Gibco, # 25200072) was added to brain tissue and incubated for 3 min at 37°C before the tissue was dissociated using three Pasteur pipettes having progressively decreasing bore sizes. 100 µl defined trypsin inhibitor (Gibco, # R007100) containing 0.01 mg/ml DNase1 was added, and the solution was centrifuged at 300 x g in an Eppendorf 5425 centrifuge. The pellet was resuspended in complete growth media (Neurobasal A (Gibco, #10888022), 0.02% Mouse FGF-basic Recombinant protein (Invitrogen, #RP-8626), 0.02% Recombinant Mouse EGF (Gibco, #PMG8044), 0.5% Pen Strep (Gibco, #15140122), 0.008% 25 mg/ml Heparin sodium salt (Sigma Aldrich, #H3393), 1% Glutamax (Gibco, #35050-061), 2% B-27 Supplement

without vitamin A (Gibco, #12587) before plating in a 100 mm dish coated with natural mouse Laminin (Gibco, 23017) and poly-D-lysine (Gibco, #A38904-01). Upon reaching confluency, cells were passaged by incubating in 5 mL Accutase (Invitrogen, #00-4555-56) for 5 minutes at 37°C. The cells were then spun down for 5 minutes at 300 x g in an Eppendorf 5425 centrifuge and replated at an appropriate density.

Polyribosome Profiling. Polyribosome profiling was performed similar to as previously described. Primary NSC cultures were passed once prior to isolation. 100 mg/ml (66.6 $\mu$ L) cycloheximide (CHX, VWR, #94271) was added to each dish and incubated at 37°C for 15 minutes. The cells were dissociated in 500  $\mu$ L lysis buffer (0.25 M sucrose, 50 mM Tris/HCl (pH7.5, Sigma Aldrich, #93363), 5 mM MgCl<sub>2</sub> (Sigma Aldrich, #M1028), 25 mM KCl (Sigma Aldrich, #P9333), 200  $\mu$ g/ml CHX (VWR, #94271), 1X HALT protease inhibitor (Thermo Scientific, #87785), 1 mM dithiothreitol (DTT, Enzo, #ALX-280-001-G005), 100 U/ml recombinant RNasin ribonuclease inhibitor (Promega, #N2511), scraped into a 1.5 mL microcentrifuge tube, and incubated for 15 minutes on ice. Lysates were homogenized five times with a Dounce homogenizer. 50  $\mu$ L was removed and 150  $\mu$ L TRIzol LS reagent (Ambion, #10296010) was added for RNA Total isolation. The remaining lysates were centrifuged for 10 minutes at 500 x g at 4°C. 10% sodium deoxycholate and 10% NP-40 was added, and the samples were incubated on ice for thirty minutes. Prepared lysates were loaded onto 10 mL continuous sucrose gradients that consisted of 17.5-50% sucrose (as well as 30 mM Tris-HCl (pH7.5, Sigma Aldrich, #93363), 30 mM MgCl<sub>2</sub> (Sigma Aldrich, #M1028), 600 mM NaCl (Fisher Scientific,

#BP358-10), 200  $\mu\text{g/ml}$  CHX (VWR, #94271), 2 mM DTT (Enzo, #ALX-280-001-G005), and UltraPure DEPC treated  $\text{H}_2\text{O}$  (Invitrogen, #750023). The gradients were balanced using lysis buffer and were centrifuged for 1.5 hours at 280,000 x g in a SW-41 Ti swinging bucket rotor with the acceleration speed set to max and the deceleration speed set to coast. Seven 1080  $\mu\text{L}$  fractions were then removed from the top of the sucrose gradients leaving 3 mL of the heaviest sucrose fractions. TRIzol LS reagent (9 mL) (Ambion, #10296010) was added and stored at  $-80^\circ\text{C}$  overnight. The solutions were then split into two equal parts and 1.2 mL of chloroform (Sigma Aldrich, #372978) was added to each tube. The tubes were incubated for three minutes before centrifugation at 12,000 x g for 15 minutes at  $4^\circ\text{C}$ . The aqueous layer was then removed and 3 mL isopropanol (Fisher Chemical, #A416-1) and 1  $\mu\text{L}$  GlycoBlue co-precipitant (Invitrogen, #AM9516) was added. The tubes were then moved to the  $-80^\circ\text{C}$  freezer to precipitate overnight. Samples were then centrifuged for ten minutes at 12,000 x g at  $4^\circ\text{C}$  and the supernatants discarded. Pellets were resuspended in 6 mL 75% EtOH (Sigma Aldrich, #E7023) and vortexed before centrifugation for five minutes at 7,500 x g at  $4^\circ\text{C}$ . The supernatants were discarded, and the pellets allowed to air dry for 8 minutes before resuspension in 50  $\mu\text{L}$  UltraPure Distilled water (Invitrogen, #10977-015). The samples were incubated for 15 minutes at  $57^\circ\text{C}$  in a water bath before being recombined into one polysomal RNA fraction each. Chloroform (Sigma Aldrich, #372978) was added to each cell lysate that was collected during polysomal profiling as a total RNA fraction. The tubes were incubated for three minutes before centrifugation at 12,000 x g for 15 minutes at  $4^\circ\text{C}$ . The aqueous layer was then removed and 100  $\mu\text{L}$  isopropanol (Fisher Chemical,

#A416-1) and 1  $\mu$ L GlycoBlue co-precipitant (Invitrogen, #AM9516) was added. The tubes were then moved to the  $-80^{\circ}\text{C}$  freezer to precipitate overnight. Samples were centrifuged for ten minutes at  $12,000 \times g$  at  $4^{\circ}\text{C}$  and the supernatants discarded. Pellets were resuspended in 200  $\mu$ L 75% EtOH (Sigma Aldrich, #E7023) and vortexed before centrifugation for five minutes at  $7,500 \times g$  at  $4^{\circ}\text{C}$ . The supernatants were discarded, and the pellets allowed to air dry for 8 minutes before resuspension in 50  $\mu$ L UltraPure Distilled water (Invitrogen, #10977-015). The samples were incubated for 15 minutes at  $57^{\circ}\text{C}$  in a water bath before library prep.

RNA Sequencing and Bioinformatics. Library preparation and RNA quality assessment was undertaken by Kaitlyn Williams of the Clemson University Genomics and Bioinformatics Facility. Libraries were constructed using the NEBNext<sup>®</sup> Ultra<sup>™</sup> II RNA Library Prep Kit for Illumina<sup>®</sup> (New England Biolabs Inc., #E7770S) and the NEBNext<sup>®</sup> Poly (A) mRNA Magnetic Isolation Module (New England Biolabs Inc., #E7490S). These libraries were dual indexed using the NEBNext<sup>®</sup> Multiplex Oligos for Illumina<sup>®</sup> (Dual Index Primers Set 1) (New England Biolabs Inc., #E7600S). The libraries were quantified and qualified using Qubit (Thermo-Fischer, #Q32852) and Tape Station (Agilent, # 5067-5579). Pooled libraries were sequenced using 150 bp paired end reads on a NovaSeq 6000 SP v1.5 (300 cycles) flow cell (Illumina, #20028400). Reads were trimmed for adapter sequences using FastQ Toolkit (v. 2.2.5) and aligned to UCSC mm10 using RNA-SEQ Alignment (STAR, v. 2.6.1A) on BaseSpace (Illumina). Aligned sequences were further analyzed on BaseSpace (Illumina) using RNA-SEQ Differential

Expression (v. 1.0.1 which utilizes DESEQ2)<sup>98</sup>. Differentially enriched mRNAs were plotted by Pheatmap (R studios, R package version 1.0.12. <https://CRAN.R-project.org/package=pheatmap>)<sup>99</sup>. mRNA transcripts with less than 100 counts were excluded from the analysis and the top 200 transcripts were used for GO term analysis. Gene ontology analysis was performed using gProfiler with a set significance threshold of 0.01 (Raudvere et al., 2019). The topmost abundant transcripts were those with the highest mean expression values. The topmost differentially expressed transcripts were those with the highest fold change between conditions, regardless of direction of change. Pathways were assessed using CytoScape (version 3.10) and Wikipathways.

## CHAPTER THREE

### *Tsc2* inactivation generates hamartomas

A version of this data is published in iScience:

Riley, V.A., Shankar, V., Holmberg, J.C., Sokolov, A.M., Neckles, V.N., Williams, K., Lyman, R., Mackay, T.F.C., and Feliciano, D.M. (2023). *Tsc2* coordinates neuroprogenitor differentiation. *iScience*. 10.1016/j.isci.2023.108442.

All experiments and data analysis in Chapter III were performed by Victoria Riley. Genotyping PCRs were performed by Victoria Riley, Sulagna Mukherjee, Melanie Garcia, Victoria Neckles, and Anthony Minerva.

## **Abstract**

TSC is caused by inactivating mutations in either the TSC1 or TSC2 gene. This results in the upregulation of mTORC1 signaling which is involved in the regulation of translation, neural stem cell (NSC) differentiation, and other aspects of development. Similarly, subependymal giant cell astrocytoma (SEGA), a large growth that can form in the TSC brain, is caused by loss of heterozygosity of either of these genes in NSCs. Given this, studying *Tsc2* loss in NSCs is important in order to gain insight into SEGA formation and etiology. Therefore, the consequences of *Tsc2* loss in murine NSCs were investigated and a model of TSC hamartomas generated in order to investigate possible mechanisms of SEGA formation. One possible mechanism of SEGA formation was that mutant NSCs were contributing to lesion formation through aberrant neurogenesis. To study this, *Tsc2* was inactivated in postnatal ventricular-subventricular zone (V-SVZ) NSCs by electroporation which resulted in multiple hamartomas within the striatum. Striatal hamartomas had a heterogeneous glial-neuronal phenotype, contained immature markers, and formed only in mutant conditions. This indicated that striatal hamartomas were reminiscent of TSC SEGA. In addition, heterotopic neurons were found within the striatum of mutant mice. Neurons were cytomegalic with increased dendritic complexity. The generation of both growths and heterotopic neurons indicated potential aberrations in striatal neurogenesis. Alternatively, the loss of *Tsc2* could also have resulted in abnormalities in other developmental processes, such as gliogenesis or cellular migration, which subsequently affect the cellular composition and distribution of the striatum. Given this, future studies must be undertaken to identify the precise role that *Tsc2* plays in these

processes and their secondary effects. Taken all together, these studies implicate *Tsc2* in the regulation of stem cell differentiation, striatal development, and TSC hamartoma formation.

## **Introduction**

SEGAs are catastrophic hamartomas that form in various brain regions, including the striatum, but are most commonly found near the lateral ventricles of the brain in the Foramen of Monro (Adriaensen et al., 2009; Kingswood et al., 2017; Yeung et al., 1997). Histologically, SEGAs are characterized by a glial-fibrillary matrix, glial and neuronal cells, immature cells, multinucleated giant cells, microglia, and other immune cells as well as a low mitotic index (Bongaarts et al., 2017; Kim et al., 2001; Martin et al., 2017). Despite their low mitotic index, SEGAs can grow in the brain, eventually causing obstruction, cerebral spinal fluid buildup, hydrocephalus, and death without surgical or pharmacological intervention (Feliciano, 2020; Franz et al., 2006). SEGAs and their development have been previously modelled in mice as described in Chapter one and two.

Given results in mouse models, multipotent neural stem cells (NSCs) are considered to be the cell of origin for TSC hamartomas (Feliciano et al., 2011; Fu et al., 2012; Magri et al., 2011; Rushing et al., 2019; Zhou et al., 2011; Zordan et al., 2018). TSC2 mutations in NSCs are believed to cause the majority of SEGAs through biallelic inactivation via loss of heterozygosity (LOH), wherein a patient will have a mutation in one allele of a gene, and it is only when the second allele becomes inactivated, that hamartoma growth takes place (Crino et al., 2010; Green et al., 1994; Henske et al., 1996; S. Jozwiak et al., 2004; Knudson, 1971; Kwiatkowski et al., 2004; Niida et al., 2001; Sepp et al., 1996). LOH is one of the driving factors behind TSC growth formation and is found in other TSC hamartoma types besides SEGAs (Au et al., 1999; Bongaarts et al.,

2017; Giannikou et al., 2016; Green et al., 1994; Henske et al., 1996; Martin et al., 2017; Niida et al., 2001). For example, renal angiomyolipoma, cortical tubers, and cardiac rhabdomyomas have all shown LOH upon mutational analysis (Au et al., 1999; Crino et al., 2010; Henske et al., 1996; Martin et al., 2017). LOH has been shown to only affect hamartomatous tissue whereas surrounding tissue has one functional allele. Cells that have one functioning copy of a TSC allele appear to have relatively normal cell physiology and don't appear to majorly contribute to TSC pathology (Riley et al., 2022; S. F. Tavazoie et al., 2005; H. Zhang et al., 2003). That being said, LOH is important for SEGA formation. However, the timing and mechanism of LOH as well as the cell of origin of SEGA are still being debated.

In order to examine these issues, multiple animal models of SEGA and TSC currently exist (Rushing et al., 2019; Zhou et al., 2011; Zordan et al., 2018). These models typically inactivate either of the TSC genes in the NSCs of the ventricular-subventricular zone (V-SVZ) in order to generate growths within the lateral ventricle, indicating that a NSC is likely the cell of origin for SEGA. In order to investigate hamartoma formation and SEGA-genesis, a model of TSC hamartomas has been generated. This model is different from other models of SEGA because it is generated following focal *Tsc2* inactivation in a subset of cells lining the entire lateral ventricle at an early time point in development. This mimics the somatic mosaicism commonly found in TSC and typical SEGA development which occurs following LOH in an NSC.

In this chapter, *Tsc2* was biallelically inactivated in NSCs to mimic LOH and generate hamartomas. It was previously discovered that *Tsc2* inactivation resulted in

abnormal transcription and translation (Chapter two) where *Tsc2* null NSCs appeared to express aberrant mRNA transcripts and produce abnormal proteins, such as those related to stemness. It was hypothesized that this phenomenon might influence NSC differentiation, neurogenesis, and contribute to hamartoma formation. In order to investigate the cellular phenotypes and hamartomas that accompany *Tsc2* loss, *Tsc2* null NSCs and their progeny were examined *in vivo* in the V-SVZ and striatum. It was hypothesized that hamartomas would retain some aspects of stemness which could contribute to lesion formation.

## Results

### *Postnatal electroporation of the V-SVZ resulted in *Tsc2* inactivation in NSCs*

Mice were obtained with alleles containing LoxP sites around exons 2 and 4 of the *Tsc2* allele, henceforth called conditional *Tsc2* alleles. Subsequent introduction of CRE recombinase resulted in the inactivation of *Tsc2*. As exons 2 through 4 contain the sequence that encodes the binding sequence of *Tsc2* to *Tsc1*, exon excision results in failure of the encoded GTPase activating protein to form and function as described previously (Hernandez et al., 2007; Riley et al., 2022). These mice were bred to mice with a Tomato reporter gene (RFP) which produced red fluorescence upon recombination via CRE (Figure 3.1.A). CRE was introduced to the NSCs of the lateral ventricle via postnatal electroporation. Electroporation is a technique that involves the intraventricular injection of plasmid DNA into the lateral ventricle. The DNA is integrated into NSCs lining the ventricle upon the permeabilization of cellular membranes following the application of electrical current (Figure 3.1.B). Following electroporation, the plasmid DNA will be diluted each time the cell divides.

Recombination was confirmed via long range PCR specific for recombined and non-recombined versions of the *Tsc2* allele (Figure 3.1.D). Both mutant and non-recombined alleles are present due to the focal nature of electroporation. Genotypes were also verified for all mice via PCR specific for the wildtype and conditional *Tsc2* allele (Figure 3.1.D).

Electroporation of CRE and green fluorescent protein (GFP) plasmids into neonatal P1 mice having wildtype, heterozygous, or conditional *Tsc2* alleles was

performed to mimic somatic *Tsc2* monoallelic and biallelic inactivation and to generate a model of TSC. Mice were subsequently euthanized at P30 and P60 (Figure 3.1.C). Electroporation of CRE and GFP resulted in the deletion of *Tsc2* from a small amount of NSCs that line the lateral ventricle as well as their progeny. The cells that would have undergone electroporation first would retain the GFP plasmid DNA whereas later born cells would only express the genetic CRE-recombined RFP protein. This allows original electroporated cells to be differentiated from their later-born progeny.

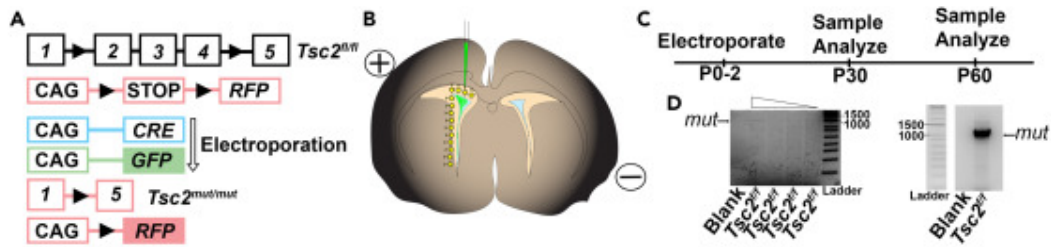


Figure 3.1 *Postnatal electroporation of the V-SVZ resulted in Tsc2 inactivation in NSCs*  
 A. Schematic diagram of conditional *Tsc2* and inducible *RFP* genes. *Tsc2* is mutated and *RFP* is expressed when *CRE* recombinase is present, B. Schematic diagram of *CAG-CRE* and *CAG-GFP* (Green) plasmid electroporation which induces genomic *CAG-RFP* leading to co-expression (yellow), C. Timeline of electroporation and analysis, D. Long-range PCR of *Tsc2* wildtype and mutant alleles following electroporation of *CRE*-recombinase with varying starting amounts and low exposure to confirm precise size (left, approximately 1090 base pairs) and high exposure demonstrating efficient recombination (right).

*mTORC1 activity was increased in the mutant SVZ and striatum following Tsc2 inactivation*

Loss of *Tsc2* upregulates the mTORC1 signaling pathway (Kwiatkowski et al., 2004). Hyperactivation of mTORC1 signaling following electroporation was confirmed by quantifying p4EBP expression, a substrate of mTORC1. Mutant mice had increased p4EBP expression in the V-SVZ when compared to *Tsc2<sup>wt/wt</sup>* mice (Figure 3.2.A-D, *Tsc2<sup>wt/wt</sup>*, N = 6, n = 49, mean =  $1.00 \pm 0.057$  SEM vs. *Tsc2<sup>mut/mut</sup>*, N = 8, n = 53, mean =  $1.51 \pm 0.081$  SEM, \*\*\*\* =  $p < 0.0001$ ). Adjacent to the V-SVZ, the mutant striatum had elevated levels of p4EBP expression when compared to the *Tsc2<sup>wt/wt</sup>* striatum (Figure 3.2.E-F, *Tsc2<sup>wt/wt</sup>*, N = 6, n = 29, mean =  $1.00 \pm 0.06$  SEM vs. *Tsc2<sup>mut/mut</sup>*, N = 8, n = 79, mean =  $1.898 \pm 0.013$  SEM, \*\*\*\* =  $p < 0.0001$ ). This confirms that mTORC1 signaling is upregulated due to the inactivation of the *Tsc2* gene.

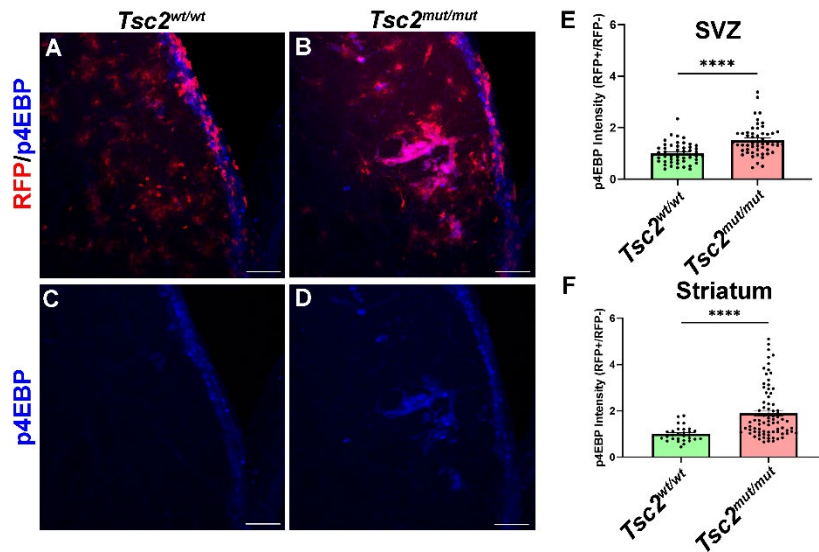


Figure 3.2 *mTORC1* activity was increased in the mutant SVZ and striatum following *Tsc2* inactivation

A, B. p4EBP and RFP expression in *Tsc2*<sup>wt/wt</sup> and *Tsc2*<sup>mut/mut</sup>. C, D. p4EBP expression in *Tsc2*<sup>wt/wt</sup> and *Tsc2*<sup>mut/mut</sup>. E. Quantification of p4EBP expression in the SVZ at P30. *Tsc2*<sup>wt/wt</sup>, N = 6, n = 49, mean =  $1.00 \pm 0.057$  SEM vs. *Tsc2*<sup>mut/mut</sup>, N = 8, n = 53, mean =  $1.51 \pm 0.081$  SEM. F. Quantification of p4EBP expression in the striatum at P30. *Tsc2*<sup>wt/wt</sup>, N = 6, n = 29, mean =  $1.00 \pm 0.06$  SEM vs. *Tsc2*<sup>mut/mut</sup>, N = 8, n = 79, mean =  $1.898 \pm 0.013$  SEM: \*\*\*\* =  $p < 0.0001$ . Data are represented as mean  $\pm$  SEM. Scale bar = 75  $\mu$ m.

*Tsc2* inactivation resulted in differences in striatal morphology

In addition to hyperactive mTORC1 signaling, striatal cytoarchitecture was also atypical following *Tsc2* inactivation. Striatal cytoarchitecture differed in mutant mice in ways reminiscent of TSC including cytomegalic cells, misplaced neurons (Figure 3.3), and striatal hamartomas (Figure 3.4.A-H).

Striatal hamartomas were identified as groups of at least eight overlapping cells in the striatum (Figure 3.5). Striatal hamartomas could be categorized by their anatomical appearance wherein type 1 lesions were elongated, compact, and linear and type 2 lesions were more diffuse and round similar to those seen in middle artery occlusion models of ischemia (Figure 3.5.D) (Yamashita et al., 2006). Due to this difference, lesions were grouped based on circularity (*Type I*, N = 8, n = 13, mean =  $0.368 \pm 0.027$  SEM vs. *Type II*, N = 16, n = 92, mean  $0.1022 \pm 0.005$  SEM,  $p < 0.0001$ , Figure 3.5.E). It was found on average that type 1 lesions were larger than type 2 lesions at P30 (*Type I*, N = 8, n = 13, mean  $1,764 \mu\text{m} = 216.8 \pm \text{SEM}$  vs. *Type II*, N = 16, n = 92, mean =  $5,273 \mu\text{m} \pm 333.7$  SEM,  $p = 0.0002$ , Figure 3.5.F). Both types of lesions were found at both P30 and P60, indicating their stability and/or longevity within the brain (Figure 3.6).

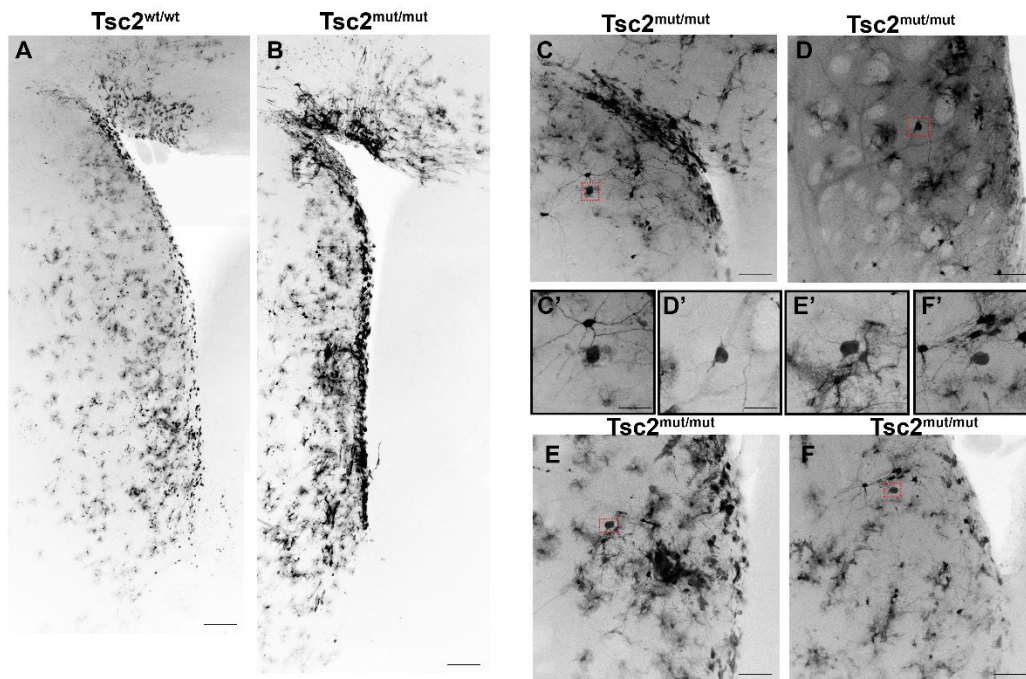


Figure 3.3 *Tsc2* loss resulted in the formation of abnormalities similar to human TSC

A. 10X composite of  $Tsc2^{wt/wt}$  V-SVZ and striatum, B. 10X composite of  $Tsc2^{mut/mut}$  V-SVZ and striatum, C-F. Examples of giant cells (red boxes) in the  $Tsc2^{mut/mut}$  striatum with digital zoom (C'-F'), Scale bar = 75  $\mu\text{m}$  (20X), 150  $\mu\text{m}$  (10X), 300  $\mu\text{m}$  (5X), 18.75  $\mu\text{m}$  (digital zoom)

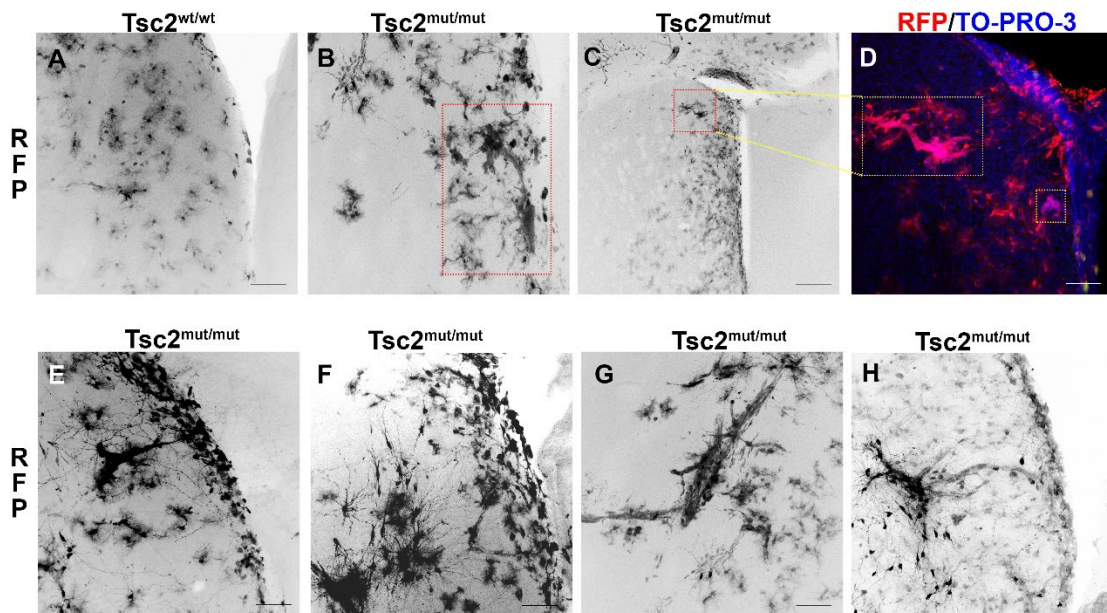


Figure 3.4 *Tsc2* inactivation resulted in striatal hamartomas

A. 20X image of a *Tsc2*<sup>wt/wt</sup> V-SVZ and striatum demonstrating lack of striatal hamartomas, B. 20X image of a *Tsc2*<sup>mut/mut</sup> V-SVZ and striatum with striatal hamartomas (red box), C. 5X image of *Tsc2*<sup>mut/mut</sup> V-SVZ and striatum with hamartoma, D. 20X image of striatal hamartoma from C, blue is Topro-3-Iodide, E-H. 20X images of striatal hamartomas demonstrating different morphology and location. Scale bar = 75  $\mu$ m (20X), 300  $\mu$ m (5X).

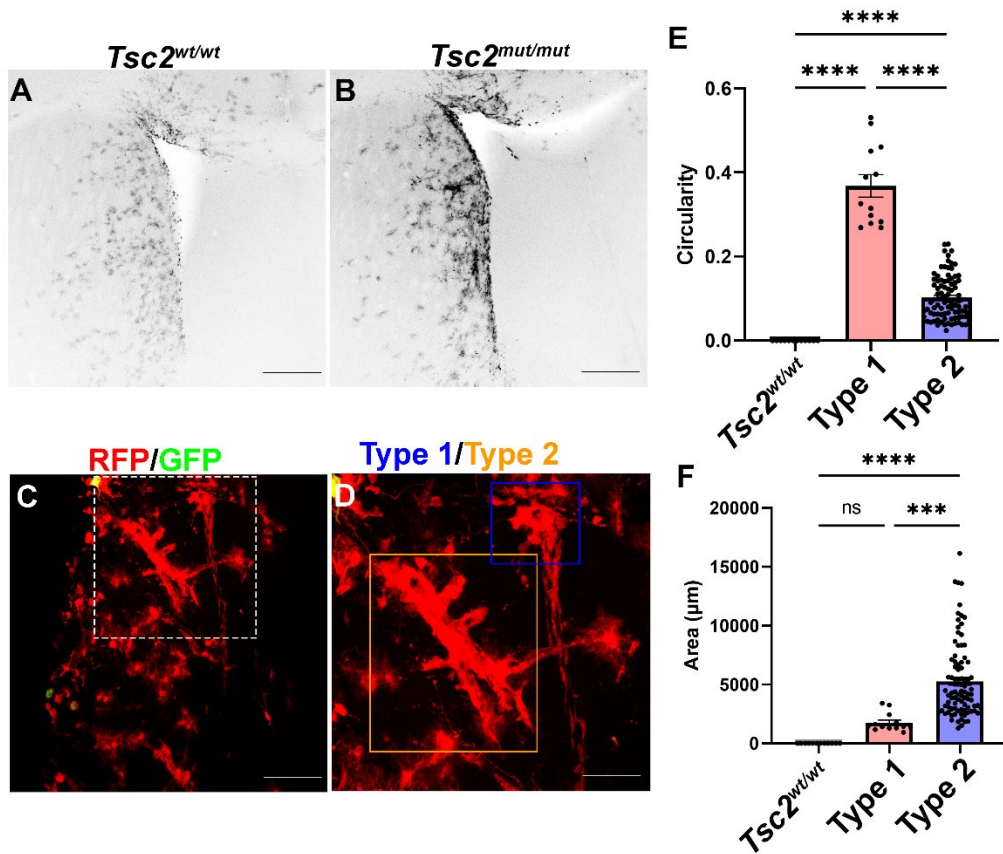


Figure 3.5 *Two categories of hamartomas were noted in the mutant striatum*

A. 5X image of a *Tsc2<sup>wt/wt</sup>* V-SVZ and striatum, B. 5X image of a *Tsc2<sup>mut/mut</sup>* V-SVZ and striatum, C. 20X image of striatal lesions (white box), D. Digital zoom of C demonstrating Type 1 (blue box) and Type 2 (orange box) striatal hamartoma, E. Quantification of hamartoma circularity at P30, *Tsc2<sup>wt/wt</sup>*, N = 12, n = 0, mean = 0.00 ± 0.000 SEM vs. *Type I*, N = 8, n = 13, mean = 0.368 ± 0.027 SEM vs. *Type II*, N = 16, n = 91, mean 0.1022 ± 0.005 SEM, F. Quantification of hamartoma size at P30, *Tsc2<sup>wt/wt</sup>*, N = 12, n = 0, mean = 0.00 ± 0.000 SEM vs. *Type I*, N = 8, n = 13, mean 1764 μm = 216.8 ± SEM vs. *Type II*, N = 16, n = 91, mean = 5,273 μm ± 333.7 SEM, \*\*\* = p = 0.0002, \*\*\*\* = p < 0.0001. Data are represented as mean ± SEM. Scale bar = 75 μm (20X), 300 μm (5X).

Striatal hamartomas formed in every mutant sample measured at P30 and P60 but did not form in *Tsc2<sup>wt/wt</sup>* brains (Figure 3.5.A, B). Hamartomas appeared with an average of two hamartomas per brain section at P30. This frequency lessened to one hamartoma per brain section at P60 (Figure 3.6.C,  $p < 0.01$ ). Striatal hamartoma area was also assessed and it was found that at P30, striatal hamartomas had an area of  $4813 \pm 312.3 \mu\text{m}^2$  which increased to  $6394 \pm 419.2 \mu\text{m}^2$  at P60 (Figure 3.6.F, *Tsc2<sup>wt/wt</sup>*, N = 12, n = 0, mean =  $0.00 \pm 0.00$  SEM vs. *Tsc2<sup>mut/mut</sup>*, N = 16, n = 105, mean =  $4813 \pm 312.3$  SEM vs. P60, *Tsc2<sup>wt/wt</sup>*, N = 8, n = 0, mean =  $0.00 \pm 0.00$  SEM vs. *Tsc2<sup>mut/mut</sup>* N = 12, n = 157, mean =  $6394 \pm 419.2$ ,  $p < 0.1$ ). Taken together, striatal hamartomas are frequently and widely formed throughout the striatum of the mutant mouse and appear to progress in size as the mouse matures.

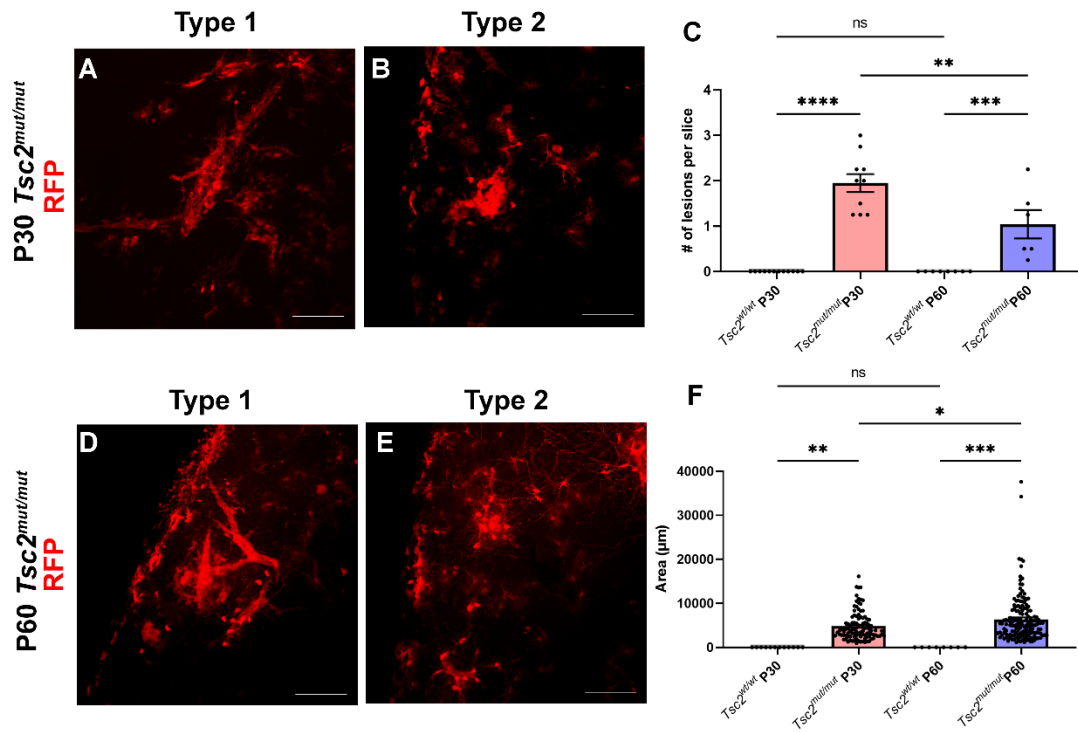


Figure 3.6 *Striatal hamartomas increased in size but not frequency with age*

A. Type 1 striatal hamartoma at P30, B. Type 2 striatal hamartoma at P30, C. Frequency of striatal hamartomas per slice at P30, *Tsc2*<sup>wt/wt</sup>, N = 12, n = 0, mean = 0.00 ± 0.00 SEM vs. *Tsc2*<sup>mut/mut</sup>, N = 10, n = 78, mean = 1.95 ± 0.200 SEM vs. P60, *Tsc2*<sup>wt/wt</sup>, N = 12, n = 0, mean = 0.00 ± 0.00 SEM vs. *Tsc2*<sup>mut/mut</sup>, N = 6, n = 25, mean = 1.042 ± 0.3124 SEM, D. Type 1 striatal hamartoma at P60, E. Type 2 striatal hamartoma at P60, F. Area quantification of striatal hamartomas at P30, *Tsc2*<sup>wt/wt</sup>, N = 12, n = 0, mean = 0.00 ± 0.00 SEM vs. *Tsc2*<sup>mut/mut</sup>, N = 16, n = 105, mean = 4813 ± 312.3 SEM vs. P60, *Tsc2*<sup>wt/wt</sup>, N = 8, n = 0, mean = 0.00 ± 0.00 SEM vs. *Tsc2*<sup>mut/mut</sup> N = 12, n = 157, mean = 6394 ± 419.2, SEM, \* = p < 0.1, \*\* = p < 0.01, \*\*\* = p < 0.001, \*\*\*\* = p < 0.0001, Data are represented as mean ± SEM. Scale bar = 75 µm.

### *Striatal hamartomas expressed marker of stem cells*

Given the previous hypothesis that  $Tsc2^{mut/mut}$  NSCs may be retaining their stem-like phenotype which could contribute to hamartoma formation, it was hypothesized that the striatal hamartomas could be a result of aberrant neurogenesis. To investigate this, immunohistochemistry was performed on wildtype, heterozygous, and mutant brains to assess Sox2 levels. Sox2 is a transcription factor that is used as a pluripotency marker and to identify stem cells (Ellis et al., 2004). Striatal hamartomas were comprised of cells that had Sox2 activity, indicating the presence of stem cells or stem cell proteins within the hamartomas (Figure 3.7). Hamartomas and ectopic Sox2 activity were not noted in either the  $Tsc2^{wt/mut}$  or  $Tsc2^{wt/wt}$  condition.

Furthermore, striatal hamartomas had cells that had Nestin activity (Figure 3.8). Nestin, as mentioned previously, is a neurofilament protein that is specific to NSCs (Lendahl et al., 1990). Its expression confirmed that there are NSCs present in the striatal hamartomas. Heterotopic NSCs in the striatum could potentially contribute to lesion formation.

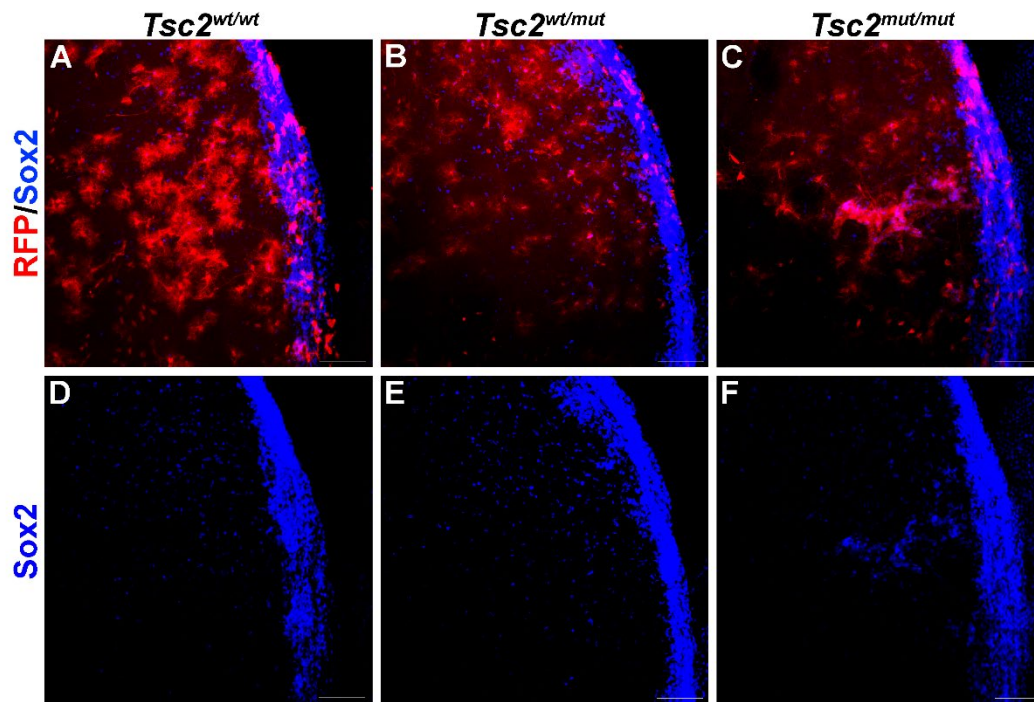


Figure 3.7 *Striatal hamartomas expressed Sox2*

A. RFP and Sox2 expression in *Tsc2*<sup>wt/wt</sup> B. *Tsc2*<sup>wt/mut</sup>, and C. *Tsc2*<sup>mut/mut</sup>. D. Sox2 expression in *Tsc2*<sup>wt/wt</sup> E. *Tsc2*<sup>wt/mut</sup>, and F. *Tsc2*<sup>mut/mut</sup>. Scale bar = 75  $\mu$ m.

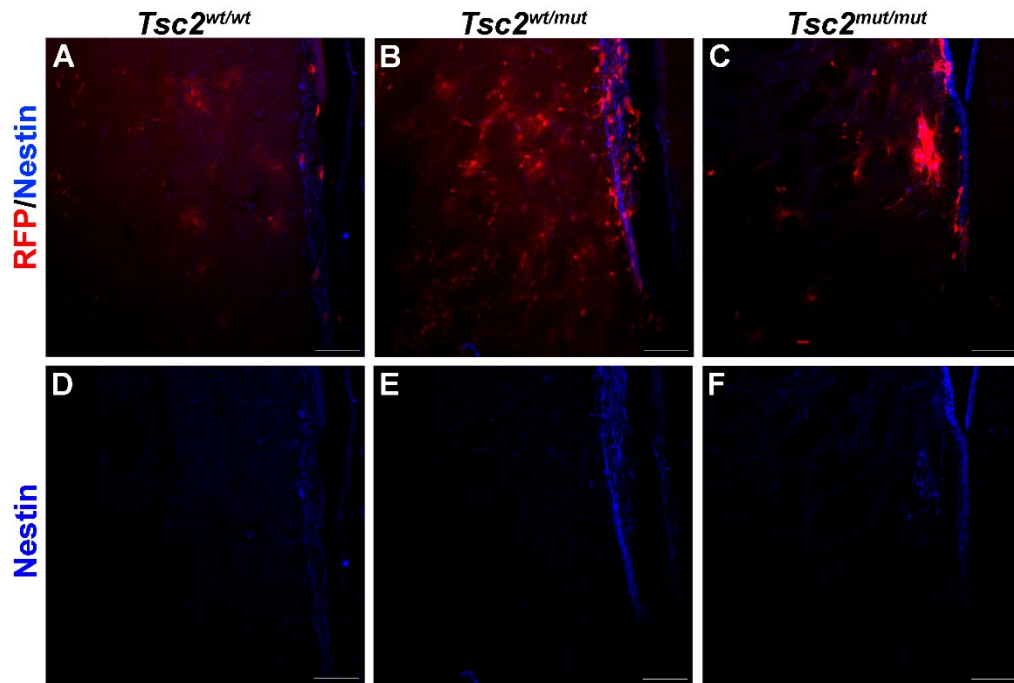


Figure 3.8 *Striatal hamartomas expressed Nestin*

A. RFP and Nestin (blue) expression in *Tsc2*<sup>wt/wt</sup> B. *Tsc2*<sup>wt/ut</sup>, and C. *Tsc2*<sup>mut/ut</sup>. D. Nestin (blue) expression in *Tsc2*<sup>wt/wt</sup> E. *Tsc2*<sup>wt/ut</sup>, and F. *Tsc2*<sup>mut/ut</sup>. Scale bar = 75  $\mu$ m.

*Striatal hamartomas expressed glutamine synthetase*

To continue investigating whether neuro- or gliogenesis was affected in striatal hamartomas, the expression of markers specific for cell types that would result from these processes was examined. Striatal hamartomas had cells that expressed glutamine synthetase (Figure 3.9). Glutamine synthetase is an enzyme that plays a role in glutamate recycling and is commonly used as a marker of glial cells, such as astrocytes (Anlauf & Derouiche, 2013). Astrocytes are one of the primary cell types that are produced via NSCs at the time of electroporation and their presence could indicate that NSCs are contributing glia to striatal hamartomas.

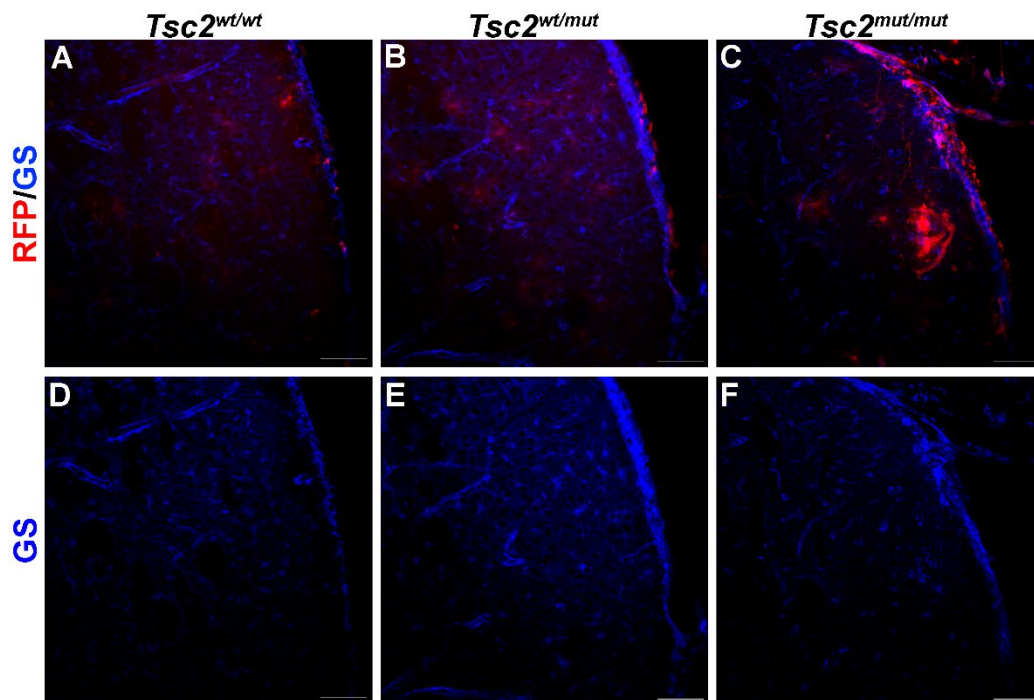


Figure 3.9 Striatal hamartomas expressed Glutamine Synthetase

A. RFP (red) and GS (blue) expression in *Tsc2*<sup>wt/wt</sup> B. *Tsc2*<sup>wt/mt</sup>, and C. *Tsc2*<sup>mut/mt</sup>. D. GS (blue) expression in *Tsc2*<sup>wt/wt</sup> E. *Tsc2*<sup>wt/mt</sup>, and F. *Tsc2*<sup>mut/mt</sup>. Scale bar = 75  $\mu$ m.

*Striatal hamartomas contain neuroblasts and neurons*

Striatal hamartomas also had cells that expressed DCX (Figure 3.10). DCX is a microtubule associated protein that is used to identify migrating neuroblasts (Gleeson et al., 1999). Neuroblasts are immature neurons that migrate through the brain during neurogenesis. DCX<sup>+</sup> neuroblasts, upon arrival at their destination, mature into post-mitotic neurons (Lim & Alvarez-Buylla, 2016). DCX<sup>+</sup> neuroblasts have previously been implicated in hamartoma formation and it's possible that similar mechanisms behind formation are occurring in this model (Feliciano et al., 2012; Magri et al., 2011; Zhou et al., 2011).

Striatal hamartomas also contained cells that expressed NeuN (Figure 3.11). NeuN is a nuclear protein that identifies mature, post-mitotic neurons (Mullen et al., 1992). Striatal hamartomas contained NeuN<sup>+</sup> neurons, indicating that fully developed, mature cells exist within hamartomas. The presence of neuroblasts and mature neurons, taken together, could indicate that NSCs are contributing to striatal hamartomas via aberrant neurogenesis. However further studies will need to be done to verify the precise mechanism.

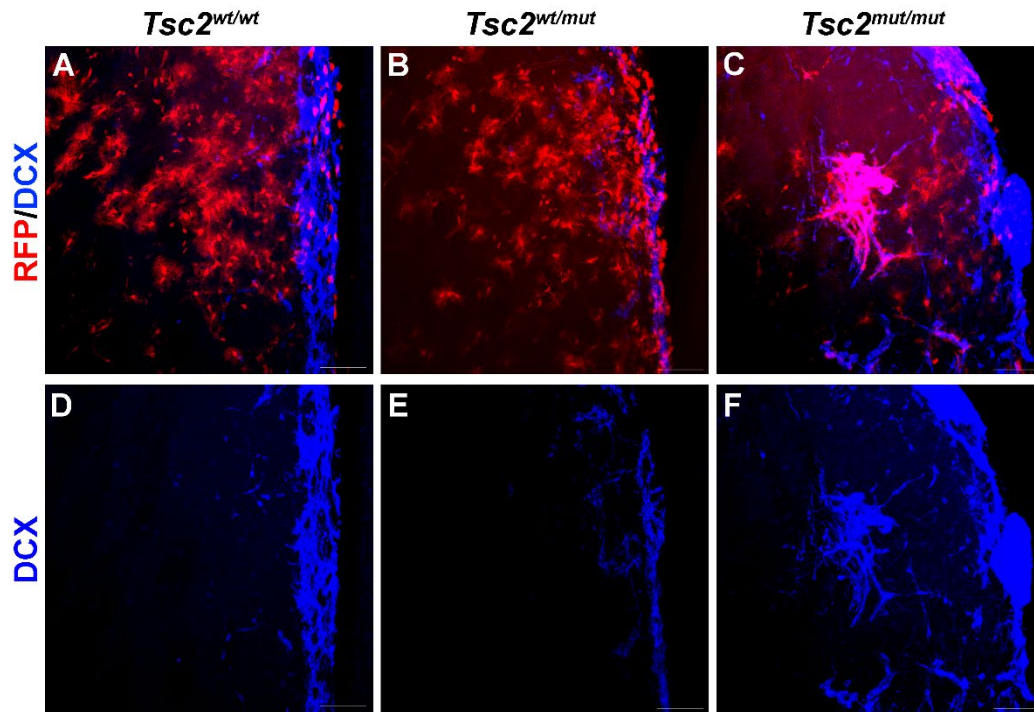


Figure 3.10 *Striatal hamartomas expressed DCX*

A. RFP and DCX (blue) expression in *Tsc2*<sup>wt/wt</sup> B. *Tsc2*<sup>wt/mut</sup>, and C. *Tsc2*<sup>mut/mut</sup>. D. DCX (blue) expression in *Tsc2*<sup>wt/wt</sup> E. *Tsc2*<sup>wt/mut</sup>, and F. *Tsc2*<sup>mut/mut</sup>. Scale bar = 75  $\mu$ m.

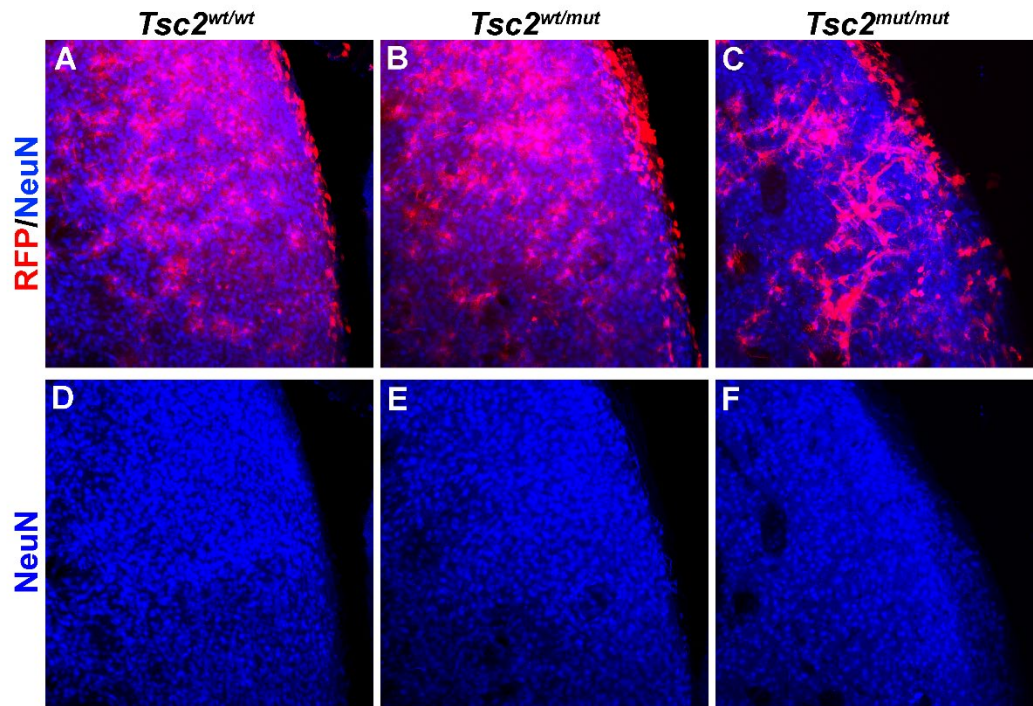


Figure 3.11 *Striatal hamartomas expressed NeuN*

A. RFP and NeuN (blue) expression in *Tsc2*<sup>wt/wt</sup> B. *Tsc2*<sup>wt/mut</sup>, and C. *Tsc2*<sup>mut/mut</sup>. D. NeuN (blue) expression in *Tsc2*<sup>wt/wt</sup> E. *Tsc2*<sup>wt/mut</sup>, and F. *Tsc2*<sup>mut/mut</sup>. Scale bar = 75  $\mu$ m.

*Many cells in striatal hamartomas have stem cell marker expression*

Given that multiple cell types seemed to exist in striatal hamartomas, the cell types were quantified using classical markers of cell identity. RFP<sup>+</sup> and either p4EBP, Sox2, GS, DCX, or NeuN positive cells were counted on raw images and the percentage of marker expression per hamartoma was calculated. Notably, all cells in the striatal hamartomas expressed p4EBP indicating mTORC1 activation following *Tsc2* loss (Figure 3.2, 3.12). Glial cells, which include NSCs and astrocytes, were identified using GS and were found in 49% of cells within striatal hamartomas (Figure 3.12). Similarly, the neuronal lineage was investigated and it was found that 67% of cells in striatal hamartomas were DCX<sup>+</sup> neuroblasts, and 54.2% were NeuN<sup>+</sup> neurons (Figure 3.12). Lastly, stem cells were identified using Sox2 and were found in 93.8% of cells within the striatal hamartomas (Figure 3.12). While co-labeling studies were not performed, given the large percentages of each marker in striatal hamartomas, it is likely that there is considerable overlap in marker expression and potential mixed cellular identity, a phenomenon commonly seen in TSC SEGA. Additionally, the majority of cells in striatal hamartomas expressed Sox2 (93.8%) which could potentially contribute cells to facilitate lesion formation. These results are similar to reports of other TSC lesions in the mouse and human that contained primarily neuroblasts and immature cells (Bongaarts et al., 2017; Giannikou et al., 2021; Kim et al., 2001; Magri et al., 2011; Martin et al., 2017; Zhou et al., 2011).

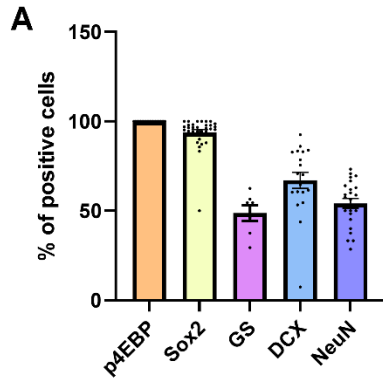


Figure 3.12 The cellular composition of striatal hamartomas

A. Percentage of cells that stained positive for Sox2+ NSCs (93.8% ± 1.618 SEM), GS+ glia (49% ± 4.429 SEM), DCX+ neuroblasts (67% ± 4.496 SEM), and NeuN+ neurons (54.2% ± 2.722 SEM) in striatal hamartomas at P30

*Tsc2 inactivation resulted in heterotopic neurons in the striatum*

Upon examination of the NeuN<sup>+</sup> neurons in striatal hamartomas, the presence of heterotopic, or misplaced neurons in the striatum outside of striatal hamartomas was observed. Heterotopic cells were present lateral to the mutant SVZ in the postnatal striatum. These cells appeared morphologically similar to neurons and expressed the marker, NeuN (Figure 3.13.A-B). Neurons were seen in *Tsc2<sup>mut/mut</sup>* and *Tsc2<sup>wt/wt</sup>* striata but were vastly more numerous in the mutant condition, possibly implicating *Tsc2* expression further in the regulation of neurogenesis. When measured, the distribution of the striatal neurons was not altered between mutant and wildtype conditions, implying that cell type production may not be altered in *Tsc2* mutant condition, only quantity of neurons produced (Figure 3.13.C,  $D_p < 0.001$ ).

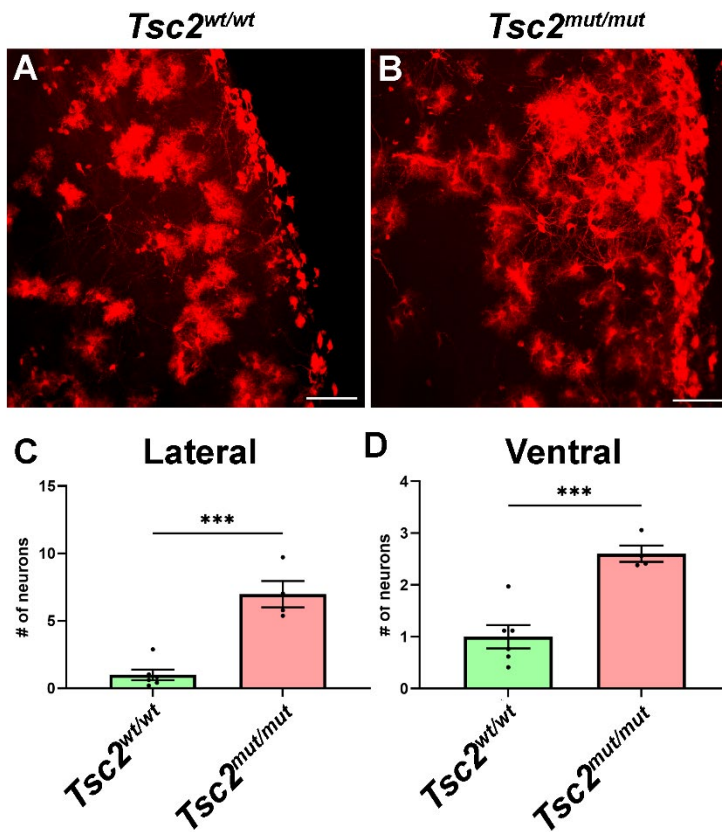


Figure 3.13 *Tsc2* inactivation resulted in heterotopic neurons in the striatum

A. 20X image of the *Tsc2*<sup>wt/wt</sup> striatum, B. 20X image of the *Tsc2*<sup>mut/mut</sup> striatum, C. Neuron counts in the lateral striatum at P30 *Tsc2*<sup>wt/wt</sup>, N=6, n=29, mean = 1.000 ± 0.3977 SEM vs. *Tsc2*<sup>mut/mut</sup>, N=4, n=135, mean = 6.983 ± 0.9791 SEM D. Neuron counts in the ventral striatum at P30 *Tsc2*<sup>wt/wt</sup>, N=6, n=204, mean = 1.000 ± 0.2249 SEM vs. *Tsc2*<sup>mut/mut</sup>, N=4, n=354, mean = 2.603 ± 0.1568 SEM, \*\*\*= p < 0.001, Data are represented as mean ± SEM. Scale bar = 75 μm.

*Heterotopic neurons in the mutant striatum are morphologically different than controls*

To assess the morphological aspects of heterotopic neurons, morphological characteristics were assessed. Soma size is a well-known indicator of mTORC1 hyperactivation and increased soma size can influence cell signaling as well as synaptic function. At P30, it was found that *Tsc2<sup>mut/mut</sup>* neurons were significantly enlarged in the striatum when compared to *Tsc2<sup>wt/wt</sup>* striatal neurons (Figure 3.14 *Tsc2<sup>wt/wt</sup>*, N = 6, n = 95, mean =  $1 \pm 0.01988$  SEM vs. *Tsc2<sup>mut/mut</sup>*, N = 12, n = 164, mean =  $1.231 \pm 0.02856$  SEM,  $p < 0.0001$ ). This trend continued at P60 where neuronal soma size increased in mutant neurons and was 150% larger than in *Tsc2<sup>wt/wt</sup>* striatal neurons (Figure 3.15., *Tsc2<sup>wt/wt</sup>*, N = 6, n = 88, mean =  $1 \pm 0.04671$  SEM vs. *Tsc2<sup>mut/mut</sup>*, N = 10, n = 227, mean =  $1.501 \pm 0.03473$  SEM,  $p < 0.0001$ ). This indicates that loss of *Tsc2* during development results in the hyperactivation of mTORC1 signaling in mature neurons and maintains these defects through maturation.

NSCs have been shown to have regional identity as well as intrinsic identity, meaning that the types of cells that they produce are predetermined (Merkle et al., 2007). At the time of electroporation (postnatal day 1), the majority of neurons produced should be destined for the OB and it is possible that neurons present in the striatum migrated there incorrectly. However, striatal neurons did not resemble the typical neurons that would be produced at this time in the postnatal OB, possibly indicating that these neurons are not a result of errors in migration. For examples of OB neuron morphology, see Chapter four.

The presence of heterotopic neurons with abnormal neuronal morphology could have far reaching implications for synaptic signaling and activity in the striatum which could further have implications for the neurological manifestations of TSC.

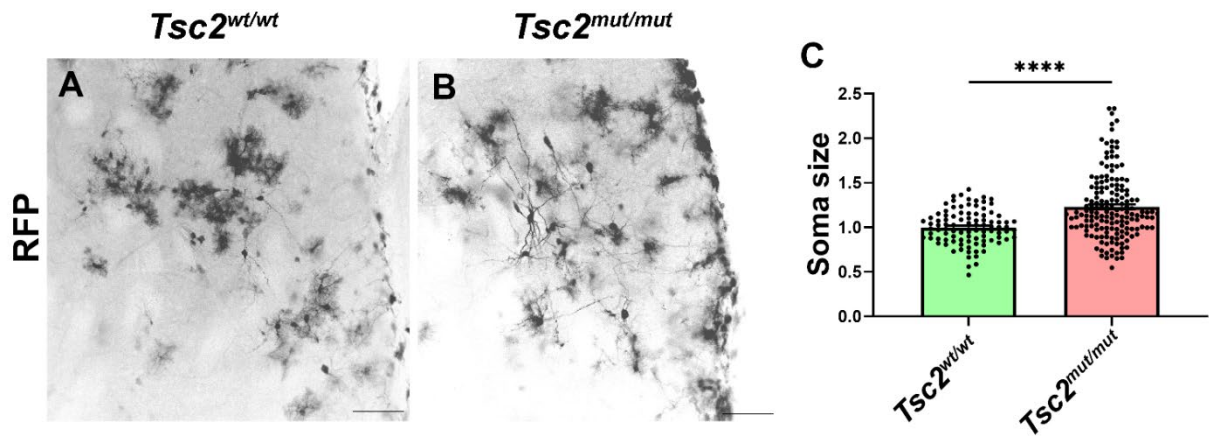


Figure 3.14 *Neuronal morphology is aberrant in the Tsc2 null striatum at P30*

A. 20X image of *Tsc2*<sup>wt/wt</sup> V-SVZ and striatum, B. 20X image of *Tsc2*<sup>mut/mut</sup> V-SVZ and striatum, C. *Tsc2*<sup>wt/wt</sup>, N = 6, n = 95, mean =  $1 \pm 0.01988$  SEM vs. *Tsc2*<sup>mut/mut</sup>, N = 12, n = 164, mean =  $1.231 \pm 0.02856$  SEM, \*\*\*\* =  $p < 0.0001$ , Data are represented as mean  $\pm$  SEM. Scale bar = 75  $\mu$ m (20X)

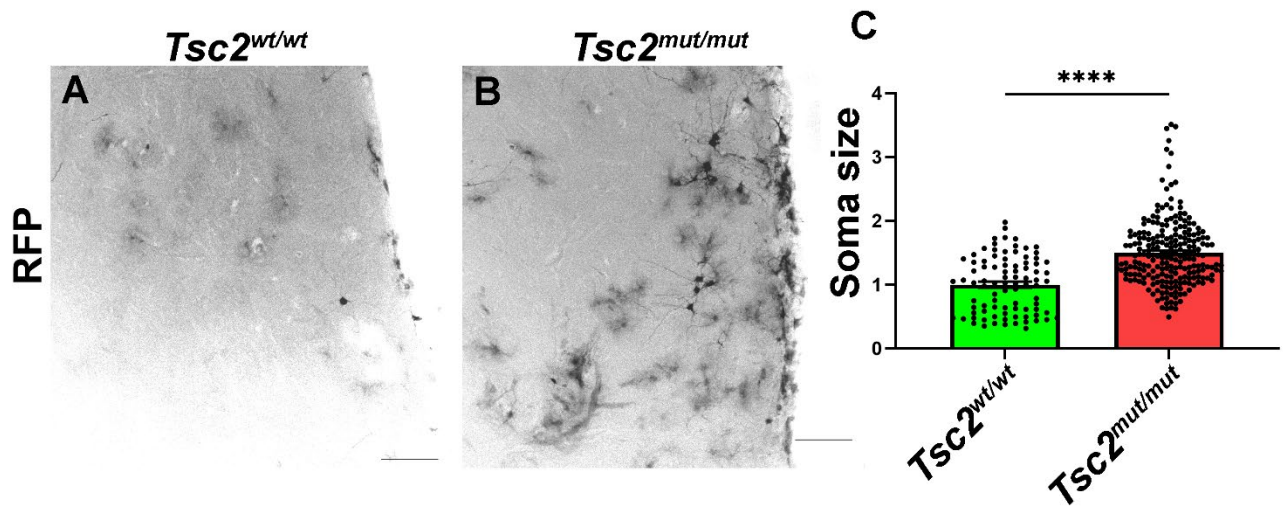


Figure 3.15 *Neurons are larger than wildtype in the mutant striatum at P60*

A. 20X image of  $Tsc2^{wt/wt}$  V-SVZ and striatum, B. 20X image of  $Tsc2^{mut/mut}$  V-SVZ and striatum, C. Quantification of soma size at P60  $Tsc2^{wt/wt}$ ,  $N = 6$ ,  $n = 88$ , mean =  $1 \pm 0.04671$  SEM vs.  $Tsc2^{mut/mut}$ ,  $N = 10$ ,  $n = 227$ , mean =  $1.501 \pm 0.03473$  SEM, \*\*\*\* =  $p < 0.0001$ . Data are represented as mean  $\pm$  SEM. Scale bar =  $75 \mu\text{m}$ .

## Discussion

Striatal hamartomas in the *Tsc2<sup>mut/mut</sup>* mice are partially reminiscent of human SEGAs. They have a mixed neuronal-glial phenotype, likely form from neural progenitor cells, and require biallelic inactivation to occur at the time points measured. The goal of this study was to characterize the cellular and molecular phenotypes associated with *Tsc2* loss in NSCs. *Tsc2* loss from perinatal NSCs resulted in the acquisition of phenotypes characteristic of TSC including cytomegalic cells, ectopic striatal neurons, and striatal hamartomas (Figure 3.4, 3.13, 3.14, 3.15). Cytomegalic cells and ectopic neurons were strewn throughout the striatum and were larger than neurons found in the wildtype condition (Figure 3.13, 3.14, 3.15). These neurons were significantly more numerous in the *Tsc2* null condition when compared to control conditions potentially influencing striatal neuronal circuitry and behavioral phenotypes (Figure 3.13). In addition to ectopic striatal neurons, *Tsc2* loss also resulted in the formation of large striatal hamartomas (Figure 3.4). These hamartomas were heterogeneous and contained many cell types including neurons, neuroblasts, glia, and NSCs, similar to human SEGA (Figure 3.12) (Bongaarts et al., 2017; Gelot & Represa, 2020; Giannikou et al., 2021; Martin et al., 2017).

The neurons produced by a specific NSC is determined intrinsically via the expression of specific transcription factors within that NSC (Merkle et al., 2007). The heterogeneity of SEGA could be tied to this phenomenon in that the cell of origin for SEGA could affect its final presentation and cellular composition. In this study, striatal hamartomas seem to appear in distinct types with differing cellular morphology, similar

to SEGAs. This may be due to their cell of origin. As multiple types of NSCs are present in the V-SVZ of the lateral ventricle and are targeted by electroporation, NSCs that produce different subtypes of cells could be responsible for different types of striatal hamartomas.

In chapter two, it was shown that *Tsc2* inactivation results in differentially regulated transcription and translation that could potentially lead to the aberrant expression of mRNA transcripts at the incorrect time and level of expression. One possible consequence of this is the potential retention of NSC factors, such as Sox2, in maturing or differentiating cells. Markers of immaturity or stemness have previously been noted in human and murine TSC hamartomas (Bongaarts et al., 2017, 2022; Gelot & Represa, 2020; Kim et al., 2001; Magri et al., 2011; Martin et al., 2017; Zordan et al., 2018). Cells retaining immature markers are hypothesized to potentially maintain some aspects of stemness and neurogenic potential outside of normal developmental timing. Indeed, murine models have shown that when mTORC1 signaling is abnormally activated it can lead to the retention of the stem cell marker Sox2 and an inability for cells to transition out of stemness (Baser et al., 2019). A similar phenomenon has been seen previously where the ectopic expression of Sox2 has been shown to induce abnormal neurogenic potential in striatal and cortical cells (Heinrich et al., 2014; Niu et al., 2013). However, for the experiments done in this chapter, cycling NSCs were used for both mutant and wildtype conditions, which would be expected to express pluripotency markers. Therefore, the retention of stemness and stem-like transcripts could not be fully investigated as the experimental conditions precluded these analyses. That

being said, these analyses should be investigated more thoroughly in the future to verify if stem cell-like transcripts are being retained in the mutant *Tsc2* condition.

If a retention of stem-like states were found in the mutant condition, this could potentially contribute to hamartoma formation where cells retaining aspects of immaturity allow them to divide and produce daughter cells in abnormal regions and number, leading to a buildup of cells that become the hamartoma. Indeed, in mouse models it has been postulated that aberrant neurogenesis is responsible for SEGA-genesis (Feliciano et al., 2012; Magri et al., 2011; Zhou et al., 2011). This hypothesis is corroborated by the fact that TSC brain hamartomas often display mixed neuronal and glial characteristics (Bongaarts et al., 2017, 2022; Giannikou et al., 2021; Kim et al., 2001; Martin et al., 2017). This duality could be syndromic of an inability to fully differentiate or move past a stem cell-like phenotype. Additionally, it has been postulated previously that SENs/SEGAs develop progressively, beginning with astrocytic NSCs that produce neuroblasts and neurons to contribute to hamartoma formation, implicating abnormal neurogenesis in hamartoma development (Gelot & Represa, 2020; Zordan et al., 2018). Indeed, these phenomena mimic what is seen in this chapter wherein hamartomas retain stem-like proteins and have multiple cell lineages present within them (Figure 3.7-11). It is possible that Sox2 and Nestin positive stem cells in the hamartomas are producing the neuroblasts, neurons, and other glia seen in the striatal hamartomas (Figure 3.7-11). However, this would need to be investigated further as this analysis does not differentiate between cells that were produced by NSCs within the striatal hamartoma and those produced by NSCs in the V-SVZ. This mechanism of growth formation would

be similar to those seen in models of cancer with cancer stem cells (Batlle & Clevers, 2017).

That being said, striatal hamartomas and ectopic neurons could be produced by alternative mechanisms to that described above. Another possible mechanism is that striatal hamartomas form due to errors in migration as seen in mouse models of SENs (Zhou et al., 2011; Zordan et al., 2018). The formation of growths in the striatum has also been noted in an ischemia model caused by middle cerebral artery occlusion (Jin et al., 2003). In this model, there were significant increases in DCX+ neuroblast number following ischemia in wide areas of the striatum (Jin et al., 2003). These neuroblasts migrated from the SVZ and formed cellular chains that appeared to track blood vessels and spherical aggregates, similar to the two types of striatal hamartoma seen in the *Tsc2* mutant in this chapter (Figure 3.5) (Jin et al., 2003). Additionally, a similar phenomenon has been noted in response to inflammation resulting from LPS injection into the striatum, implying that inflammation may be the culprit responsible for abnormal striatal neurogenesis and hamartoma formation as opposed to injury (Chapman et al., 2015).

In this vein, cortical tubers and SEGAs found in TSC are known to occur in conjunction with brain inflammation (Bongaarts et al., 2017, 2022; Martin et al., 2017; Prabowo et al., 2013; Zordan et al., 2018). This could potentially indicate that inflammation is either caused by or contributes to hamartoma formation in the TSC brain. Another factor that causes or is a consequence of inflammation in the TSC brain is epileptic activity, which could contribute to TSC hamartoma progression (B. Zhang et al., 2015). As an alternative mechanism to striatal hamartoma generation, it is possible that

inflammatory environments in the TSC brain contribute to the induction of aberrant neurogenesis in different brain regions, including the striatum which then contributes to hamartoma formation and other TSC symptoms. While none of these possible mechanisms have been investigated in this chapter, it is worthwhile to examine them further to determine the exact mechanisms behind hamartoma formation.

## Methods

Animals. Clemson University Institutional Animal Care and Use Committee approved experiments, and all guidelines set forth by the Clemson University Institutional Animal Care and Use Committee and were compliant with the Animal Care and Use Review Office (ACURO), a component of the USAMRDC Office of Research Protections (ORP) within the Department of Defense (DoD). Red fluorescent protein (RFP<sup>+/-</sup>, <sup>+/+</sup>) (B6. CgGt (ROSA)26Sortm9 (CAG-tdTomato)<sup>Hze/J</sup>) (Strain #007909), *Tsc2*<sup>tm1.1Mjg/J</sup> (Strain #027458) were acquired from Jackson Laboratories. Mice were housed under pathogen-free conditions with a 12-h light/dark cycle and fed ad libitum.

PCR. The tissue was incubated in 50 mM NaOH and 0.2 mM EDTA at 50°C overnight. An equal volume of 100 mM Tris-HCl was added to samples. Samples were subject to routine genotyping using Taq DNA Polymerase with the following conditions: Initial denaturation step at 98°C for 2 min, followed by 35 cycles of denaturation at 95°C for 30 s, an annealing step at 60°C for 30 s, and an extension at 72°C for 30 seconds followed by a final extension at 72°C for 3 min. Samples were loaded onto a 1.7% agarose gel with 1X Blue Juice and run at 100 V for 20–30 mins. Mice having conditional *Tsc2* alleles are distinguished by endpoint genotyping PCR using the following primer sequences, 5'-ACAATGGGAGGCACATTACC-3' and 5'-AAGCAGCAGGTCTGCAGTG-3'. Tomato (RFP) genes were identified for Stock #7914 using the following primer sequences, 5'-AAGGGAGCTGCAGTGGAG TA-3' and 5'-CCGAAAATCTGTGGGAAG TC-3' and

5'-GGCATTAAAGCAGCGTATCC-3' and 5'CTGTTTCCTGTACGGCATGG-3'. Long-range PCR was performed as previously described.

Immunohistochemistry. Euthasol® was administered by intraperitoneal injection to sedate mice followed by swift decapitation. Brains were dissected in room temperature PBS, transferred to 4% paraformaldehyde (in PBS), and incubated overnight at 4°C. Brains were rinsed in PBS and mounted in 3% agarose. A Leica VTS 1000 vibratome was used to slice brains coronally in 150-300 µm sections. Sections were blocked in PBS containing 0.1% Triton X-100, 0.1% Tween-20 and 2% BSA for 1 hour at room temperature. Sections were washed in PBS containing 0.1% Tween-20 three times. Sections were incubated in primary antibody; anti-Dcx (1:500; Santa Cruz Biotechnology sc-8066 and sc-271390), anti-Sox2 (1:500; Invitrogen 14-9811-82) anti-pS6 (1:500; Cell Signaling Technology; Ser 240/244, 61H9, #4838), anti-Nestin (1:500; Novus Biologicals; #NB100-1604), anti-p4EBP (1:500; Cell Signaling Technology; Thr37/46, 236B4; #2855), anti-glutamine synthetase (1:500; Sigma Aldrich; #G2781), and anti-NeuN (1:500; Sigma Aldrich; #MAB377) overnight at 4°C. Sections were subjected to three additional washes in PBS containing 0.1% Tween-20. Sections were incubated with the appropriate secondary antibody (Alexa Fluor series; 1:500; Invitrogen) overnight at 4°C. Sections were mounted in ProLong Antifade Mountant (Thermo Fisher). Each staining was replicated on the indicated number of mice per condition. Images were acquired on a spectral confocal microscope (Leica SPE) with a ×20 dry objective (N.A.

0.75). Low-magnification images were acquired with  $\times 10$  dry or a  $\times 5$  dry (N.A. 0.15) objective.

Image Analysis. Images ( $\times 20$ ) of RFP positive cells were uploaded to FIJI (ImageJ 1.5 g). The freehand selection tool was used to trace a region of interest (ROI) on electroporated and non-electroporated cells in the same Z section and a mean gray value measured to quantify the staining intensity of p4EBP and normalized. Ratios of staining in electroporated and non-electroporated cells were compared for RFP positive cells in  $Tsc2^{wt/wt}$  and  $Tsc2^{mut/mut}$  conditions to account for immunohistochemical variation. All values were normalized to the average intensity of the ratio of electroporated divided by non-electroporated cells in  $Tsc2^{wt/wt}$  conditions.

Images ( $\times 20$ ) were used to measure soma size. Images were uploaded as described above and the freehand selection tool was used to trace soma size in  $Tsc2^{wt/wt}$  and  $Tsc2^{mut/mut}$  conditions.

Images ( $\times 20$ ) were used to measure neuronal number in the striatum. Images were uploaded as described above and the Cell Counter plug-in was used to mark RFP positive cells with a neuronal morphology. The total number of neurons were calculated within the striatum and divided into lateral and ventral regions by eye.

For lesion analysis, lesions were defined in images ( $\times 20$ ) as containing approximately eight or more overlapping RFP positive cells present within the striatum and in an individual Z-section. RFP+ cells were counted in the lesion and assessed for either Sox2, p4EBP, DCX, GS, or NeuN on a per cell basis. Circularity and area were measured in maximum intensity projections. The area of the lesions was then circumscribed using the freehand selection tool and the area and circularity quantified. Hamartomas were considered Type 1 when circularity values were 0.269-0.531 and Type 2 when circularity values were 0.024-0.23.

Measurements were made on original image files without enhancements or thresholding. Figures were created by converting LIF files into TIFF format images using FIJI. Images were uploaded into Photoshop (Adobe, version 2022). Merged images containing multiple fluorophores were subject to brightness and contrast changes and RGB levels were optimized. Changes were applied across the entirety of each image. For individual-colored images, the RGB images were duplicated, and individual colors were removed. To make black and white images, the RFP channel was converted to gray scale and inverted.

Statistics. Data were graphed and analyzed with GraphPad Prism software (Version 8.2.0, GraphPad Software Inc.). Statistical significance was determined by Student's *t* test where indicated. One-way analysis of variance (ANOVA) with Tukey's multiple comparisons test was performed where indicated, \* =  $p < 0.05$ , \*\* =  $p < 0.01$ , \*\*\* =

$p < 0.001$ , \*\*\*\* =  $p < 0.0001$ ).  $p$  values less than 0.05 were considered significant unless otherwise noted. No methods were used to determine whether the data met assumptions of the statistical approach. All experiments were performed on 6–17 mice per condition per time point.  $N$  (number of mice) and  $n$  (number of cells or hamartomas) are listed where applicable. Error bars are reported as standard error mean.

## CHAPTER FOUR

### ***Tsc2* inactivation results in morphological abnormalities in the Olfactory Bulb**

A version of this data is published in Frontiers of Molecular Neuroscience:

Riley, V.A., Holmberg, J.C., Sokolov, A.M., and Feliciano, D.M. (2022). *Tsc2* shapes OB granule cell molecular and morphological characteristics. *Front Mol Neurosci* 15. 10.3389/fnmol.2022.970357.

Experiments presented in chapter IV were conducted as follows.

Electroporations, tamoxifen injections, dissections, immunohistochemistry, RNA isolations, and image analysis were performed by Victoria Riley. Computational and bioinformatic analysis was performed by Dr. David Feliciano. Library preparation, RNA quality assessment, RNA sequencing, and bioinformatic analysis of the RNA sequencing data was performed by Azenta Life Sciences (formerly GeneWiz)

## Abstract

Many of the neurological symptoms of TSC are believed to be caused by malformations in the cerebral cortex. These malformations are mainly comprised of neurons. It is therefore useful to study neurons that have lost *Tsc2* in order to see how their molecular and cellular morphology could contribute to the disorder. The olfactory bulb (OB) of the brain is particularly useful for the study of neurons because it has a well-defined organization and mechanism of development. In this chapter, OB granule cell (GC) neurons were investigated. In order to examine the role that the *Tsc2* gene plays in the development of mature GC neurons of the OB, *Tsc2* was inactivated in perinatal ventricular-subventricular zone (V-SVZ) neural stem cells (NSCs) by electroporation. This resulted in RFP+ *Tsc2*<sup>mut/mut</sup> neurons in the GC layer of the OB. These neurons were cytomegalic and had increased pS6 levels, indicating increased mTORC1 signaling. Additionally, the OB appeared disorganized when compared to controls. In addition to examining neurons that had lost *Tsc2* during development, *Tsc2* loss was also assessed in mature post-mitotic neurons. It was found that *Tsc2* did not play a large role in the maintenance of mature neuronal morphology. OB transcriptome profiling revealed a network of significantly differentially expressed genes following loss of *Tsc2* during development that altered neural circuitry. Taken together, this shows that *Tsc2* is crucial for neurogenesis and neuronal development.

## Introduction

Given the correlation between hamartomas and the neurological manifestations of TSC, it is believed that the disruption of cortical neuronal cytoarchitecture is responsible for these symptoms. It is therefore necessary to examine neurons that have lost TSC genes in more detail.

Mouse models have been generated that look at the role of TSC genes in neurons specifically and how they contribute to the pathology of TSC. In one model, it was found that *Tsc1* loss in synapsin<sup>+</sup> neurons led to the generation of spontaneous seizure activity due to decreased inhibitory activity (Meikle et al., 2007; Zhao & Yoshii, 2019). This reduction in inhibitory activity could potentially contribute to excitation/inhibition imbalances and epilepsy. In another study, *Tsc1* was inactivated in both alleles simultaneously under the  $\alpha$ CaMKII promoter (Ehninger et al., 2008). This resulted in the loss of *Tsc1* from neurons in the postnatal forebrain (Ehninger et al., 2008). Neuronal loss of *Tsc1* led to non-cell autonomous effects wherein seizures caused by increased mTORC1 activity led to the generation of increased activity and mTORC1 activation in other brain regions (McMahon et al., 2015). This indicates that *Tsc1* loss from a small subset of cells can cause new regions of abnormality worsening symptoms. This could have far reaching implications for whole brain TSC pathology and could explain the severity of the disorder despite the focal nature of cells affected.

Given that these models did not differentiate between excitatory and inhibitory neurons which could contribute to these manifestations, models that inactivated TSC genes in either subset were generated. In one model, *Tsc2* was inactivated in neurons that

expressed NEX, a protein implicated in neuronal differentiation that should be present in neurons with an excitatory lineage (Crowell et al., 2015; Schwab et al., 1998). These mice had increased mTORC1 activity in the cortex but the patterning of the cortex was relatively normal. Additionally, the mice did not have obvious seizures, though no technical seizure detection tests were undertaken (Crowell et al., 2015).

Another *in vivo* model inactivated *Tsc1* in inhibitory progenitor cells and neurons expressing *Dlx5/6* (Fu et al., 2012). Interestingly, in this model, groups of large cells were noted in the cortex that had increased levels of pS6 expression and co-expressed NeuN and GAD67, an inhibitory neuron marker (Fu et al., 2012). Like the excitatory neuron model, seizures were not detected in these mice despite prolonged EEG monitoring, indicating that loss of *Tsc1* in inhibitory neurons may not be enough for epileptogenesis (Fu et al., 2012). However, when the mice were induced to have seizures, they displayed a lower seizure threshold, possibly as a result of the reduced number of inhibitory neurons in the cortex (Fu et al., 2012).

Taken together, the loss of TSC genes and hyperactivation of mTORC1 precisely regulate the ratio of excitation and inhibition in the brain. However, loss of *Tsc1* or *Tsc2* from only a subset of neurons does not result in obvious seizure activity. It is only in mouse models that inactivate TSC genes in all neuron types or in neural progenitor cells which will go on to produce neurons that have seizure activity. It is therefore likely that differential regulation in these cell types contributes to seizure activity and TSC pathogenesis. In this chapter, inhibitory neurons generated from *Tsc2<sup>mut/mut</sup>* neural stem

cells (NSCs) were examined more closely in a new brain region. Additionally, mature inhibitory neurons that have lost *Tsc2* were examined. This was done by utilizing the OB.

The OB is a macroscopic structure in the mouse brain that facilitates odor processing and recognition (Shiple & Ennis, 1996). The cytoarchitectonic organization of the OB and its cell types make it a useful model for studying types of neurons that may populate harder to study regions. The six layers of the OB include: the olfactory nerve layer which contains the cell bodies of the olfactory sensory neurons, the glomerular layer which contains the glomeruli and juxtglomerular cells, the external plexiform layer which contains the cell bodies of the tufted cells, the mitral cell layer which contains the cell bodies of the mitral cells, the internal plexiform layer which contains the axons of mitral and tufted cells, and, lastly, the granule cell layer which contains the cell bodies of the granule cells (Figure 4,1,B) (Shiple & Ennis, 1996).

The olfactory nerve layer of the nasal epithelium is comprised of the olfactory sensory neurons (OSN) (Shiple & Ennis, 1996). Each neuron contains the receptor for one odorant that can be detected in the environment (Shiple & Ennis, 1996). OSNs project their axons toward large structures in the OB called glomeruli (Shiple & Ennis, 1996). When an odor triggers OSNs, they propagate that signal to the glomeruli where it activates individual mitral and tufted cells (Shiple & Ennis, 1996). These cells then project the information further down their primary dendrites into the primary olfactory cortex where odor processing concludes (Lledo & Lagier, 2006). The tufted/mitral cells are large projection neurons that are considered the principal cells of the olfactory circuit (Jackowski et al., 1978). Mitral cell activity is regulated by granule cells that populate the

granule cell layer (Jackowski et al., 1978; Rall et al., 1966). Specifically, when mitral cells are excited, this excitation propagates into their primary dendrite which goes to the olfactory cortex but also into their secondary dendrites which interface in the external plexiform layer with the apical dendrites of granule cells in a reciprocal dendrodendritic synapse (Jackowski et al., 1978; Rall et al., 1966). When the mitral cell's secondary dendrites are active, they release the excitatory neurotransmitter glutamate which is taken up by NMDA and non-NMDA receptors on the granule cell gemmules (a kind of synaptic bouton) (Isaacson & Strowbridge, 1998; Jackowski et al., 1978). This excites the granule cell causing it to synapse. As granule cells are inhibitory interneurons, they release the neurotransmitter GABA from that same gemmule resulting in the inhibition of the original mitral cell (Isaacson & Strowbridge, 1998; Jackowski et al., 1978; Rall et al., 1966). As granule cells interface with multiple mitral cells at once, this inhibition also affects neighboring cells providing both inhibition of a single activated mitral cell as well as a method of adaption toward olfactory stimuli (Rall et al., 1966).

OB neurogenesis begins at E14.5 but the majority occurs perinatally. Neurogenesis is ongoing and persists throughout adulthood in mice, though at a protracted rate as age increases (Lim & Alvarez-Buylla, 2016). In order to account for the increase in neurons, the OB has been shown to increase in size throughout the first year of life (Platel et al., 2019). To facilitate OB neurogenesis, adult NSCs remain quiescent in the ventricular-subventricular zone (V-SVZ) until after birth when they take over neurogenesis (Fuentelba et al., 2015). Postnatal neurogenesis in the V-SVZ is similar to embryonic neurogenesis except that neurons are destined for the OB instead of the cortex

(Doetsch & Alvarez-Buylla, 1996; Lois & Alvarez-Buylla, 1993). To accomplish this, adult NSCs first divide to generate TACs. These TACs further divide to generate neuroblasts. Neuroblasts have short processes on either side of the cell that are connected to the neuroblast directly preceding and following it, leading to the presence of chains of neuroblasts that migrate down a pathway called the rostral migratory stream and potentially along blood vessels (Jankovski & Sotelo, 1996; Lim & Alvarez-Buylla, 2016; Whitman et al., 2009). These migrating neuroblasts are surrounded by GFAP<sup>+</sup> astrocytes which extend many processes through which the neuroblasts migrate, termed the glial sheath (Jankovski & Sotelo, 1996). The migrating neuroblasts rely on migratory cues that are independent of the OB (Kirschenbaum et al., 1999). Upon reaching the OB core, young neurons will migrate radially to populate the granular and glomerular cell layers. They will then mature and integrate into OB circuitry (Figure 4.1.A) (Lim & Alvarez-Buylla, 2016). These neurons do not replace specific dying neurons but rather join the pre-existing circuitry (Platel et al., 2019). There are multiple subtypes of neurons in the OB each of which is generated and pre-determined by stem cells in the V-SVZ that express specific transcription factors based on their region of origin (Doetsch & Alvarez-Buylla, 1996). Further, it has been found that cells destined for the glomerular cell layer decrease as the mouse ages resulting in primarily granule cells that are produced postnatally (Batista-Brito et al., 2008).

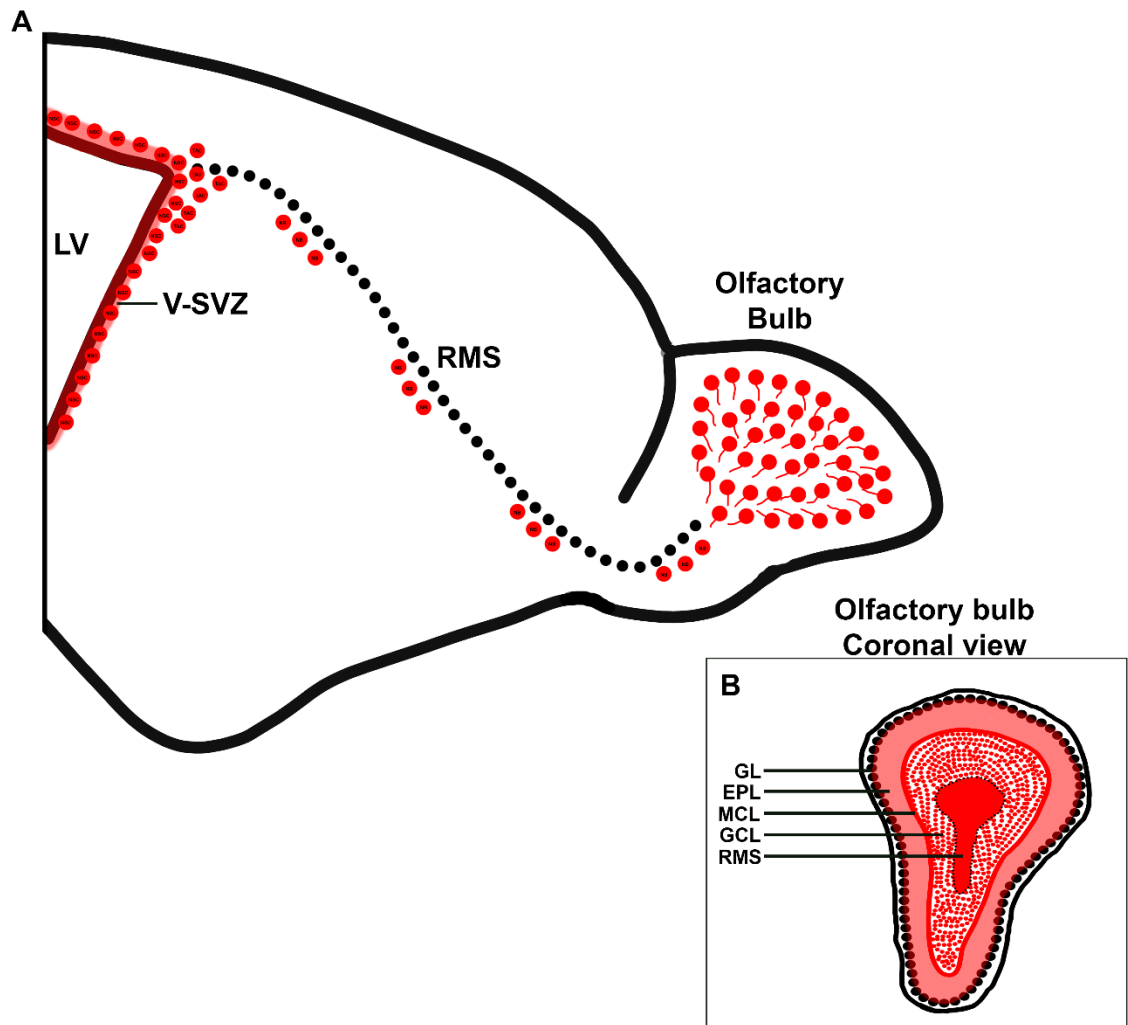


Figure 4. 1 *Olfactory bulb neurogenesis*

A. A drawing of a sagittal section of the adult mouse brain, B. A drawing of a coronal section of the OB, LV=lateral ventricle, V-SVZ=ventricular-subventricular zone, RMS=rostral migratory stream, GL=glomerular layer, EPL=external plexiform layer, MCL=mitral cell layer, GCL=granule cell layer

Granule cells of the OB have been previously looked at in the context of TSC (Feliciano et al., 2012; Zhou et al., 2011). When *Tsc1* was inactivated in NSCs it resulted in migration deficits and fewer granule cells within the granule cell layer of the OB (Zhou et al., 2011). Further studies showed that the neuroblasts from the V-SVZ migrated more slowly to the OB and once reaching the OB, were disorganized and cytomegalic (Feliciano et al., 2012). Further olfactory micronodules were shown to occur both in the olfactory bulb and rostral migratory stream, not unlike those previously seen in patient samples (de León et al., 1988; Feliciano et al., 2012). Taken together, these studies indicate that *Tsc1* plays a significant role in inhibitory granule cell morphology. However, the role of *Tsc2* in these inhibitory neurons has not been established.

Given that postnatal V-SVZ neurogenesis results in mature inhibitory neurons in the OB, it is important to investigate the effects of *Tsc2* inactivation in NSCs and their progeny. In this chapter, the molecular and cellular consequences of reduced *Tsc2* expression in OB granule inhibitory interneurons were examined in order to measure the effect of *Tsc2* loss on GC morphology. Differences in neuron morphology have previously been shown to play a role in neuronal behavior, therefore studying how mutations in this gene affect morphology can be potentially useful for predicting changes in neuron functionality and, ultimately, how that morphology contributes to the symptoms of TSC.

## Results

### *Postnatal electroporation of the V-SVZ resulted in *Tsc2* inactivation in NSCs*

Mice were obtained with alleles identical to those described in Chapter 3 (Figure 4.2.A). Briefly these mice had LoxP sites inserted into the *Tsc2* gene which, upon introduction of CRE, would result in the recombination of the gene and consequent inactivation. Additionally, these mice had an inserted RFP reporter gene that would cause red fluorescence following recombination. This led to all cells with inactivated *Tsc2* also fluorescing red. Electroporation of CRE recombinase and GFP plasmids into neonatal mice having either wildtype or conditional *Tsc2* alleles was performed to mimic somatic *Tsc2* biallelic inactivation and resulted in the loss of *Tsc2* from V-SVZ NSCs and their progeny, including granule cell OB neurons (Figure 4.2.B, D). Mice were electroporated at postnatal day (P) 1 and subsequently euthanized at P30 and P60 (Figure 4.2.C). They were further assessed to determine the effect of *Tsc2* loss in OB neurons.

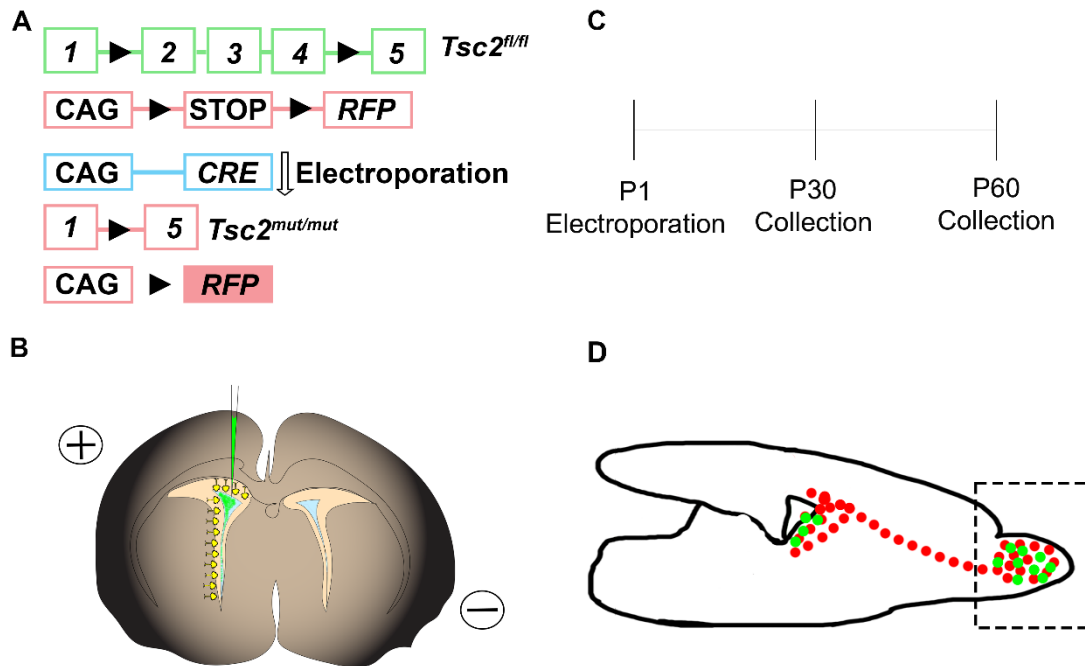


Figure 4.2 Postnatal electroporation of the V-SVZ resulted in *Tsc2* inactivation in the OB

A. Schematic diagram of conditional *Tsc2* and inducible *RFP* genes. *Tsc2* is mutated and *RFP* is expressed when CRE recombinase is present. Triangles denote LoxP sites, B. Postnatal electroporation introduces plasmid DNA into the ventricular space of neonatal mice which is translocated into the cells lining the ventricle following electrical stimulation. C. Experimental schema D. Electroporation results in the focal deletion of *Tsc2* from NSCs lining the ventricle as well as their progeny in the OB. Green and red circles indicate the *RFP* and GFP fluorescent cells that would be generated following electroporation of CAG-CRE and CAG-GFP, including V-SVZ NSCs and their progeny, A box is drawn around the olfactory bulb.

*mTORC1 activity is increased in granule cells following Tsc2 inactivation*

Recombination of *Tsc2* in V-SVZ NSCs resulted in the generation of red granule cells with inactivated *Tsc2* in the OB. Strikingly, OB neuronal organization was disorganized following *Tsc2* inactivation, with a number of neurons forming cell clusters within the mutant OB as opposed to the even radial distribution seen in the heterozygous and control mice (Figure 4.3). Abnormal distribution and organization are common phenotypes that are seen in the cortex and hippocampus of TSC mouse models (Carson et al., 2012; Feliciano et al., 2011; Goto et al., 2011; Magri et al., 2011, 2013; Uhlmann, Apicelli, et al., 2002; Way et al., 2009; L. H. Zeng et al., 2011). This potentially indicates that *Tsc2* loss has similar effects on affected neurons regardless of the region measured.

To further confirm the results of recombination, mTORC1 activity was also assessed. The mTORC1 substrate pS6 was used as it is more commonly expressed in mature neurons than the mTORC1 substrate, p4EBP (Figure 4.4.B-I). Mutant OB granule cells had increased levels of p-S6 expression when compared to RFP+ neurons in the *Tsc2*<sup>wt/mut</sup> or *Tsc2*<sup>wt/wt</sup> OB (Figure 4.4.A, H-I; *Tsc2*<sup>wt/wt</sup>, n = 155 cells, N = 7 mice, mean = 0.8680 ± 0.01966, *Tsc2*<sup>wt/mut</sup> n = 212, N = 8 mice, mean = 1.013 ± 0.05985, *Tsc2*<sup>mut/mut</sup> n = 301, N = 9 mice, mean = 1.965 ± 0.07024, \*\*\*\*=*p* < 0.0001) Therefore, pS6 analysis confirmed that mTORC1 pathway activity increased following *Tsc2* inactivation.

Loss of *Tsc2* resulted in morphological and molecular changes in OB granule cell neurons that could have impacts on neuron functionality (Figure 4.3, 4). These changes underscore the importance of *Tsc2* in NSCs and the crucial role it plays in the

development of mature neurons, i.e., neurogenesis. In order to parse apart the role that *Tsc2* plays in the development of neurons and the effect it has on already neuronal maturation, *Tsc2* was inactivated in post-mitotic mature neurons.

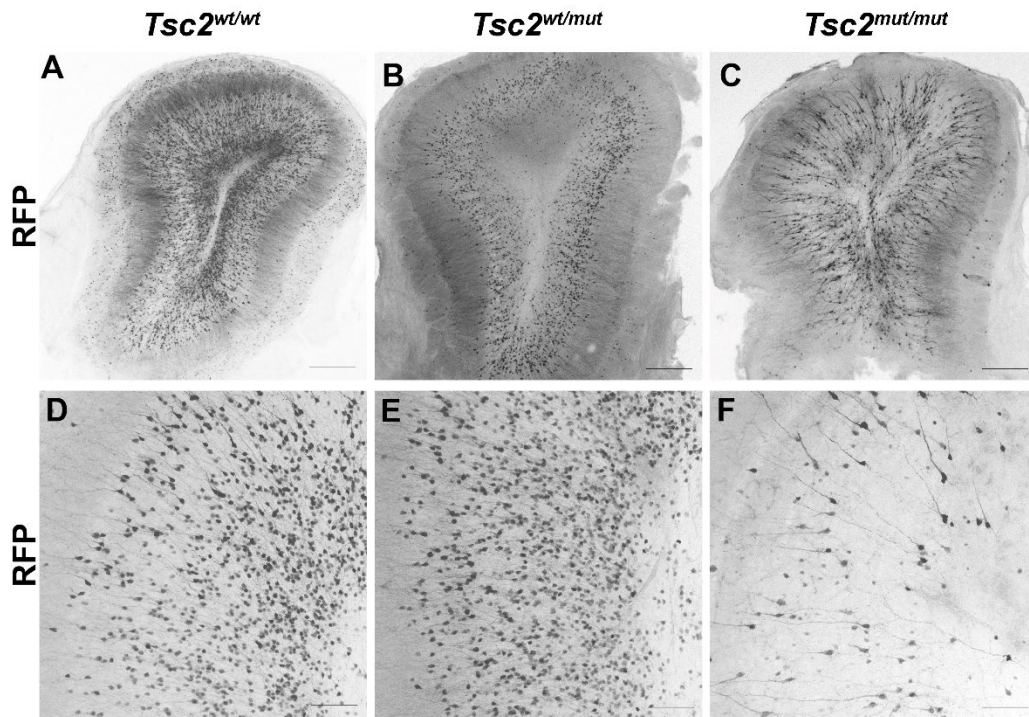


Figure 4.3 *OB morphology and organization is disrupted following Tsc2 inactivation*  
 A. 5X image of  $Tsc2^{wt/wt}$  OB, B. 5X image of  $Tsc2^{wt/mt}$  OB, C. 5X image of  $Tsc2^{mut/mt}$  OB, D. 20X image of  $Tsc2^{wt/wt}$  OB, E. 20X image of  $Tsc2^{wt/mt}$  OB, F. 20X image of  $Tsc2^{mut/mt}$  OB, Scale bar = 75  $\mu\text{m}$  (20X), 300  $\mu\text{m}$  (5X).

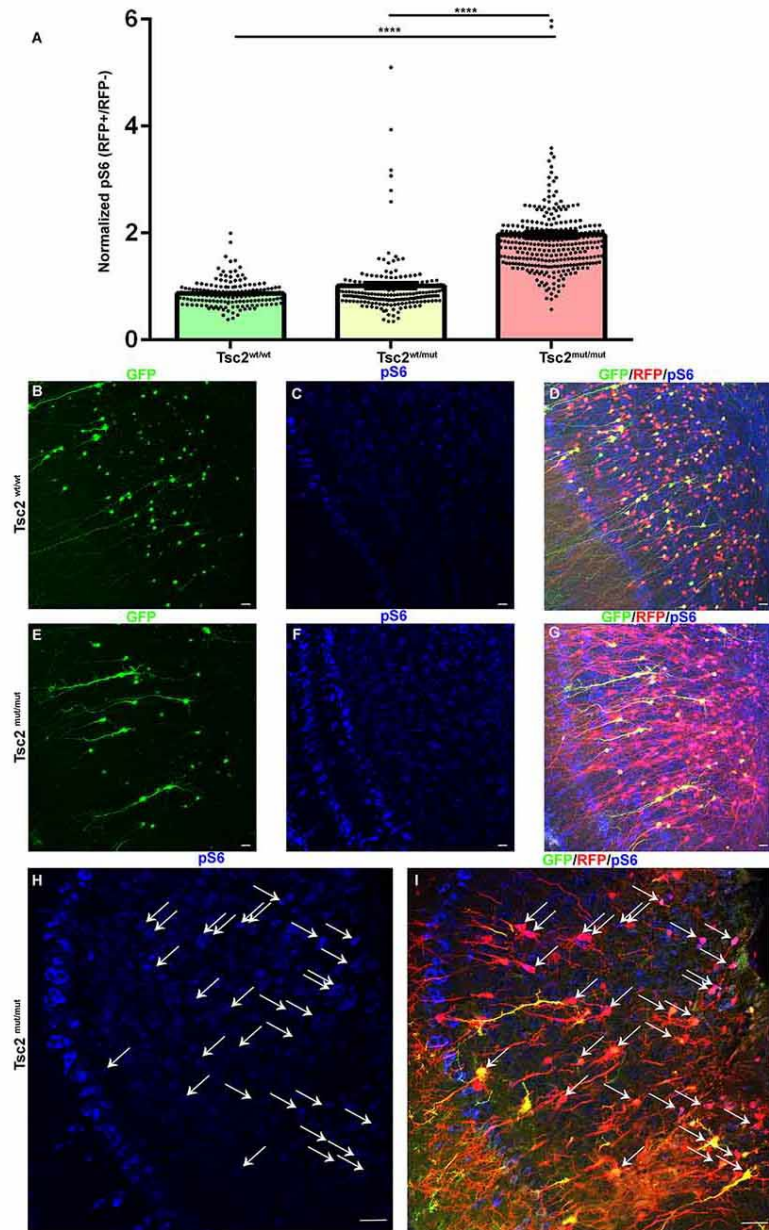


Figure 4.4 mTORC1 activity is increased in OB granule cells

A. Quantification of relative pS6 levels, B–I. 20× confocal images of coronal sections of OB GCs labeled with GFP (green) demonstrating recombination and expression of RFP (red), and pS6 staining (blue). Arrows indicate *Tsc2*<sup>mut/mut</sup> GCs with elevated pS6. \*\*\*\*= $p < 0.0001$ . Data are represented as mean  $\pm$  SEM. This analysis was performed by Dr. David Feliciano.

### *Tsc2 inactivation in mature OB neurons*

In order to assess the effects of *Tsc2* inactivation in already established neurons, neonatal mice were electroporated with plasmids containing CRE-ERT2 and GFP into Nestin-CRE-ERT2 inducible mice and injected them with tamoxifen at P30 (Figure 4.5.A, B). When mice are injected with tamoxifen in electroporated Nestin-CRE-ERT2 mice, it resulted in recombination in the V-SVZ NSCs as well as in electroporated OB granule cells that contained CRE-ERT2. Recombination in these cells resulted in labelled, fully developed neurons in the OB that had lost *Tsc2* after maturation as opposed to during development. The mature neurons would be co-labelled with RFP from genetic recombination as well as GFP from the original electroporation. This allowed for the ability to distinguish between neurons that had lost *Tsc2* during (RFP+ only) or after development (RFP+ and GFP+) (Figure 4.5.B, H). As a control, GFP/RFP double positive granule cells from GFP and tdTomato electroporations represent mature neurons retaining *Tsc2* (Figure 4.5.G).

### *Mature granule cell neurons are mostly unchanged following Tsc2 inactivation*

Following *Tsc2* inactivation in fully developed neurons at P30, mice were euthanized at P60 and their brains collected. mTORC1 signaling was assessed and pS6 activity was not changed in mature *Tsc2* null neurons when compared to controls (*Tsc2*<sup>wt/wt</sup>, n = 228 cells, N = 4 mice, mean = 2.155 ± 0.09378 vs. *Tsc2*<sup>mut/mut</sup>, n = 236 cells, N = 4 mice, Mean = 1.889 ± 0.1010, P = 0.0548, Figure 4.5.C). Similar pS6 levels in both mutant and control conditions could indicate that S6 is not readily

phosphorylated in these cells or that mTORC1 signaling is not hyperactive, further this finding could indicate that *Tsc2* and its regulation of mTORC1 may not be crucial in mature neurons. Similarly, mature granule cells had similar levels of dendritic arborization regardless of *Tsc2* activation (*Tsc2*<sup>wt/wt</sup>, n = 110 cells, N = 4 mice, mean =  $149.4 \pm 10.97$ , *Tsc2*<sup>mut/mut</sup>, n = 110 cells, N = 4 mice, Mean =  $168.8 \pm 9.743$ , P = 0.1867, Figure 4.5.E-F). Similar levels of dendritic arborization indicate that GCs of the OB are similarly patterned and likely have similar connectivity, though this is not measured in this analysis. Despite these similarities, there was a modest (5%) difference in soma size following *Tsc2* inactivation (*Tsc2*<sup>wt/wt</sup>, n = 881 cells, N = 4 mice, mean =  $58.34 \pm 0.6904$ , *Tsc2*<sup>mut/mut</sup>, n = 1,341 cells, N = 4 mice, Mean =  $55.56 \pm 0.5082$ , P = 0.0010, Figure 4.5.D). Taken together, this indicates that *Tsc2* and its regulation of mTORC1 signaling does not play or plays a minor role in the maintenance of neuron morphology once neurons are established in the OB.

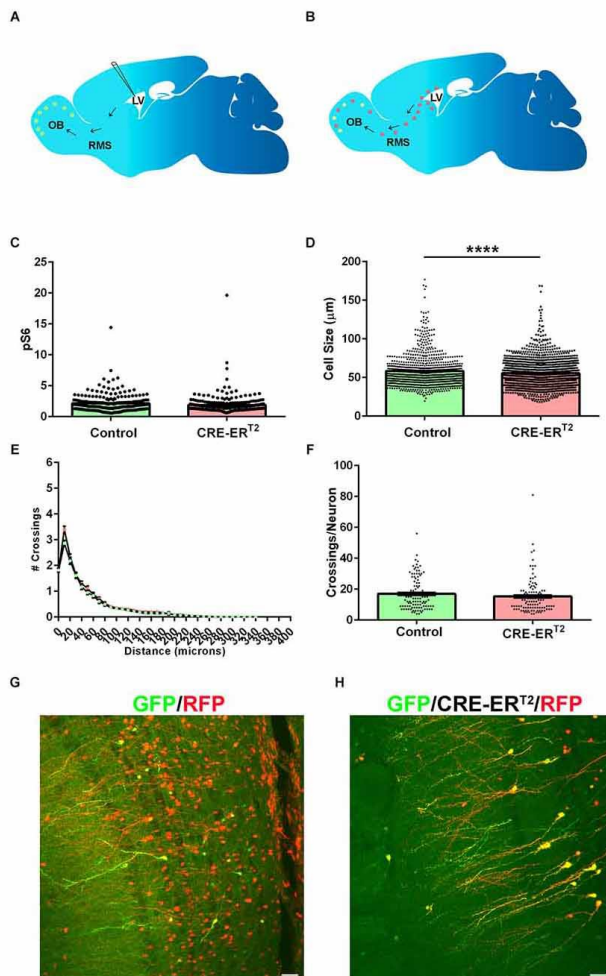


Figure 4.5 *Tsc2* was inactivated in mature granule cell neurons of the OB

A. Schematic diagram of neonatal electroporation and presence of GFP OB GCs prior to recombination at P30, B. Schematic diagram of neonatal electroporation with the presence of GFP and RFP positive OB GCs at P60 after P30 tamoxifen induced recombination, C. Quantification of pS6 expression in the OB at P60, *Tsc2*<sup>wt/wt</sup>, n = 228 cells, N = 4 mice, Mean = 2.155 ± 0.09378 vs. *Tsc2*<sup>mut/mut</sup>, n = 236 cells, N = 4 mice, Mean = 1.889 ± 0.0.1010, P = 0.0548, D. Quantification of cell size, *Tsc2*<sup>wt/wt</sup>, n = 881 cells, N = 4 mice, Mean = 58.34 ± 0.6904, *Tsc2*<sup>mut/mut</sup>, n = 1,341 cells, N = 4 mice, Mean = 55.56 ± 0.5082, P = 0.0010, E. Sholl analysis of *Tsc2*<sup>wt/wt</sup>, n = 110 cells, N = 4 mice, Mean = 149.4 ± 10.97 and *Tsc2*<sup>mut/mut</sup>, n = 110 cells, N = 4 mice, Mean = 168.8 ± 9.743, P = 0.1867, F. Quantification of the number of dendrite crossings per GC, G. RFP (red) and GFP (green) cells in OB GCs in control conditions, H. RFP (red) and GFP

(green) cells in OB GCs in CRE-ER<sup>T2</sup> conditions confirm recombination, \*\*\*\* =  $p < 0.0001$ . Data are represented as mean  $\pm$  SEM.

*Tsc2 mutant OBs show increased expression of transcripts associated with synaptic activity*

Given that *Tsc2* inactivation from NSCs resulted in aberrant neuron morphology, the molecular consequences of this difference were assessed using bulk RNA sequencing. Nestin-CRE-ERT2 mice were obtained as in Chapter 2. These mice were used to generate a global deletion of *Tsc2* in all NSCs and their progeny. This model was used in order to increase the proportion of cells that underwent recombination and therefore decrease the chance of contaminating wildtype cells in the dataset. Mice were injected with tamoxifen at P2 and P3 to induce recombination in Nestin<sup>+</sup> NSCs of the OB. Mice were euthanized at P60 and their OBs excised. RNA was then isolated from the whole OB and sequenced. Following differential expression analysis with DESeq2, samples were found to be related by condition and volcano plots demonstrated groups of significantly differently expressed transcripts between the two conditions (Figure 4.6. A, C). Significantly upregulated and downregulated transcripts in the OB following loss of *Tsc2* were visualized with heat maps. In all, 1,208 transcripts were differentially expressed (Figure 4.6.B,  $p < 0.05$ ). Of these differentially expressed genes, a subset of 51 significantly different ( $p_{adj} < 0.01$ ) were examined and found to be involved in the regulation of neuron death and calcium-dependent protein binding (Figure 4.6.D). This same subset of transcripts was used in a GO term analysis that used a curated set of transcripts associated with neuronal synapses called SynGO. SynGO analysis demonstrated potential changes in synapse organization, metabolism, transport, synaptic signaling, and processes in presynaptic and postsynaptic structure (Figure 4.6.E). These transcripts were then used in

network analysis to identify important nodes and node interactions (Figure 4.6.E). At the core of this network was *Homer1*, a mGluR coupling protein. Importantly, *Homer1* was also among the most highly expressed and significantly increased transcripts in the entire dataset (Figures 4.6 B, E). *Homer1* is a crucial part of the post synaptic density, a large protein complex that facilitates excitatory neuron synaptic activity and facilitates aspects of synaptic plasticity and dendritic spine formation (Bottai et al., 2001). This indicates that neuronal circuitry and synaptic plasticity may be altered following loss of *Tsc2*. Indeed, synaptic plasticity has been shown to be altered in TSC and the loss of *Tsc1* has previously been shown to cause an increase in immediate early gene expression in the hippocampus (Auerbach et al., 2011; Bateup et al., 2013; V. Costa et al., 2016; L.-H. Zeng et al., 2007).

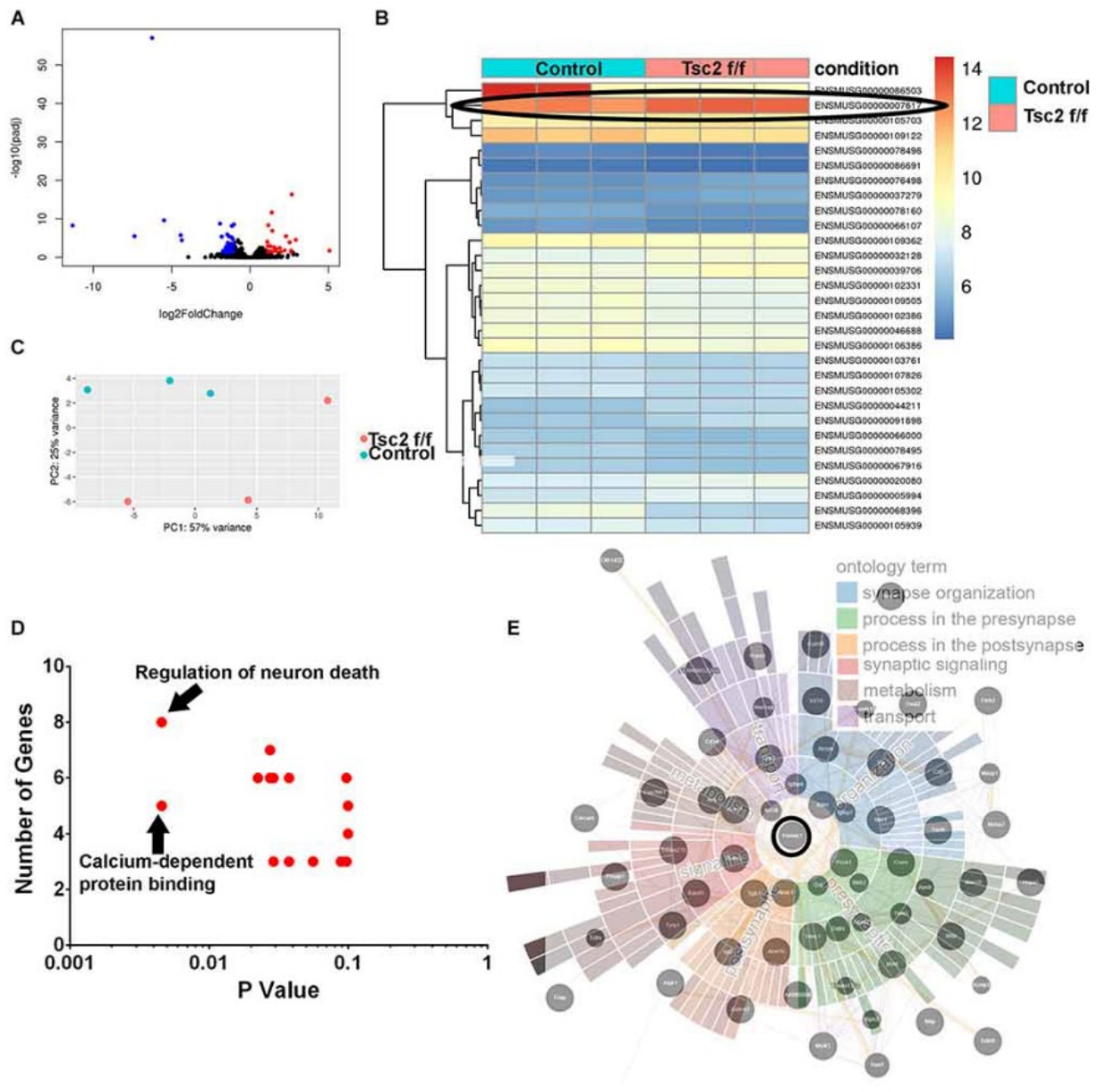


Figure 4.6 Bulk RNA sequencing of the *Tsc2* mutant OB

A. Volcano plot of RNA-seq of *Tsc2*<sup>wt/wt</sup> and *Tsc2*<sup>mut/mut</sup> OBs, Colored dots represent significantly enriched transcripts (red=upregulated, blue=downregulated) B. Heat map of RNA-seq data from *Tsc2*<sup>wt/wt</sup> and *Tsc2*<sup>mut/mut</sup>, C. PCA analysis of *Tsc2*<sup>wt/wt</sup> and *Tsc2*<sup>mut/mut</sup> OB RNA-seq data with (ENSMUSG000000007617=Homer1) circled, D. GO terms listed based on P-values and the total number of transcripts represented in terms are

differentially represented, E. Network analysis of differentially expressed transcripts with Homer1 circled and SynGo terms overlapping network nodes.

## Discussion

The role of *Tsc1* in OB granule cells (GCs) has been previously established (Feliciano et al., 2012; Zhou et al., 2011). In this chapter, the role of *Tsc2* was investigated. *Tsc2* mutations usually result in more severe symptoms of TSC and therefore it is worthwhile to investigate *Tsc2* independently. Loss of *Tsc2* resulted in disorganization as well as the upregulation of mTORC1 substrate pS6 in the inhibitory granule cells of the OB (Figure 4.3, 4.4). Additionally, the effect of losing *Tsc2* in mature post-mitotic neurons was measured. It was found that mature neurons that had lost *Tsc2* did not have increased pS6 expression or differences in dendritic arborization when compared to control mice but did have a minor increase in soma size in the mutant condition (Figure 4.5). This indicates that *Tsc2* is relatively unnecessary for mature granule cell morphological maintenance. This further implies that *Tsc2* is potentially critical for a tightly regulated developmental window wherein morphological characteristics such as soma size and dendritic arborization are determined. This means that full functional loss of *Tsc2* at different developmental stages could result in the variable presentation commonly seen in TSC. By studying these different developmental stages, crucial time points may be elucidated that can be investigated more fully, leading to potential insights into the pathogenicity of TSC and possible new mechanisms of therapeutics and the timing of therapeutic delivery.

Given that there were not many morphological changes to the GCs in the OB, GCs that were developed after *Tsc2* loss in NSCs were examined further. RNA sequencing was performed in order to investigate the effects of *Tsc2* loss in NSCs on

inhibitory neurons of the OB. Differential expression and GO term analysis showed that the most significantly differentially expressed transcripts in the mutant OB had terms associated with synapse organization, metabolism, transport, synaptic signaling, and processes in presynaptic and postsynaptic structure. One such transcript was *Homer1*. *Homer1* exists in multiple isoforms that have different effects in the cell. *Homer1a* is an immediate early gene that acts as dominant negative isoform that upon binding to mGluR causes mGluR dissociation from the post synaptic density and the constitutive activation of mGluR signaling even in the absence of glutamate (Bottai et al., 2001). *Homer1a* competes for binding of mGluR with the other isoforms of *Homer1*, *Homer1b* and *Homer1c* which are constitutively active, dimerize, and bind to mGluR to facilitate downstream signaling in the presence of glutamate. Therefore, the *Homer1a* isoform functions to swiftly modulate the activity of the post synaptic density, synaptic function, and multiple forms of synaptic plasticity (Bottai et al., 2001). *Homer1* and other proteins of the post-synaptic density have previously been implicated in the etiology of non-syndromic autism spectrum disorders and intellectual delay and may also contribute to TSC neuropsychiatric phenotypes (Kelleher et al., 2012). Indeed, altered synaptic plasticity has been seen in human TSC patients (Auerbach et al., 2011; Bateup et al., 2013; V. Costa et al., 2016; L.-H. Zeng et al., 2007). Similarly, *Homer1* and other synaptic proteins could contribute to altered synaptic activity and expression in the murine olfactory bulb and TSC brains, potentially contributing to symptoms such as epilepsy. It remains to be seen whether the morphological changes in the OB are causal or consequential to increased activity. However, this abnormal activity could have further

implication for the neuropsychiatric manifestations of TSC and future studies are needed to determine the pathological significance and cellular specificity.

It has previously been shown that activation of the mTORC1 pathway in neurons can result in seizure activity in multiple brain regions in a non-cell autonomous fashion (McMahon et al., 2015). This could potentially contribute to the severe symptoms of TSC and global effects despite the small number of cells affected. In this chapter, electroporation resulted in focal deletion of *Tsc2* from a small subset of cells, mimicking TSC in patients. Interestingly, focal deletion resulted in large, obvious phenotypes, such as the disorganization of the OB, which were minimally observed in the global model of TSC using Nestin-CRE-ER<sup>T2</sup> (Figure 4.3). It is unclear if these phenotypes are nonexistent in the global model or if the level of severity resulting from the number of affected cells occludes the observation. Another possibility to explain this phenomenon is that the hyperactivation of mTORC1 signaling in neurons requires significant amounts of nutrients and signaling molecules which are scarcer in a global model due to demand. This lack of resources could potentially prevent more intense phenotypes from occurring.

Taken together, this chapter demonstrates the importance of *Tsc2* in the development and regulation of olfactory bulb granule cell neurons including morphological characteristics and synaptic activity. This regulation seems to take place during a specific developmental time window, underscoring the role that *Tsc2* plays in development, NSCs, and neurogenesis. The alterations noted here could have far-reaching implications for the neurological presentations of TSC and further studies need to be undertaken to measure direct contributions.

## Methods

Animals. Clemson University Institutional Animal Care and Use Committee approved experiments, and all guidelines set forth by the Clemson University Institutional Animal Care and Use Committee and were compliant with the Animal Care and Use Review Office (ACURO), a component of the USAMRDC Office of Research Protections (ORP) within the Department of Defense (DoD). Red fluorescent protein (RFP<sup>+/-</sup>, <sup>+/+</sup>) (B6. CgGt (ROSA)26Sortm9 (CAG-tdTomato)<sup>Hze/J</sup>) (Strain #007909), C57BL/6-Tg (Nes-Cre/ERT2)<sup>K<sup>Eisc</sup>/J</sup> (Strain #:016261), *Tsc2*<sup>tm1.1Mjg/J</sup> (Strain #027458) were acquired from Jackson Laboratories. Mice were housed under pathogen-free conditions with a 12-h light/dark cycle and fed ad libitum.

PCR. The tissue was incubated in 50 mM NaOH and 0.2 mM EDTA at 50°C overnight. An equal volume of 100 mM Tris-HCl was added to samples. Samples were subject to routine genotyping using Taq DNA Polymerase with the following conditions: Initial denaturation step at 98°C for 2 min, followed by 35 cycles of denaturation at 95°C for 30 s, an annealing step at 60°C for 30 s, and an extension at 72°C for 30 seconds followed by a final extension at 72°C for 3 min. Samples were loaded onto a 1.7% agarose gel with 1X Blue Juice and run at 100 V for 20–30 mins. Mice having conditional *Tsc2* alleles are distinguished by endpoint genotyping PCR using the following primer sequences, 5'-ACAATGGGAGGCACATTACC-3' and 5'-AAGCAGCAGGTCTGCAGTG-3'. Tomato (RFP) genes were identified for Stock #7914 using the following primer sequences, 5'-AAGGGAGCTGCAGTGGAG TA-3' and 5'-CCGAAAATCTGTGGGAAG TC-3' and

5'-GGCATTAAAGCAGCGTATCC-3' and 5'CTGTTCCGTACGGCATGG-3'. *Nestin-CRE-ER<sup>T2</sup>* mice were genotyped with 5'ATGCAGGCAAATTTTGGTGT-3' and 5'-CGCCGCTACTTCTTTTCAAC-3' or 5'ATACCGGAGATCATGCAAGC-3' and 5'-GGCCAGGCTGTTCTTCTTAG-3' and 5' CTAGGCCACAGAATTGAAAGATCT-3' (Internal Positive Control) and 5' GTAGGTGGAAATTCTAGCATCATCC-3' (Internal Positive Control). Long-range PCR was performed as previously described.

Electroporation and Tamoxifen injection. Neonatal mice were electroporated as previously described. Mouse pups were injected with equal concentrations and volumes of DNA plasmids diluted in phosphate buffered saline (PBS) with 0.1% fast green. Electroporated plasmids are as follows; CAG-CRE (Plasmid #13775, Addgene) and CAG-GFP (Plasmid #11150, Addgene). DNA was injected into the lateral ventricles and delivered using a borosilicate glass micropipette generated from pulled capillary tubes. Borosilicate capillary tubes were pulled with a P97 Sutter micropipette puller. Tweezer electrodes (model 520; BTX) were rinsed in 0.9% saline solution and swept over the head of neonatal pups using five, 100-volt square pulses of 50 ms duration with 950-ms intervals that were applied using a pulse generator (ECM830; BTX). *Nestin-CRE-ERT2* mouse pups were weighed and injected with approximately 20 µg/g (Z)-4-Hydroxytamoxifen (Sigma Aldrich, #H7904).

Immunohistochemistry. Euthasol® was administered by intraperitoneal injection to sedate mice followed by swift decapitation. Brains were dissected in room temperature

PBS, transferred to 4% paraformaldehyde (in PBS), and incubated overnight at 4°C. Brains were rinsed in PBS and mounted in 3% agarose. A Leica VTS 1000 vibratome was used to slice brains coronally in 150-300 µm sections. Sections were blocked in PBS containing 0.1% Triton X-100, 0.1% Tween-20 and 2% BSA for 1 hour at room temperature. Sections were washed in PBS containing 0.1% Tween-20 three times. Sections were incubated in primary antibody; anti-Dcx (1:500; Santa Cruz Biotechnology sc-8066 and sc-271390), anti-Sox2 (1:500; Invitrogen 14-9811-82) anti-pS6 (1:500; Cell Signaling Technology; Ser 240/244, 61H9, #4838), anti-Nestin (1:500; Novus Biologicals; #NB100-1604), anti-p4EBP (1:500; Cell Signaling Technology; Thr37/46, 236B4; #2855), anti-glutamine synthetase (1:500; Sigma Aldrich; #G2781), and anti-NeuN (1:500; Sigma Aldrich; #MAB377) overnight at 4°C. Sections were subjected to three additional washes in PBS containing 0.1% Tween-20. Sections were incubated with the appropriate secondary antibody (Alexa Fluor series; 1:500; Invitrogen) overnight at 4°C. Sections were mounted in ProLong Antifade Mountant (Thermo Fisher). Each staining was replicated on the indicated number of mice per condition. Images were acquired on a spectral confocal microscope (Leica SPE) with a ×20 dry objective (N.A. 0.75). Low-magnification images were acquired with ×10 dry or a ×5 dry (N.A. 0.15) objective.

Image Analysis. Images (×20) of RFP positive cells were uploaded to FIJI (ImageJ 1.5 g). The freehand selection tool was used to trace a region of interest (ROI) on electroporated and non-electroporated cells in the same Z section and a mean gray value

measured to quantify the staining intensity of phospho-S6 and normalized. Ratios of staining in electroporated and non-electroporated cells were compared for RFP positive cells in  $Tsc2^{wt/wt}$  and  $Tsc2^{mut/mut}$  conditions to account for immunohistochemical variation. All values were normalized to the average intensity of the ratio of electroporated divided by non-electroporated cells in  $Tsc2^{wt/wt}$  conditions.

Images ( $\times 20$ ) were used to measure dendrite morphology. Images were uploaded as described above and Simple Neurite tracer plug-in was used to trace dendrite processes of RFP positive cells. Sholl analysis was performed at 10  $\mu\text{m}$  intervals to quantify dendrite arborization using the Sholl plug-in. The total number of dendritic crossings were calculated by taking the sum of crossings at 10  $\mu\text{m}$  intervals for each traced neuron and averaging the total number of crossings per neuron in each condition.

Images of the OB were uploaded to FIJI and subject to a custom macro or traced by hand using the freehand selection tool. Briefly, results were cleared, channels were split, and a maximum Z projection of RFP was made. Automated thresholding using Renyi Entropy was performed with images inverted and resulting binary image subjected to binary watershed. Resulting binary images were subject to particle analysis using custom settings (size = 20–400 circularity = 0.5–1.00) to only capture somas and the size and number of particles were saved along with drawing of particles. The size of particles was used for quantification of soma size in the OB(Riley et al., 2022).

Measurements were made on original image files without enhancements. Figures were created by converting LIF files into TIFF format images using FIJI. Images were uploaded into Photoshop (Adobe, version 2022). Merged images containing multiple fluorophores were subject to brightness and contrast changes and RGB levels were optimized. Changes were applied across the entirety of each image. For individual-colored images, the RGB images were duplicated, and individual colors were removed. To make black and white images, the RFP channel was converted to gray scale and inverted.

RNA sequencing. OBs (two for each mouse, from three mice each condition) were collected and homogenized in 500  $\mu$ l TRIzol reagent (ThermoFisher). Samples were incubated for 5 min at 4°C and 100  $\mu$ l chloroform was subsequently added. Samples were centrifuged for 15 min at 12,000 $\times$  g at 4°C and the aqueous layer was collected and transferred to a 1.5 ml centrifuge tube. 250  $\mu$ l of isopropanol was added to samples and incubated for ten minutes at 4°C. The samples were centrifuged for ten minutes at 12,000 $\times$  g at 4°C and the supernatant discarded. Pellets were resuspended in 500  $\mu$ l 75% ethanol and vortexed before being centrifuged for 5 min at 7,500 $\times$  g at 4°C. Pellets were allowed to dry and rehydrated in 35  $\mu$ l of RNase free ultrapure water. Samples were incubated at 60°C for 15 min to complete RNA isolation. RNA concentrations and purity were assessed using a NanoDrop Lite Spectrophotometer (Thermo Scientific). Sample quantity and RIN values were determined.

RNA concentration, RNA quality, library preparation, and some bioinformatic analyses were performed by Azenta Life Sciences. RNA concentration and quality was verified by Qubit assay and Agilent TapeStation analysis which confirmed RNA integrity. Libraries were prepared using NEBNext Ultra RNA Library Preparation Kit according to the manufacturer's protocol (New England Biolabs). Samples were sequenced using 150 base pair end reads on an Illumina HiSeq. Read adapter sequences and nucleotides with poor quality were trimmed using Trimmomatic 0.36 and mapped to the *Mus musculus* GRCm38 reference genome available on ENSEMBL using the STAR aligner. 98.28% of reads were mapped with an average quality Q score of 35.69. 402,490,214 reads over the six samples had an average of 66,000,935 reads per sample. RNA sequencing aligner was executed using splicing aligner. The subread package was used to calculate unique exon hit counts. Unique exon hit counts were analyzed using differential expression analysis (DESeq2) and differential splice variant expression (DEXseq) analysis. Correlation between samples and treatment was performed by PCA plot. A heatmap of the top 30 genes based on p-adjusted value were subject to bi-cluster analysis to check for correlation between samples. The Feliciano lab performed the following bioinformatic analyses. Gene ontology analysis was performed by implementing GeneSCF, gene networks were identified by Cytoscape 3.60 using Genemania, and SynGO analysis was performed as previously described (Morton et al., 2018).

Statistics. Data were graphed and analyzed with GraphPad Prism software (Version 8.2.0, GraphPad Software Inc.). Statistical significance was determined by Student's t-test

(tamoxifen experiments), one-way analysis of variance (ANOVA; ROI and total number of crossings analysis) with multiple comparisons test, or two-way ANOVA with Tukey's multiple comparisons test (Sholl analysis). All experiments were performed on 4–11 mice per condition per time point. N (number of mice) and n (number of cells) are listed where applicable. Error bars are reported as standard error mean.

## CHAPTER FIVE

### Conclusion

#### Discussion

The purpose of the work presented here was to provide insight into *Tsc2* activity during neurogenesis using the developmental disorder, Tuberous Sclerosis Complex. *Tsc2* regulates mTORC1 signaling which can play a key role in neural stem cell (NSC) biology and facilitate the transition of NSC cell states. In TSC, decreased mTORC1 signaling is prevented and NSCs are aberrantly affected. In this work, the transcriptome and translome of *Tsc2* null NSCs was examined and it was found that transcripts primarily associated with translation were affected in both datasets. This indicated that the most highly altered processes in TSC NSCs are likely those associated with translation which can have downstream effects on protein production, cell identity, and development. Additionally, translational regulation was found to be disrupted wherein mRNA transcripts were differentially translated in *Tsc2* null mice when compared to wildtype, meaning that some transcripts appeared to be variably translated depending on condition. This phenomenon varied across transcripts and did not appear to have a specific trend indicating the vast and precise role that *Tsc2* expression plays in NSCs. The disconnect of transcription and translation regulation resulted in differences in translational efficiency for different mRNA transcripts and could potentially have resulted in the retention of NSC transcripts in otherwise mature cells.

Mouse models of TSC have shown that NSCs and their progeny are aberrant in the disorder. In TSC, subependymal nodules (SENs), subependymal giant cell

astrocytomas (SEGAs), astrocytes, and giant cells all have been shown to express markers of immaturity including the stem cell markers: nestin, BLBP, Tbr2, and vimentin (Ess et al., 2004; Goto et al., 2011; Magri et al., 2011; Uhlmann, Wong, et al., 2002; Way et al., 2009). As previously stated, it has been shown that there is a decrease in mTORC1 signaling preceding differentiation in wildtype conditions which is not possible in cells with inactivated TSC genes (Blair et al., 2018). This was exemplified in a cerebral organoid model of TSC. When TSC null organoids are prompted to differentiate, they are unable to downregulate the stem cell marker, Nestin during differentiation (Zordan et al., 2018). This could be an example of certain stem-like proteins that remain within the cell following loss of *Tsc2*. The retention of unwanted stem like features could have considerable influence on TSC pathology and contribute to growth formation and progression.

Indeed, when the consequences of *Tsc2* loss were examined *in vivo* it was discovered that mice had large striatal hamartomas that contained Sox2<sup>+</sup> and Nestin<sup>+</sup> cells, indicating their potential stem-like nature. These markers have previously been seen in SEGA samples and indicate that striatal hamartomas were reminiscent of SEGAs. Further the striatal lesions were heterogenous containing cells positive for DCX, NeuN, and GS, possibly indicating that active neuro- and gliogenesis is taking place in the striatum. Though future studies must be done to verify that this is actually occurring.

In addition to the striatal hamartomas, *Tsc2* loss from perinatal NSCs resulted in the acquisition of phenotypes characteristic of TSC including giant cells and ectopic cytomegalic neurons. Cytomegalic neurons were found at a higher quantity in the *Tsc2*

null condition when compared to control conditions which could have impacts on striatal neuronal circuitry and functionality. Giant cells and cytomegalic, ectopic neurons are pathognomic for TSC and provide evidence that these mouse models are representative of TSC pathology.

Given the effects that *Tsc2* loss had on striatal neurogenesis, the typical end site of neurogenesis in the ventricular-subventricular zone (V-SVZ) was also examined: the OB. Like the V-SVZ and striatum, the OB was disorganized and contained cytomegalic neurons with increased pS6 activity. Transcriptomic profiling of the OB showed that the mutant condition had increased levels of mRNA associated with synaptic activity, including the immediate early gene, *Homer1*. This agrees with prior studies that have shown that loss of TSC genes can alter synaptic activity in the cortex and hippocampus, indicating that some aspects of the effects of *Tsc2* loss in inhibitory neurons may be universal. Alterations in synaptic activity could have numerous implications for TSC including contributions to epileptogenesis and the development of neuropsychiatric manifestations. Looking further at the impact of TSC on synaptic activity and the regulation of early response genes will be important for future studies. Additionally, these sequencing results have shown that loss of *Tsc2* in NSCs has far reaching effects on neurogenesis and neural activity.

Currently in the TSC field, there has been debate about whether LOH is necessary for symptoms of TSC, including SEGA. Throughout this work it was shown that *Tsc2* was required to be inactivated in both alleles in order to generate phenotypes typical of TSC. Indeed, for the majority of analyses in the OB, it was shown that monoallelic

inactivation was insufficient to generate phenotypes significantly different from the wildtype condition. Striatal hamartomas were also a result of biallelic inactivation of *Tsc2* in NSCs and did not form in any heterozygote or wildtype mouse observed, indicating that biallelic inactivation is necessary for TSC murine growth formation. LOH has previously been noted in TSC hamartomas and this work provides supporting evidence that biallelic inactivation is required for growth formation. However, it should be noted that LOH in TSC and the biallelic inactivation presented here are not identical in mechanism. In TSC, patients are commonly born with a germline heterozygous mutation and it is upon somatic inactivation of the second allele that hamartoma formation takes place (Bongaarts et al., 2017; Crino et al., 2010; Kwiatkowski et al., 2004). This contrasts with this work where *Tsc2* is lost in neural stem cells in both alleles simultaneously. Therefore, this model does not examine the effects of biallelic inactivation in a heterozygous background or the contributions of that heterozygosity to disorder phenotypes. It is unclear what the implication of different modes of biallelic inactivation may be and further studies are needed to delineate these processes.

NSCs result in the production of neurons and astrocytes. Therefore, it is often questioned whether it is the NSCs that contribute to TSC pathology or their progeny. To investigate this further, the effect of *Tsc2* loss in mature neurons was examined. Loss of *Tsc2* from mature neurons resulted in no drastic phenotypes with the exception of a slight but significant increase in soma size (Figure 4.5.D). This indicates that *Tsc2* loss is potentially not required for neuronal maintenance and results in more dramatic phenotypes when lost from progenitor cells. It is possible that when *Tsc2* is lost in

progenitor cells, it results in more cell types ultimately being affected or it could indicate that *Tsc2* is more crucial in NSCs when compared to other cell types. Astrocytes were not investigated in this study and should be examined in the future.

Similarly, it should be noted that during electroporation, all cells of the lateral ventricle will be targeted and theoretically lose *Tsc2* functionality. This means that multiple cell types are affected and could potentially contribute to the phenotypes seen in *Tsc2<sup>mut/mut</sup>* brains. The vast majority of cells that line the lateral ventricle at postnatal day one are NSCs making it likely that NSCs are the primary cell type affected and contributing to striatal hamartoma formation (Doetsch et al., 1997). However, this work does not delineate between different cell types and their role in this process nor does it preclude the notion that multiple cell types are contributing to the observed phenomenon. Similarly, different types of striatal hamartomas occurred and manifested in different regions of the striatum, potentially indicating multiple cells of origin for growths in TSC. Additionally, loss of TSC genes in neural progenitor cells has been shown previously to result in growth formation, making it likely that our model inactivates *Tsc2* in these cells (Feliciano et al., 2011, 2012; Magri et al., 2013; Zhou et al., 2011).

The findings discussed here demonstrate the importance of *Tsc2* in neurogenesis. However, it should be noted that there are limitations to this work. In this work, it is shown that loss of *Tsc2* results in altered regulation of translation and transcription in NSCs. This led to the hypothesis that NSCs in the V-SVZ are retaining stem cell like transcripts that “confuse” cell identity and possibly contribute to aberrant neurogenesis

and hamartoma formation. However, the exact mechanisms behind this and what contributes to these phenotypes still need to be elucidated.

Further, this study was done on proliferating activated NSCs that were kept in an enriched media. NSCs in media are not necessarily representative of *in vivo* NSCs and do not necessarily undergo the same developmental processes. Similarly, *Tsc2* and mTORC1 may not behave similarly in all cell types and SEGAs do not present with high rates of proliferation (Rushing et al., 2019). This means that our observations on dividing NSCs are limited and may not have any forbearance on other types of cells or neural stem cell states. At the time of the experiment, no NSCs should be present in the striatum. However, cells in the mutant condition express stem cell markers in striatal hamartomas. This indicates that in the case of hamartomas, stem cell identity seems to be retained and points to the more widespread applicability of our model.

Similarly, in the *Tsc2<sup>mut/mut</sup>* brains, there is evidence of striatal hamartomas, giant cells, disorganization, and cytomegalic heterotopic neurons. While these malformations arose from the inactivation of *Tsc2*, the mechanism of generation of these phenotypes or why they occur in some mutant brains but not others were not investigated. This is likely due to a specific cell type or state that is being targeted by electroporation in some mice but not others. In order to circumvent this limitation in the future, studies must be done to narrow down the specific cell type responsible for the generation of these phenotypes.

SEGAs are generally removed from within the lateral ventricles of the brain near the Foramen of Monro (Crino, 2010). However, this does not indicate that SEGAs necessarily initiate in these areas. Instead, SEGAs often appear to originate in the

parenchyma of the brain and SEGAs grow toward the ependymal lining and V-SVZ resulting in their typical ventricular presentation. In our models this was recapitulated and hamartomas formed within the striatum adjacent to the V-SVZ. The evidence that striatal hamartomas and SEGAs represent the same phenomenon include shared transcriptomic profiles, a mixed glial-neuronal composition, the presence of immature and mature cells, and the necessity of biallelic inactivation for development. Further, SEGAs have been noted in other brain regions besides the Foramen of Monro, including the frontal lobe, lateral ventricle, and third ventricle (Bollo et al., 2009; Bongaarts et al., 2022; Jiang et al., 2017). They have also been characterized in the basal ganglia which includes the striatum (Işık et al., 2010). Taken altogether, it is likely that striatal hamartomas are partially representative of SEGAs and this model is useful for the study of TSC and SEGAs-genes.

In addition to SEGAs-genes, this model can be utilized to study giant cells, ectopic neurons, and translational regulation. It could also be useful to study new treatment modalities, as more insight into the mechanisms behind the pathogenicity of TSC will generate new ideas surrounding what to treat as well as how and when to treat it. In the future, using this model, the cells of origin of the striatal hamartomas should be investigated as well as the mechanisms behind growth formation. Other abnormalities seen in the mice should also be investigated such as the heterotopic neurons and giant cells. These are typical presentations of TSC and valuable information could be gleaned from this model. Functional studies of striatal and OB neurons should also be performed and their influence on circuitry and behavior examined.

Taken altogether, this thesis shows that *Tsc2* plays a role in the regulation of neurogenesis through its downstream effects on translation. *Tsc2* inactivation is detrimental in NSCs where regulation of translation is important for development and could be responsible for the abnormalities, such as striatal hamartomas, seen in the *Tsc2*<sup>mut/mut</sup> condition.

## REFERENCES

- Adriaensen, M. E. A. P. M., Schaefer-Prokop, C. M., Stijnen, T., Duyndam, D. A. C., Zonnenberg, B. A., & Prokop, M. (2009). Prevalence of subependymal giant cell tumors in patients with Tuberous Sclerosis and a review of the literature. *European Journal of Neurology*, *16*(6), 691–696. <https://doi.org/10.1111/j.1468-1331.2009.02567.x>
- Anlauf, E., & Derouiche, A. (2013). Glutamine Synthetase as an Astrocytic Marker: Its Cell Type and Vesicle Localization. *Frontiers in Endocrinology*, *4*. <https://doi.org/10.3389/fendo.2013.00144>
- Au, K. S., Hebert, A. A., Roach, E. S., & Northrup, H. (1999). Complete Inactivation of the TSC2 Gene Leads to Formation of Hamartomas. *American Journal of Human Genetics*, *65*, 1790–1795.
- Auerbach, B. D., Osterweil, E. K., & Bear, M. F. (2011). Mutations causing syndromic autism define an axis of synaptic pathophysiology. *Nature*, *480*(7375), 63–68. <https://doi.org/10.1038/nature10658>
- Basak, O., Krieger, T. G., Muraro, M. J., Wiebrands, K., Stange, D. E., Frias-Aldeguer, J., Rivron, N. C., van de Wetering, M., van Es, J. H., van Oudenaarden, A., Simons, B. D., & Clevers, H. (2018). Troy+ brain stem cells cycle through quiescence and regulate their number by sensing niche occupancy. *Proceedings of the National Academy of Sciences of the United States of America*, *115*(4), E610–E619. <https://doi.org/10.1073/pnas.1715911114>
- Baser, A., Skabkin, M., Kleber, S., Dang, Y., Gülcüler Balta, G. S., Kalamakis, G., Göpferich, M., Ibañez, D. C., Schefzik, R., Lopez, A. S., Bobadilla, E. L., Schultz, C., Fischer, B., & Martin-Villalba, A. (2019). Onset of differentiation is post-transcriptionally controlled in adult neural stem cells. *Nature*, *566*(7742), 100–104. <https://doi.org/10.1038/s41586-019-0888-x>
- Baser, A., Skabkin, M., & Martin-Villalba, A. (2017). Neural stem cell activation and the role of protein synthesis. *Brain Plasticity*, *3*(1), 27–41. <https://doi.org/10.3233/bpl-160038>
- Bateup, H. S., Johnson, C. A., Denefrio, C. L., Saulnier, J. L., Kornacker, K., & Sabatini, B. L. (2013). Excitatory/Inhibitory Synaptic Imbalance Leads to Hippocampal Hyperexcitability in Mouse Models of Tuberous Sclerosis. *Neuron*, *78*(3), 510–522. <https://doi.org/10.1016/j.neuron.2013.03.017>
- Batista-Brito, R., Close, J., Machold, R., & Fishell, G. (2008). The distinct temporal origins of olfactory bulb interneuron subtypes. *Journal of Neuroscience*, *28*(15), 3966–3975. <https://doi.org/10.1523/jneurosci.5625-07.2008>
- Battle, E., & Clevers, H. (2017). Cancer stem cells revisited. In *Nature Medicine* (Vol. 23, Issue 10, pp. 1124–1134). Nature Publishing Group. <https://doi.org/10.1038/nm.4409>
- Benvenuto, G., Li, S., Brown, S. J., Braverman, R., Vass, W. C., Cheadle, J. P., Halley, D. J., Sampson, J. R., Wienecke, R., & DeClue, J. E. (2000). The Tuberous Sclerosis-1 (TSC1) gene product hamartin suppresses cell growth and augments the

- expression of the TSC2 product tuberlin by inhibiting its ubiquitination. *Oncogene*, *19*, 6306–6316.
- Beretta, L., Gingras, A. C., Svitkin, Y. V., Hall, M. N., & Sonenberg, N. (1996). Rapamycin blocks the phosphorylation of 4E-BP1 and inhibits cap-dependent initiation of translation. *EMBO Journal*, *15*(3), 658–664. <https://doi.org/10.1002/j.1460-2075.1996.tb00398.x>
- Blair, J. D., Hockemeyer, D., & Bateup, H. S. (2018). Genetically engineered human cortical spheroid models of Tuberous Sclerosis. *Nature Medicine*, *24*(10), 1568–1578. <https://doi.org/10.1038/s41591-018-0139-y>
- Blair, J. D., Hockemeyer, D., Doudna, J. A., Bateup, H. S., & Floor, S. N. (2017). Widespread translational remodeling during human neuronal differentiation. *Cell Reports*, *21*(7), 2005–2016. <https://doi.org/10.1016/j.celrep.2017.10.095>
- Boer, K., Crino, P. B., Gorter, J. A., Nellist, M., Jansen, F. E., Spliet, W. G. M., Van Rijen, P. C., Wittink, F. R. A., Breit, T. M., Troost, D., Wadman, W. J., & Aronica, E. (2010). Gene expression analysis of Tuberous Sclerosis Complex cortical tubers reveals increased expression of adhesion and inflammatory factors. *Brain Pathology*, *20*(4), 704–719. <https://doi.org/10.1111/j.1750-3639.2009.00341.x>
- Bollo, R. J., Berliner, J. L., Fischer, I., Miles, D. K., Thiele, E. A., Zagzag, D., & Weiner, H. L. (2009). Extraventricular subependymal giant cell tumor in a child with tuberous sclerosis complex. *Journal of Neurosurgery: Pediatrics*, *4*, 85–90.
- Bongaarts, A., Giannikou, K., Reinten, R. J., Anink, J. J., Mills, J. D., Jansen, F. E., Spliet, W. G. M., Den Dunnen, W. F. A., Coras, R., Blümcke, I., Paulus, W., Scholl, T., Feucht, M., Kotulska, K., Jozwiak, S., Buccoliero, A. M., Caporalini, C., Giordano, F., Genitori, L., ... Aronica, E. (2017). Subependymal giant cell astrocytomas in Tuberous Sclerosis Complex have consistent TSC1/TSC2 biallelic inactivation, and no BRAF mutations. *Oncotarget*, *8*(56), 95516–95529. [www.impactjournals.com/oncotarget](http://www.impactjournals.com/oncotarget)
- Bongaarts, A., Mijnsbergen, C., Anink, J. J., Jansen, F. E., Spliet, W. G. M., den Dunnen, W. F. A., Coras, R., Blümcke, I., Paulus, W., Gruber, V. E., Scholl, T., Hainfellner, J. A., Feucht, M., Kotulska, K., Jozwiak, S., Grajkowska, W., Buccoliero, A. M., Caporalini, C., Giordano, F., ... Aronica, E. (2022). Distinct DNA Methylation Patterns of Subependymal Giant Cell Astrocytomas in Tuberous Sclerosis Complex. *Cellular and Molecular Neurobiology*, *42*(8), 2863–2892. <https://doi.org/10.1007/s10571-021-01157-5>
- Bongaarts, A., Van Scheppingen, J., Korotkov, A., Mijnsbergen, C., Anink, J. J., Jansen, F. E., Spliet, W. G. M., Den Dunnen, W. F. A., Gruber, V. E., Scholl, T., Samuelli, S., Hainfellner, J. A., Feucht, M., Kotulska, K., Jozwiak, S., Grajkowska, W., Buccoliero, A. M., Caporalini, C., Giordano, F., ... Aronica, E. (2020). The coding and non-coding transcriptional landscape of subependymal giant cell astrocytomas. *Brain*, *143*(1), 131–149. <https://doi.org/10.1093/brain/awz370>
- Bottai, D., Guzowski, J. F., Schwarz, M. K., Kang, S. H., Xiao, B., Lanahan, A., Worley, P. F., & Seeburg, P. H. (2001). Synaptic Activity-Induced Conversion of Intronic to Exonic Sequence in Homer 1 Immediate Early Gene Expression. *The Journal of Neuroscience*.

- Carbonara, C., Longa, L., Grosso, E., Mazzucco, G., Borrone, C., Garrè, M. L., Brisigotti, M., Filippi, G., Scabar, A., Giannotti, A., Falzoni, P., Monga, G., Garini, G., Gabrielli, M., Riegler, P., Danesino, C., Ruggieri, M., Magro, G., & Migone, N. (1996). Apparent preferential loss of heterozygosity at TSC2 over TSC1 chromosomal region in tuberous sclerosis hamartomas. *Genes Chromosomes and Cancer*, *15*(1), 18–25. [https://doi.org/10.1002/\(SICI\)1098-2264\(199601\)15:1<18::AID-GCC3>3.0.CO;2-7](https://doi.org/10.1002/(SICI)1098-2264(199601)15:1<18::AID-GCC3>3.0.CO;2-7)
- Carson, R. P., Van Nielen, D. L., Winzenburger, P. A., & Ess, K. C. (2012). Neuronal and glia abnormalities in Tsc1-deficient forebrain and partial rescue by rapamycin. *Neurobiology of Disease*, *45*(1), 369–380. <https://doi.org/10.1016/j.nbd.2011.08.024>
- Chapman, K. Z., Ge, R., Monni, E., Tatarishvili, J., Ahlenius, H., Arvidsson, A., Ekdahl, C. T., Lindvall, O., & Kokaia, Z. (2015). Inflammation without neuronal death triggers striatal neurogenesis comparable to stroke. *Neurobiology of Disease*, *83*, 1–15. <https://doi.org/10.1016/j.nbd.2015.08.013>
- Chassé, H., Boulben, S., Costache, V., Cormier, P., & Morales, J. (2017). Analysis of translation using polysome profiling. *Nucleic Acids Research*, *45*(3), e15. <https://doi.org/10.1093/nar/gkw907>
- Choo, A. Y., Yoon, S.-O., Kim, S. G., Roux, P. P., & Blenis, J. (2008). Rapamycin differentially inhibits S6Ks and 4E-BP1 to mediate cell-type-specific repression of mRNA translation. [www.pnas.org/cgi/doi/10.1073/pnas.0809136105](http://www.pnas.org/cgi/doi/10.1073/pnas.0809136105)
- Costa, M. R., Ortega, F., Brill, M. S., Beckervordersandforth, R., Petrone, C., Schroeder, T., Götz, M., & Berninger, B. (2011). Continuous live imaging of adult neural stem cell division and lineage progression in vitro. *Development*, *138*(6), 1057–1068. <https://doi.org/10.1242/dev.061663>
- Costa, V., Aigner, S., Vukcevic, M., Sauter, E., Behr, K., Ebeling, M., Dunkley, T., Friedlein, A., Zoffmann, S., Meyer, C. A., Knoflach, F., Lugert, S., Patsch, C., Fjeldskaar, F., Chicha-Gaudimier, L., Kiiialainen, A., Piraino, P., Bedoucha, M., Graf, M., ... Jagasia, R. (2016). mTORC1 inhibition corrects neurodevelopmental and synaptic alterations in a human stem cell model of Tuberous Sclerosis. *Cell Reports*, *15*(1), 86–95. <https://doi.org/10.1016/j.celrep.2016.02.090>
- Crino, P. B. (2010). The pathophysiology of tuberous sclerosis complex. *Epilepsia*, *51*(SUPPL. 1), 27–29. <https://doi.org/10.1111/j.1528-1167.2009.02438.x>
- Crino, P. B. (2020). mTORopathies: A Road Well-Traveled. *Epilepsy Currents*, *20*(6), 64S-66S. <https://doi.org/10.1046/j.1535-7597.2003.03411.x>
- Crino, P. B., Aronica, E., Baltuch, G., & Nathanson, K. L. (2010). Biallelic TSC gene inactivation in tuberous sclerosis complex. *Neurology*, *74*, 1716–1723. <http://chromium.liacs.nl/LOVD2/TSC/home.php>
- Crowell, B., Lee, G. H., Nikolaeva, I., Dal Pozzo, V., & D’Arcangelo, G. (2015). Complex neurological phenotype in mutant mice lacking Tsc2 in excitatory neurons of the developing forebrain. *ENeuro*, *2*(6). <https://doi.org/10.1523/eneuro.0046-15.2015>
- de León, G. A., Zaeri, N., & Foley, C. M. (1988). Olfactory hamartomas in tuberous sclerosis. *Journal of the Neurological Sciences*, *87*(2–3), 187–194. [https://doi.org/10.1016/0022-510X\(88\)90244-4](https://doi.org/10.1016/0022-510X(88)90244-4)

- De Vries, P. J., Whittemore, V. H., Leclezio, L., Byars, A. W., Dunn, D., Ess, K. C., Hook, D., King, B. H., Sahin, M., & Jansen, A. (2015). Tuberous Sclerosis associated neuropsychiatric disorders (TAND) and the TAND checklist. *Pediatric Neurology*, *52*(1), 25–35. <https://doi.org/10.1016/j.pediatrneurol.2014.10.004>
- Dibble, C. C., Elis, W., Menon, S., Qin, W., Klekota, J., Asara, J. M., Finan, P. M., Kwiatkowski, D. J., Murphy, L. O., & Manning, B. D. (2012). TBC1D7 is a third subunit of the TSC1-TSC2 complex upstream of mTORC1. *Molecular Cell*, *47*(4), 535–546. <https://doi.org/10.1016/j.molcel.2012.06.009>
- DiMario Jr, F. J. (2004). Brain abnormalities in Tuberous Sclerosis Complex. *Journal of Child Neurology*, *19*(9), 650–657.
- Doetsch, F., & Alvarez-Buylla, A. (1996). Network of tangential pathways for neuronal migration in adult mammalian brain. *Proceedings of the National Academy of Sciences*, *93*, 14895–14900.
- Doetsch, F., Caillé, I., Lim, D. A., Manuel García-Verdugo, J., & Alvarez-Buylla, A. (1999). Subventricular zone astrocytes are neural stem cells in the adult mammalian brain. *Cell*, *97*, 703–716.
- Doetsch, F., Manuel García-Verdugo, J., & Alvarez-Buylla, A. (1997). Cellular composition and three-dimensional organization of the subventricular germinal zone in the adult mammalian brain. *The Journal of Neuroscience*, *17*(13), 5046–5061.
- Dulken, B. W., Leeman, D. S., Boutet, S. C., Hebestreit, K., & Brunet, A. (2017). Single-cell transcriptomic analysis defines heterogeneity and transcriptional dynamics in the adult neural stem cell lineage. *Cell Reports*, *18*(3), 777–790. <https://doi.org/10.1016/j.celrep.2016.12.060>
- Ehninger, D., Han, S., Shilyansky, C., Zhou, Y., Li, W., Kwiatkowski, D. J., Ramesh, V., & Silva, A. J. (2008). Reversal of learning deficits in a Tsc2<sup>+/-</sup> mouse model of Tuberous Sclerosis. *Nature Medicine*, *14*(8), 843–848. <https://doi.org/10.1038/nm1788>
- Eichmüller, O. L., Corsini, N. S., Vértessy, Á., Morassut, I., Scholl, T., Gruber, V. E., Peer, A. M., Chu, J., Novatchkova, M., Hainfellner, J. A., Paredes, M. F., Feucht, M., & Knoblich, J. A. (2022). Amplification of human interneuron progenitors promotes brain tumors and neurological defects. *Science*, *375*(6579). <https://doi.org/10.1126/science.abf5546>
- Ellis, P., Fagan, B. M., Magness, S. T., Hutton, S., Taranova, O., Hayashi, S., McMahon, A., Rao, M., & Pevny, L. (2004). SOX2, a persistent marker for multipotential neural stem cells derived from embryonic stem cells, the embryo or the adult. *Developmental Neuroscience*, *26*(2–4), 148–165. <https://doi.org/10.1159/000082134>
- Ess, K. C., Kamp, C. A., Tu, B. P., & Gutmann, D. H. (2005). Developmental origin of subependymal giant cell astrocytoma in tuberous sclerosis complex. *Neurology*, *64*, 1446–1449.
- Ess, K. C., Uhlmann, E. J., Li, W., Li, H., Declue, J. E., Crino, P. B., & Gutmann, D. H. (2004). Expression profiling in Tuberous Sclerosis Complex (TSC) knockout mouse astrocytes to characterize human TSC brain pathology. *Glia*, *46*(1), 28–40. <https://doi.org/10.1002/glia.10324>

- European Tuberous Sclerosis Consortium. (1993). Identification and characterization of the Tuberous Sclerosis gene on chromosome 16. *Cell*, *75*, 1305–1315.
- European Tuberous Sclerosis Consortium. (2001). Mutational analysis in a cohort of 224 tuberous sclerosis patients indicates increased severity of TSC2, compared with TSC1, disease in multiple organs. *American Journal of Human Genetics*, *68*, 64–80.
- Fame, R. M., & Lehtinen, M. K. (2019). Sister, sister: ependymal cells and adult neural stem cells are separated at birth by geminin family members. *Neuron*, *102*(2), 278–279. <https://doi.org/10.1016/j.neuron.2019.02.040>
- Feliciano, D. M. (2020). The Neurodevelopmental Pathogenesis of Tuberous Sclerosis Complex (TSC). In *Frontiers in Neuroanatomy* (Vol. 14). Frontiers Media S.A. <https://doi.org/10.3389/fnana.2020.00039>
- Feliciano, D. M. (2023). Modeling genetic mosaicism of the mammalian target of rapamycin pathway in the cerebral cortex. *Frontiers in Mammal Science*, *2*. <https://doi.org/10.3389/fmamm.2023.1231778>
- Feliciano, D. M., Quon, J. L., Su, T., Taylor, M. M., & Bordey, A. (2012). Postnatal neurogenesis generates heterotopias, olfactory micronodules and cortical infiltration following single-cell TSC1 deletion. *Human Molecular Genetics*, *21*(4), 799–810. <https://doi.org/10.1093/hmg/ddr511>
- Feliciano, D. M., Su, T., Lopez, J., Platel, J. C., & Bordey, A. (2011). Single-cell Tsc1 knockout during corticogenesis generates tuber-like lesions and reduces seizure threshold in mice. *Journal of Clinical Investigation*, *121*(4), 1596–1607. <https://doi.org/10.1172/JCI44909>
- Franz, D. N., Leonard, J., Tudor, C., Chuck, G., Care, M., Sethuraman, G., Dinopoulos, A., Thomas, G., & Crone, K. R. (2006). Rapamycin causes regression of astrocytomas in Tuberous Sclerosis Complex. *Annals of Neurology*, *59*(3), 490–498. <https://doi.org/10.1002/ana.20784>
- Fu, C., Cawthon, B., Clinkscales, W., Bruce, A., Winzenburger, P., & Ess, K. C. (2012). GABAergic interneuron development and function is modulated by the Tsc1 gene. *Cerebral Cortex*, *22*(9), 2111–2119. <https://doi.org/10.1093/cercor/bhr300>
- Fuentealba, L. C., Rompani, S. B., Parraguez, J. I., Obernier, K., Romero, R., Cepko, C. L., & Alvarez-Buylla, A. (2015). Embryonic origin of postnatal neural stem cells. *Cell*, *161*(7), 1644–1655. <https://doi.org/10.1016/j.cell.2015.05.041>
- Furutachi, S., Miya, H., Watanabe, T., Kawai, H., Yamasaki, N., Harada, Y., Imayoshi, I., Nelson, M., Nakayama, K. I., Hirabayashi, Y., & Gotoh, Y. (2015). BSlowly dividing neural progenitors are an embryonic origin of adult neural stem cells. *Nature Neuroscience*, *18*(5), 657–665. <https://doi.org/10.1038/nn.3989>
- Gandin, V., Masvidal, L., Hulea, L., Gravel, S. P., Cargnello, M., McLaughlan, S., Cai, Y., Balanathan, P., Morita, M., Rajakumar, A., Furic, L., Pollak, M., Porco, J. A., St-Pierre, J., Pelletier, J., Larsson, O., & Topisirovic, I. (2016). NanoCAGE reveals 5' UTR features that define specific modes of translation of functionally related MTOR-sensitive mRNAs. *Genome Research*, *26*(5), 636–648. <https://doi.org/10.1101/gr.197566.115>
- Gandin, V., Sikström, K., Alain, T., Morita, M., McLaughlan, S., Larsson, O., & Topisirovic, I. (2014). Polysome fractionation and analysis of mammalian

- translatomes on a genome-wide scale. *Journal of Visualized Experiments*, 87. <https://doi.org/10.3791/51455>
- Gelot, A. B., & Represa, A. (2020). Progression of fetal brain lesions in Tuberous Sclerosis Complex. *Frontiers in Neuroscience*, 14. <https://doi.org/10.3389/fnins.2020.00899>
- Giannikou, K., Malinowska, I. A., Pugh, T. J., Yan, R., Tseng, Y. Y., Oh, C., Kim, J., Tyburczy, M. E., Chekaluk, Y., Liu, Y., Alesi, N., Finlay, G. A., Wu, C. L., Signoretti, S., Meyerson, M., Getz, G., Boehm, J. S., Henske, E. P., & Kwiatkowski, D. J. (2016). Whole Exome Sequencing Identifies TSC1/TSC2 Biallelic Loss as the Primary and Sufficient Driver Event for Renal Angiomyolipoma Development. *PLoS Genetics*, 12(8). <https://doi.org/10.1371/journal.pgen.1006242>
- Giannikou, K., Zhu, Z., Kim, J., Winden, K. D., Tyburczy, M. E., Marron, D., Parker, J. S., Hebert, Z., Bongaarts, A., Taing, L., Long, H. W., Pisano, W. V., Alexandrescu, S., Godlewski, B., Nellist, M., Kotulska, K., Jozwiak, S., Roszkowski, M., Mandra, M., ... Kwiatkowski, D. J. (2021). Subependymal giant cell astrocytomas are characterized by mTORC1 hyperactivation, a very low somatic mutation rate, and a unique gene expression profile. *Modern Pathology*, 34(2), 264–279. <https://doi.org/10.1038/s41379-020-00659-9>
- Gingras, A. C., Raught, B., & Sonenberg, N. (2001). Regulation of translation initiation by FRAP/mTOR. In *Genes and Development* (Vol. 15, Issue 7, pp. 807–826). <https://doi.org/10.1101/gad.887201>
- Gingras, A., Gygi, S. P., Raught, B., Polakiewicz, R. D., Abraham, R. T., Hoekstra, M. F., Aebersold, R., & Sonenberg, N. (1999). Regulation of 4E-BP1 phosphorylation: a novel two-step mechanism. *Genes and Development*, 1422–1437.
- Gleeson, J. G., Lin, P. T., Flanagan, L. A., & Walsh, C. A. (1999). Doublecortin Is a Microtubule-Associated Protein and Is Expressed Widely by Migrating Neurons. *Neuron*, 23, 257–271.
- Goto, J., Talos, D. M., Klein, P., Qin, W., Chekaluk, Y. I., Anderl, S., Malinowska, I. A., Di Nardo, A., Bronson, R. T., Chan, J. A., Vinters, H. V., Kernie, S. G., Jensen, F. E., Sahin, M., & Kwiatkowski, D. J. (2011). Regulable neural progenitor-specific Tsc1 loss yields giant cells with organellar dysfunction in a model of Tuberous Sclerosis Complex. *Proceedings of the National Academy of Sciences*, 108(45), 1070–1079. <https://doi.org/10.1073/pnas.1106454108>
- Grabole, N., Zhang, J. D., Aigner, S., Ruderisch, N., Costa, V., Weber, F. C., Theron, M., Berntenis, N., Spleiss, O., Ebeling, M., Yeo, G. W., Jagasia, R., & Kiialainen, A. (2016). Genomic analysis of the molecular neuropathology of tuberous sclerosis using a human stem cell model. *Genome Medicine*, 8(1). <https://doi.org/10.1186/s13073-016-0347-3>
- Green, A. J., Smith, M., & Yates, J. R. W. (1994). Loss of heterozygosity on chromosome 16p13.3 in hamartomas from Tuberous Sclerosis patients. *Nature Genetics*, 6, 193–196.
- Han, S., Lio, T., Santos, M., Puga, A., Roy, J., Thiele, E. A., Mccollin, M., Stemmer-Rachamimov, A., & Ramesh, V. (2004). Phosphorylation of tuberin as a novel mechanism for somatic inactivation of the Tuberous Sclerosis Complex proteins in

- brain lesions. *Cancer Research*, *64*, 812–816.  
<http://aacrjournals.org/cancerres/article-pdf/64/3/812/2522546/zch00304000812.pdf>
- Hartman, N. W., Lin, T. V., Zhang, L., Paquelet, G. E., Feliciano, D. M., & Bordey, A. (2013). mTORC1 targets the translational repressor 4E-BP2, but not S6 kinase 1/2, to regulate neural stem cell self-renewal in vivo. *Cell Reports*, *5*(2), 433–444.  
<https://doi.org/10.1016/j.celrep.2013.09.017>
- Heinrich, C., Bergami, M., Gascón, S., Lepier, A., Viganò, F., Dimou, L., Sutor, B., Berninger, B., & Götz, M. (2014). Sox2-mediated conversion of NG2 glia into induced neurons in the injured adult cerebral cortex. *Stem Cell Reports*, *3*(6), 1000–1014. <https://doi.org/10.1016/j.stemcr.2014.10.007>
- Henske, E. P., Scheithauer, B. W., Short, M. P., Wollmann, R., Nahmias, J., Hornigold, N., Van Slegtenhorst, M., Welsh, C. T., & Kwiatkowski, D. J. (1996). Allelic loss is frequent in Tuberous Sclerosis kidney lesions but rare in brain lesions. *American Journal of Human Genetics*, *59*, 400–406.
- Hernandez, O., Way, S., McKenna III, J., & Gambello, M. (2007). Generation of a conditional disruption of the Tsc2 gene. *Genesis*, *45*, 101–106.  
<https://doi.org/10.1002/dvg>
- Holz, M. K., Ballif, B. A., Gygi, S. P., & Blenis, J. (2005). mTOR and S6K1 mediate assembly of the translation preinitiation complex through dynamic protein interchange and ordered phosphorylation events. *Cell*, *123*(4), 569–580.  
<https://doi.org/10.1016/j.cell.2005.10.024>
- Huang, J., & Manning, B. D. (2008). The TSC1-TSC2 complex: A molecular switchboard controlling cell growth. *Biochemical Journal*, *412*(2), 179–190.  
<https://doi.org/10.1042/BJ20080281>
- Isaacson, J. S., & Strowbridge, B. W. (1998). Olfactory reciprocal synapses: dendritic signaling in the CNS. *Neuron*, *20*, 749–761.
- Işik, U., Dinçer, A., Sav, A., & Özek, M. M. (2010). Basal Ganglia Location of Subependymal Giant Cell Astrocytomas in Two Infants. *Pediatric Neurology*, *42*(2), 157–159. <https://doi.org/10.1016/j.pediatrneurol.2009.09.008>
- Jackowski, A., Parnavelas, J. G., & Lieberman, A. R. (1978). The reciprocal synapse in the external plexiform layer of the mammalian olfactory bulb. *Brain Research*, *159*, 17–28.
- Jankovski, A., & Sotelo, C. (1996). Subventricular zone-olfactory bulb migratory pathway in the adult mouse: cellular composition and specificity as determined by heterochronic and heterotopic transplantation. *The Journal of Comparative Neurology*, *371*, 376–396. <https://onlinelibrary.wiley.com/doi/10.1002/>
- Jansen, A. C., Belousova, E., Benedik, M. P., Carter, T., Cottin, V., Curatolo, P., D’Amato, L., D’Augères, G. B., De Vries, P. J., Ferreira, J. C., Feucht, M., Fladrowski, C., Hertzberg, C., Jozwiak, S., Lawson, J. A., MacAya, A., Marques, R., Nabbout, R., O’Callaghan, F., ... Trollmann, R. (2019). Newly diagnosed and growing subependymal giant cell astrocytoma in adults with tuberous sclerosis complex: Results from the International TOSCA Study. *Frontiers in Neurology*, *10*(JUL). <https://doi.org/10.3389/fneur.2019.00821>

- Jansen, F. E., Braams, O., Vincken, K. L., Algra, A., Anbeek, P., Jennekens-Schinkel, A., Halley, D., Zonnenberg, B. A., van den Ouweland, A., van Huffelen, A. C., van Nieuwenhuizen, O., & Nellist, M. (2008). Overlapping neurologic and cognitive phenotypes in patients with TSC1 or TSC2 mutations. *Neurology*, *70*(12), 908–915.
- Jansen, F. E., Van Huffelen, A. C., Van Rijen, P. C., Leijten, F. S. S., Jennekens-Schinkel, A., Gosselaar, P., & Van Nieuwenhuizen, O. (2007). Epilepsy surgery in tuberous sclerosis: The Dutch experience. *Seizure*, *16*(5), 445–453.  
<https://doi.org/10.1016/j.seizure.2007.03.001>
- Jefferies, H. B. J., Fumagalli, S., Dennis, P. B., Reinhard, C., Pearson, R. B., & Thomas, G. (1997a). Rapamycin suppresses 5' TOP mRNA translation through inhibition of p70(s6k). *EMBO Journal*, *16*(12), 3693–3704.  
<https://doi.org/10.1093/emboj/16.12.3693>
- Jefferies, H. B. J., Fumagalli, S., Dennis, P. B., Reinhard, C., Pearson, R. B., & Thomas, G. (1997b). Rapamycin suppresses 5' TOP mRNA translation through inhibition of p70(s6k). *EMBO Journal*, *16*(12), 3693–3704.  
<https://doi.org/10.1093/emboj/16.12.3693>
- Jefferies, H. B. J., Reinhard, C., Kozma, S. C., & Thomas, G. (1994). Rapamycin selectively represses translation of the “polypyrimidine tract” mRNA family. *Proceedings of the National Academy of Sciences of the United States of America*, *91*(10), 4441–4445. <https://doi.org/10.1073/PNAS.91.10.4441>
- Jensen, F. E. (2009). Epileptogenic cortical dysplasia: Emerging trends in diagnosis, treatment, and pathogenesis. *Epilepsia*, *50*(SUPPL. 9), 1–2.  
<https://doi.org/10.1111/j.1528-1167.2009.02293.x>
- Jiang, T., Du, J., Raynald, Wang, J., & Li, C. (2017). Presurgical administration of mTOR inhibitors in patients with large subependymal giant cell astrocytoma associated with Tuberous Sclerosis Complex. *World Neurosurgery*, *107*, 1053.e1-1053.e6. <https://doi.org/10.1016/j.wneu.2017.08.122>
- Jin, K., Sun, Y., Xie, L., Peel, A., Mao, X. O., Bateau, S., & Greenberg, D. A. (2003). Directed migration of neuronal precursors into the ischemic cerebral cortex and striatum. *Molecular and Cellular Neuroscience*, *24*(1), 171–189.  
[https://doi.org/10.1016/S1044-7431\(03\)00159-3](https://doi.org/10.1016/S1044-7431(03)00159-3)
- Jozwiak, J., Grajkowska, W., Kotulska, K., Jozwiak, S., Zalewski, W., Zajackowska, A., Roszkowski, M., Slupianek, A., & Wlodarski, P. (2007). Brain Tumor Formation in Tuberous Sclerosis Depends on Erk Activation. *NeuroMolecular Medicine*, *117*.  
<https://doi.org/10.1385/NMM:9:2:117>
- Jozwiak, S., Kwiatkowski, D., Kotulska, K., Larysz-Brysz, M., Lewin-Kowalik, J., Grajkowska, W., & Roszkowski, M. (2004). Tuberin and hamartin expression is reduced in the majority of subependymal giant cell astrocytomas in Tuberous Sclerosis Complex consistent with a two-hit model of pathogenesis. *Journal of Child Neurology*, *19*(2), 102–106.
- Kelleher, R. J., Geigenmüller, U., Hovhannisyan, H., Trautman, E., Pinard, R., Rathmell, B., Carpenter, R., & Margulies, D. (2012). High-throughput sequencing of mGluR signaling pathway genes reveals enrichment of rare variants in autism. *PLoS ONE*, *7*(4). <https://doi.org/10.1371/journal.pone.0035003>

- Kempermann, G., Song, H., & Gage, F. H. (2015). Neurogenesis in the adult hippocampus. *Cold Spring Harbor Perspectives in Biology*, 7, 1–14. <https://doi.org/10.1101/cshperspect.a018812>
- Kim, S.-K., Wang, K.-C., Cho, B.-K., Jung, H.-W., Lee, Y. J., Chung, Y. S., Lee, J.-Y., Park, S.-H., Kim, Y.-M., Choe, G., & Chi, J. G. (2001). Biological behavior and tumorigenesis of subependymal giant cell astrocytomas. *Journal of Neuro-Oncology*, 52, 217–225.
- Kingswood, J. C., D’Augères, G. B., Belousova, E., Ferreira, J. C., Carter, T., Castellana, R., Cottin, V., Curatolo, P., Dahlin, M., De Vries, P. J., Feucht, M., Fladrowski, C., Gislimberti, G., Hertzberg, C., Jozwiak, S., Lawson, J. A., Macaya, A., Nabbout, R., O’Callaghan, F., ... Jansen, A. C. (2017). Tuberous Sclerosis registry to increase disease Awareness (TOSCA) - Baseline data on 2093 patients. *Orphanet Journal of Rare Diseases*, 12(1). <https://doi.org/10.1186/s13023-016-0553-5>
- Kirschenbaum, B., Doetsch, F., Lois, C., & Alvarez-Buylla, A. (1999). Adult subventricular zone neuronal precursors continue to proliferate and migrate in the absence of the olfactory bulb. *The Journal of Neuroscience*, 19(6), 2171–2180.
- Knudson, A. G. (1971). Mutation and cancer: statistical study of retinoblastoma. *Proceedings of the National Academy of Science*, 68(4), 820–823.
- Kwiatkowski, D. J. (2003). Rhebbing up mTOR: New insights on TSC1 and TSC2, and the pathogenesis of tuberous sclerosis. *Cancer Biology and Therapy*, 2(5), 471–476. <https://doi.org/10.4161/cbt.2.5.446>
- Kwiatkowski, D. J., Lewin-Kowalik, J., Roberts, P. S., Zhang, H., Kotulska, K., Wieslawa, G., Chan, J. A., & Jozwiak, S. (2004). Pathogenesis of Tuberous Sclerosis Subependymal Giant Cell Astrocytomas: Biallelic Inactivation of TSC1 or TSC2 Leads to mTOR Activation. *Journal of Neuropathology and Experimental Neurology*, 63, 1236–1242. <https://academic.oup.com/jnen/article/63/12/1236/2916471>
- Leclezio, L., Jansen, A., Whittemore, V. H., & De Vries, P. J. (2015). Pilot validation of the Tuberous Sclerosis-associated neuropsychiatric disorders (TAND) checklist. *Pediatric Neurology*, 52(1), 16–24. <https://doi.org/10.1016/j.pediatrneurol.2014.10.006>
- Lendahl, U., Zimmerman, L. B., & McKay, R. D. G. (1990). CNS Stem Cells Express a New Class of Intermediate Filament Protein. *Cell*, 60, 585–595.
- Lepko, T., Pusch, M., Müller, T., Schulte, D., Ehses, J., Kiebler, M., Hasler, J., Huttner, H. B., Vandenbroucke, R. E., Vandendriessche, C., Modic, M., Martin-Villalba, A., Zhao, S., Llorens-Bobadilla, E., Schneider, A., Fischer, A., Breunig, C. T., Stricker, S. H., Götz, M., & Ninkovic, J. (2019). Choroid plexus-derived miR-204 regulates the number of quiescent neural stem cells in the adult brain. *The EMBO Journal*, 38(17). <https://doi.org/10.15252/emboj.2018100481>
- Lim, D. A., & Alvarez-Buylla, A. (2016). The adult ventricular–subventricular zone (V-SVZ) and olfactory bulb (OB) neurogenesis. *Cold Spring Harbor Perspectives in Biology*, 8(5). <https://doi.org/10.1101/cshperspect.a018820>

- Liu, G. Y., & Sabatini, D. M. (2020). mTOR at the nexus of nutrition, growth, ageing and disease. In *Nature Reviews Molecular Cell Biology* (Vol. 21, Issue 4, pp. 183–203). Nature Research. <https://doi.org/10.1038/s41580-019-0199-y>
- Lledo, P. M., & Lagier, S. (2006). Adjusting neurophysiological computations in the adult olfactory bulb. *Seminars in Cell and Developmental Biology*, *17*(4), 443–453. <https://doi.org/10.1016/j.semcdb.2006.04.011>
- Llorens-Bobadilla, E., Zhao, S., Baser, A., Saiz-Castro, G., Zwadlo, K., & Martin-Villalba, A. (2015). Single-cell transcriptomics reveals a population of dormant neural stem cells that become activated upon brain injury. *Cell Stem Cell*, *17*(3), 329–340. <https://doi.org/10.1016/j.stem.2015.07.002>
- Lois, C., & Alvarez-Buylla, A. (1993). Proliferating subventricular zone cells in the adult mammalian forebrain can differentiate into neurons and glia. *Proceedings of the National Academy of Sciences*, *90*, 2074–2077.
- Lou, W. P. K., Baser, A., Klußmann, S., & Martin-Villalba, A. (2014). In vivo interrogation of central nervous system transcriptome by polyribosome fractionation. *Journal of Visualized Experiments*, *86*. <https://doi.org/10.3791/51255>
- Ma, X. M., & Blenis, J. (2009). Molecular mechanisms of mTOR-mediated translational control. *Nature Reviews Molecular Cell Biology*, *10*(5), 307–318. <https://doi.org/10.1038/NRM2672>
- Mader, S., Lee, H., Pause, A., & Sonenberg, N. (1995). The translation initiation factor eIF-4E binds to a common motif shared by the translation factor eIF-4γ and the translational repressors 4E-binding proteins. *Molecular and Cellular Biology*, *15*(9), 4990–4997. <https://doi.org/10.1128/mcb.15.9.4990>
- Magri, L., Cambiaghi, M., Cominelli, M., Alfaro-Cervello, C., Cursi, M., Pala, M., Bulfone, A., Garca-Verdugo, J. M., Leocani, L., Minicucci, F., Poliani, P. L., & Galli, R. (2011). Sustained activation of mTOR pathway in embryonic neural stem cells leads to development of Tuberous Sclerosis Complex-associated lesions. *Cell Stem Cell*, *9*(5), 447–462. <https://doi.org/10.1016/j.stem.2011.09.008>
- Magri, L., Cominelli, M., Cambiaghi, M., Cursi, M., Leocani, L., Minicucci, F., Poliani, P. L., & Galli, R. (2013). Timing of mTOR activation affects Tuberous Sclerosis Complex neuropathology in mouse models. *Disease Models and Mechanisms*, *6*(5), 1185–1197. <https://doi.org/10.1242/dmm.012096>
- Malatesta, P., Hartfuss, E., & Götz, M. (2000). Isolation of radial glial cells by fluorescent-activated cell sorting reveals a neuronal lineage. *Development*, *127*, 5253–5263.
- Martin, K. R., Zhou, W., Bowman, M. J., Shih, J., Au, K. S., Dittenhafer-Reed, K. E., Sisson, K. A., Koeman, J., Weisenberger, D. J., Cottingham, S. L., Deroos, S. T., Devinsky, O., Winn, M. E., Cherniack, A. D., Shen, H., Northrup, H., Krueger, D. A., & Mackeigan, J. P. (2017). The genomic landscape of Tuberous Sclerosis Complex. *Nature Communications*, *8*. <https://doi.org/10.1038/ncomms15816>
- McMahon, J. J., Yu, W., Yang, J., Feng, H., Helm, M., McMahon, E., Zhu, X., Shin, D., & Huang, Y. (2015). Seizure-dependent mTOR activation in 5-HT neurons promotes autism-like behaviors in mice. *Neurobiology of Disease*, *73*, 296–306. <https://doi.org/10.1016/j.nbd.2014.10.004>

- Meikle, L., Talos, D. M., Onda, H., Pollizzi, K., Rotenberg, A., Sahin, M., Jensen, F. E., & Kwiatkowski, D. J. (2007). A mouse model of Tuberous Sclerosis: neuronal loss of Tsc1 causes dysplastic and ectopic neurons, reduced myelination, seizure activity, and limited survival. *Journal of Neuroscience*, *27*(21), 5546–5558. <https://doi.org/10.1523/jneurosci.5540-06.2007>
- Merkle, F. T., Mirzadeh, Z., & Alvarez-Buylla, A. (2007). Mosaic organization of neural stem cells in the adult brain. *Science*, *317*, 381–384. <https://doi.org/10.1126/science.1140956>
- Merkle, F. T., Tramontin, A. D., Manuel García-Verdugo, J., & Alvarez-Buylla, A. (2004). Radial glia give rise to adult neural stem cells in the subventricular zone. *Proceedings of the National Academy of Sciences*, *101*(50), 17528–17532.
- Mizrak, D., Levitin, H. M., Delgado, A. C., Crotet, V., Yuan, J., Chaker, Z., Silva-Vargas, V., Sims, P. A., & Doetsch, F. (2019). Single-cell analysis of regional differences in adult V-SVZ neural stem cell lineages. *Cell Reports*, *26*(2), 394–406.e5. <https://doi.org/10.1016/j.celrep.2018.12.044>
- Moavero, R., Kotulska, K., Lagae, L., Benvenuto, A., Emberti Gialloreti, L., Weschke, B., Riney, K., Feucht, M., Krsek, P., Nabbout, R., Jansen, A. C., Wojdan, K., Borkowska, J., Sadowski, K., Hertzberg, C., Van Schooneveld, M. M., Samuelli, S., Maulisovà, A., Aronica, E., ... Curatolo, P. (2020). Is autism driven by epilepsy in infants with Tuberous Sclerosis Complex? *Annals of Clinical and Translational Neurology*, *7*(8), 1371–1381. <https://doi.org/10.1002/acn3.51128>
- Morimoto, K., & Mogami, H. (1986). Sequential CT study of subependymal giant-cell astrocytoma associated with Tuberous Sclerosis. *Journal of Neurosurgery*, *65*, 874–877.
- Morton, M. C., Neckles, V. N., Seluzicki, C. M., Holmberg, J. C., & Feliciano, D. M. (2018). Neonatal Subventricular Zone Neural Stem Cells Release Extracellular Vesicles that Act as a Microglial Morphogen. *Cell Reports*, *23*(1), 78–89. <https://doi.org/10.1016/j.celrep.2018.03.037>
- Mullen, R. J., Buck, C. R., & Smith, A. M. (1992). NeuN, a neuronal specific nuclear protein in vertebrates. *Development*, *116*, 201–211.
- Niida, Y., Stemmer-Rachamimov, A. O., Logrip, M., Tapon, D., Perez, R., Kwiatkowski, D. J., Sims, K., Maccollin, M., Louis, D. N., & Ramesh, V. (2001). Survey of somatic mutations in Tuberous Sclerosis Complex (TSC) hamartomas suggests different genetic mechanisms for pathogenesis of TSC lesions. *American Journal of Human Genetics*, *69*, 493–503.
- Niu, W., Zang, T., Zou, Y., Fang, S., Smith, D. K., Bachoo, R., & Zhang, C. L. (2013). In vivo reprogramming of astrocytes to neuroblasts in the adult brain. *Nature Cell Biology*, *15*(10), 1164–1175. <https://doi.org/10.1038/ncb2843>
- Noctor, S. C., Flint, A. C., Weissman, T. A., Dammerman, R. S., & Kriegstein, A. R. (2001). Neurons derived from radial glial cells establish radial units in neocortex. *Nature*, *409*, 714–720.
- Noctor, S. C., Martínez-Cerdeño, V., Ivic, L., & Kriegstein, A. R. (2004). Cortical neurons arise in symmetric and asymmetric division zones and migrate through

specific phases. *Nature Neuroscience*, 7(2), 136–144.

<https://doi.org/10.1038/nn1172>

- Northrup, H., Krueger, D. A., Roberds, S., Smith, K., Sampson, J., Korf, B., Kwiatkowski, D. J., Mowat, D., Nellist, M., Povey, S., de Vries, P., Byars, A., Dunn, D., Ess, K., Hook, D., Jansen, A., King, B., Sahin, M., Whittemore, V., ... Frost, M. D. (2013). Tuberous Sclerosis Complex diagnostic criteria update: Recommendations of the 2012 international Tuberous Sclerosis Complex consensus conference. *Pediatric Neurology*, 49(4), 243–254.  
<https://doi.org/10.1016/j.pediatrneurol.2013.08.001>
- Obernier, K., Cebrian-Silla, A., Thomson, M., Parraguez, J. I., Anderson, R., Guinto, C., Rodas Rodriguez, J., Garcia-Verdugo, J. M., & Alvarez-Buylla, A. (2018). Adult neurogenesis is sustained by symmetric self-renewal and differentiation. *Cell Stem Cell*, 22(2), 221–234.e8. <https://doi.org/10.1016/j.stem.2018.01.003>
- Onda, H., Crino, P. B., Zhang, H., Murphey, R. D., Rastelli, L., Rothberg, B. E. G., & Kwiatkowski, D. J. (2002). Tsc2 null murine neuroepithelial cells are a model for human tuber giant cells, and show activation of an mTOR pathway. *Molecular and Cellular Neuroscience*, 21(4), 561–574. <https://doi.org/10.1006/mcne.2002.1184>
- Ortiz-Álvarez, G., Daclin, M., Shihavuddin, A., Lansade, P., Fortoul, A., Faucourt, M., Clavreul, S., Lalioti, M. E., Taraviras, S., Hippenmeyer, S., Livet, J., Meunier, A., Genovesio, A., & Spassky, N. (2019). Adult neural stem cells and multiciliated ependymal cells share a common lineage regulated by the geminin family members. *Neuron*, 102(1), 159–172.e7. <https://doi.org/10.1016/j.neuron.2019.01.051>
- Paliouras, G. N., Hamilton, L. K., Aumont, A., Joppé, S. E., Barnab-Heider, F., & Fernandes, K. J. L. (2012). Mammalian target of rapamycin signaling is a key regulator of the transit-amplifying progenitor pool in the adult and aging forebrain. *Journal of Neuroscience*, 32(43), 15012–15026.  
<https://doi.org/10.1523/jneurosci.2248-12.2012>
- Park, S.-H., Pepkowitz, S. H., Kerfoot, C., De Rosa, M. J., Poukens, V., Wieneke, R., DeClue, J. E., & Vinters, H. V. (1997). Tuberous Sclerosis in a 20-week gestation fetus: immunohistochemical study. *Acta Neuropathologica*, 94, 180–186.
- Platel, J.-C., Angelova, A., Bugeon, S., Wallace, J., Ganay, T., Chudotvorova, I., Deloulme, J.-C., Bé Clin, C., Tiveron, M.-C., Coré, N., Murthy, V. N., & Cremer, H. (2019). Neuronal integration in the adult mouse olfactory bulb is a non-selective addition process. *ELife*. <https://doi.org/10.7554/eLife.44830.001>
- Prabowo, A. S., Anink, J. J., Lammens, M., Nellist, M., Van Den Ouweland, A. M. W., Adle-Biassette, H., Sarnat, H. B., Flores-Sarnat, L., Crino, P. B., & Aronica, E. (2013). Fetal brain lesions in Tuberous Sclerosis Complex: TORC1 activation and inflammation. *Brain Pathology*, 23(1), 45–59. <https://doi.org/10.1111/j.1750-3639.2012.00616.x>
- Qian, X., Shen, Q., Goderie, S. K., He, W., Capela, A., Davis, A. A., & Temple, S. (2000). Timing of CNS cell generation: a programmed sequence of neuron and glial cell production from isolated murine cortical stem cells. *Neuron*, 28, 69–80.

- Raju, G. P., Urion, D. K., & Sahin, M. (2007). Neonatal subependymal giant cell astrocytoma: new case and review of literature. *Pediatric Neurology*, *36*(2), 128–131. <https://doi.org/10.1016/j.pediatrneurol.2006.08.009>
- Rall, W., Shepherd, G. M., Reese, T. S., & Brightman, M. W. (1966). Dendrodendritic synaptic pathway for inhibition in the olfactory bulb. *Experimental Neurology*, *14*, 44–56.
- Raudvere, U., Kolberg, L., Kuzmin, I., Arak, T., Adler, P., Peterson, H., & Vilo, J. (2019). G:Profiler: A web server for functional enrichment analysis and conversions of gene lists (2019 update). *Nucleic Acids Research*, *47*, 191–198. <https://doi.org/10.1093/nar/gkz369>
- Redmond, S. A., Figueres-Oñate, M., Obernier, K., Nascimento, M. A., Parraguez, J. I., López-Mascaraque, L., Fuentealba, L. C., & Alvarez-Buylla, A. (2019). Development of ependymal and postnatal neural stem cells and their origin from a common embryonic progenitor. *Cell Reports*, *27*(2), 429–441.e3. <https://doi.org/10.1016/j.celrep.2019.01.088>
- Richter, J. D., & Sonenberg, N. (2005). Regulation of cap-dependent translation by eIF4E inhibitory proteins. *Nature*, *433*(7025), 477–480. <https://doi.org/10.1038/NATURE03205>
- Riley, V. A., Holmberg, J. C., Sokolov, A. M., & Feliciano, D. M. (2022). Tsc2 shapes olfactory bulb granule cell molecular and morphological characteristics. *Frontiers in Molecular Neuroscience*, *15*. <https://doi.org/10.3389/fnmol.2022.970357>
- Riley, V. A., Shankar, V., Holmberg, J. C., Sokolov, A. M., Neckles, V. N., Williams, K., Lyman, R., Mackay, T. F. C., & Feliciano, D. M. (2023). Tsc2 coordinates neuroprogenitor differentiation. *IScience*. <https://doi.org/10.1016/j.isci.2023.108442>
- Rushing, G. V., Brockman, A. A., Bollig, M. K., Leelatian, N., Mobley, B. C., Irish, J. M., Ess, K. C., Fu, C., & Ihrie, R. A. (2019). Location-dependent maintenance of intrinsic susceptibility to mTORC1-driven tumorigenesis. *Life Science Alliance*, *2*(2). <https://doi.org/10.26508/lsa.201800218>
- Sampath, P., Pritchard, D. K., Pabon, L., Reinecke, H., Schwartz, S. M., Morris, D. R., & Murry, C. E. (2008). A hierarchical network controls protein translation during murine embryonic stem cell self-renewal and differentiation. *Cell Stem Cell*, *2*(5), 448–460. <https://doi.org/10.1016/j.stem.2008.03.013>
- Sancak, Y., Bar-Peled, L., Zoncu, R., Markhard, A. L., Nada, S., & Sabatini, D. M. (2010). Ragulator-rag complex targets mTORC1 to the lysosomal surface and is necessary for its activation by amino acids. *Cell*, *141*(2), 290–303. <https://doi.org/10.1016/j.cell.2010.02.024>
- Schwab, M. H., Druffel-Augustin, S., Gass, P., Jung, M., Klugmann, M., Bartholomae, A., Rossner, M. J., & Nave, K.-A. (1998). Neuronal Basic Helix-Loop-Helix Proteins (NEX, neuroD, NDRF): Spatiotemporal Expression and Targeted Disruption of the NEX Gene in Transgenic Mice. *Journal of Neuroscience*.
- Sepp, T., Yates, J. R. W., Green, A. J., Sepp, T., Yates, W., & Green, A. J. (1996). Loss of heterozygosity in tuberous sclerosis hamartomas. *Journal of Medical Genetics*, *33*, 962–964.

- Shin, J., Berg, D. A., Zhu, Y., Shin, J. Y., Song, J., Bonaguidi, M. A., Enikolopov, G., Nauen, D. W., Christian, K. M., Ming, G. L., & Song, H. (2015). Single-cell RNA-Seq with waterfall reveals molecular cascades underlying adult neurogenesis. *Cell Stem Cell*, *17*(3), 360–372. <https://doi.org/10.1016/j.stem.2015.07.013>
- Shiple, M. T., & Ennis, M. (1996). Functional organization of olfactory system. *Journal of Neurobiology*, *30*(1), 123–176.
- Siedlecka, M., Szlufik, S., Grajkowska, W., Roszkowski, M., & Józwiak, J. (2015a). Erk activation as a possible mechanism of transformation of subependymal nodule into subependymal giant cell astrocytoma. *Folia Neuropathologica*, *53*(1), 8–14. <https://doi.org/10.5114/fn.2015.49969>
- Siedlecka, M., Szlufik, S., Grajkowska, W., Roszkowski, M., & Józwiak, J. (2015b). Erk activation as a possible mechanism of transformation of subependymal nodule into subependymal giant cell astrocytoma. *Folia Neuropathologica*, *53*(1), 8–14. <https://doi.org/10.5114/fn.2015.49969>
- Silva-Vargas, V., Maldonado-Soto, A. R., Mizrak, D., Codega, P., & Doetsch, F. (2016). Age-dependent niche signals from the choroid plexus regulate adult neural stem cells. *Cell Stem Cell*, *19*(5), 643–652. <https://doi.org/10.1016/j.stem.2016.06.013>
- Singh, V. K., Saini, A., Kalsan, M., Kumar, N., & Chandra, R. (2016). Describing the stem cell potency: the various methods of functional assessment and in silico diagnostics. *Frontiers in Cell and Developmental Biology*, *4*(NOV). <https://doi.org/10.3389/fcell.2016.00134>
- Sinson, G., Sutton, L. N., Yachnis, A. T., Duhaime, A.-C., & Schut, L. (1977). Subependymal Giant Cell Astrocytomas in Children. *Pediatric Neurosurgery*.
- Spassky, N., Merkle, F. T., Flames, N., Tramontin, A. D., García-Verdugo, J. M., & Alvarez-Buylla, A. (2005). Adult ependymal cells are postmitotic and are derived from radial glial cells during embryogenesis. *Journal of Neuroscience*, *25*(1), 10–18. <https://doi.org/10.1523/jneurosci.1108-04.2005>
- Specchio, N., Pietrafusa, N., Trivisano, M., Moavero, R., De Palma, L., Ferretti, A., Vigeveno, F., & Curatolo, P. (2020). Autism and epilepsy in patients with Tuberous Sclerosis Complex. *Frontiers in Neurology*, *11*. <https://doi.org/10.3389/fneur.2020.00639>
- Subramanian, L., Bershteyn, M., Paredes, M. F., & Kriegstein, A. R. (2017). Dynamic behaviour of human neuroepithelial cells in the developing forebrain. *Nature Communications*, *8*. <https://doi.org/10.1038/ncomms14167>
- Svitkin, Y. V., Pause, A., Haghghat, A., Pyronnet, S., Witherell, G., Belsham, G. J., & Sonenberg, N. (2001). The requirement for eukaryotic initiation factor 4A (eIF4A) in translation is in direct proportion to the degree of mRNA 5' secondary structure. *RNA*, *7*, 382–394.
- Talos, D. M., Kwiatkowski, D. J., Cordero, K., Black, P. M., & Jensen, F. E. (2008). Cell-specific alterations of glutamate receptor expression in Tuberous Sclerosis Complex cortical tubers. *Annals of Neurology*, *63*(4), 454–465. <https://doi.org/10.1002/ana.21342>
- Tavazoie, M., Van der Veken, L., Silva-Vargas, V., Louissaint, M., Colonna, L., Zaidi, B., Garcia-Verdugo, J. M., & Doetsch, F. (2008). A specialized vascular niche for

- adult neural stem cells. *Cell Stem Cell*, 3(3), 279–288.  
<https://doi.org/10.1016/j.stem.2008.07.025>
- Tavazoie, S. F., Alvarez, V. A., Ridenour, D. A., Kwiatkowski, D. J., & Sabatini, B. L. (2005). Regulation of neuronal morphology and function by the tumor suppressors Tsc1 and Tsc2. *Nature Neuroscience*, 8(12), 1727–1734.  
<https://doi.org/10.1038/nn1566>
- Tee, A. R., & Blenis, J. (2005). mTOR, translational control and human disease. *Seminars in Cell and Developmental Biology*, 16(1), 29–37.  
<https://doi.org/10.1016/j.semcdb.2004.11.005>
- Tee, A. R., Manning, B. D., Roux, P. P., Cantley, L. C., & Blenis, J. (2003). Tuberous Sclerosis Complex gene products, tuberin and hamartin, control mTOR Signaling by acting as a GTPase-activating protein complex toward Rheb. *Current Biology*, 13, 1259–1268. <https://doi.org/10.1016/S>
- Thoreen, C. C., Chantranupong, L., Keys, H. R., Wang, T., Gray, N. S., & Sabatini, D. M. (2012). A unifying model for mTORC1-mediated regulation of mRNA translation. *Nature*, 485(7396), 109–113. <https://doi.org/10.1038/nature11083>
- Tsai, J. D., Wei, C. C., Tsao, T. F., Hsiao, Y. P., Tsai, H. J., Yang, S. H., Tsai, M. L., & Sheu, J. N. (2016). Association between the growth rate of subependymal giant cell astrocytoma and age in patients with Tuberous Sclerosis Complex. *Child's Nervous System*, 32(1), 89–95. <https://doi.org/10.1007/s00381-015-2947-4>
- Tyburczy, M. E., Dies, K. A., Glass, J., Camposano, S., Chekaluk, Y., Thorner, A. R., Lin, L., Krueger, D., Franz, D. N., Thiele, E. A., Sahin, M., & Kwiatkowski, D. J. (2015). Mosaic and intronic mutations in TSC1/TSC2 explain the majority of TSC Patients with no mutation identified by conventional testing. *PLoS Genetics*, 11(11). <https://doi.org/10.1371/journal.pgen.1005637>
- Uhlmann, E. J., Apicelli, A. J., Baldwin, R. L., Burke, S. P., Livia Bajenaru, M., Onda, H., Kwiatkowski, D., & Gutmann, D. H. (2002). Heterozygosity for the Tuberous Sclerosis Complex (TSC) gene products results in increased astrocyte numbers and decreased p27-Kip1 expression in TSC2+/- cells. *Oncogene*, 21, 4050–4059.  
<https://doi.org/10.1038/sj.onc>
- Uhlmann, E. J., Wong, M., Baldwin, R. L., Bajenaru, M. L., Onda, H., Kwiatkowski, D. J., Yamada, K., & Gutmann, D. H. (2002). Astrocyte-specific TSC1 conditional knockout mice exhibit abnormal neuronal organization and seizures. *Annals of Neurology*, 52(3), 285–296. <https://doi.org/10.1002/ana.10283>
- van Slegtenhorst, M., de Hoogt, R., Hermans, C., Nellist, M., Janssen, B., Verhoef, S., Lindhout, D., van den Ouweland, A., Halley, D., Young, J., Burley, M., Jeremiah, S., Woodward, K., Nahmias, J., Fox, M., Ekong, R., Osborne, J., Wolfe, J., Povey, S., ... Kwiatkowski, D. J. (1997). Identification of the Tuberous Sclerosis gene TSC1 on chromosome 9q34. *Science*, 277, 805–808.
- Way, S. W., Mckenna, J., Mietzsch, U., Reith, R. M., Wu, H. C. J., & Gambello, M. J. (2009). Loss of Tsc2 in radial glia models the brain pathology of Tuberous Sclerosis Complex in the mouse. *Human Molecular Genetics*, 18(7), 1252–1265.  
<https://doi.org/10.1093/hmg/ddp025>

- Weiner, H. L., Carlson, C., Ridgway, E. B., Zaroff, C. M., Miles, D., LaJoie, J., & Devinsky, O. (2006). Epilepsy surgery in young children with Tuberous Sclerosis: results of a novel approach. *Pediatrics*, *117*(5), 1494–1502. <https://doi.org/10.1542/peds.2005-1206>
- Whitman, M. C., Fan, W., Rela, L., Rodriguez-Gil, D. J., & Greer, C. A. (2009). Blood vessels form a migratory scaffold in the rostral migratory stream. *Journal of Comparative Neurology*, *516*(2), 94–104. <https://doi.org/10.1002/cne.22093>
- Yamanouchi, H., Jay, V., Rutka, J. T., Takashima, S., & Becker, L. E. (1997). Evidence of abnormal differentiation in giant cells of Tuberous Sclerosis. *Pediatric Neurology*, *17*(1), 49–53.
- Yamashita, T., Ninomiya, M., Acosta, P. H., García-Verdugo, J. M., Sunabori, T., Sakaguchi, M., Adachi, K., Kojima, T., Hirota, Y., Kawase, T., Araki, N., Abe, K., Okano, H., & Sawamoto, K. (2006). Subventricular zone-derived neuroblasts migrate and differentiate into mature neurons in the post-stroke adult striatum. *Journal of Neuroscience*, *26*(24), 6627–6636. <https://doi.org/10.1523/jneurosci.0149-06.2006>
- Yeung, R. S., Katsetos, C. D., & Klein-Szanto, A. (1997). Animal model subependymal astrocytic hamartomas in the Eker rat model of Tuberous Sclerosis. *American Journal of Pathology*, *151*(5), 1477–1486.
- Young, K. M., Fogarty, M., Kessar, N., & Richardson, W. D. (2007). Subventricular zone stem cells are heterogeneous with respect to their embryonic origins and neurogenic fates in the adult olfactory bulb. *Journal of Neuroscience*, *27*(31), 8286–8296. <https://doi.org/10.1523/JNEUROSCI.0476-07.2007>
- Zeng, L. H., Rensing, N. R., Zhang, B., Gutmann, D. H., Gambello, M. J., & Wong, M. (2011). Tsc2 gene inactivation causes a more severe epilepsy phenotype than Tsc1 inactivation in a mouse model of Tuberous Sclerosis Complex. *Human Molecular Genetics*, *20*(3), 445–454. <https://doi.org/10.1093/hmg/ddq491>
- Zeng, L.-H., Ouyang, Y., Gazit, V., Cirrito, J. R., Jansen, L. A., Ess, K. C., Yamada, K. A., Wozniak, D. F., Holtzman, D. M., Gutmann, D. H., & Wong, M. (2007). Abnormal Glutamate Homeostasis and Impaired Synaptic Plasticity and Learning in a Mouse Model of Tuberous Sclerosis Complex. *Neurobiology of Disease*, *28*(2), 184–196.
- Zhang, B., Zou, J., Rensing, N. R., Yang, M., & Wong, M. (2015). Inflammatory mechanisms contribute to the neurological manifestations of tuberous sclerosis complex. *Neurobiology of Disease*, *80*, 70–79. <https://doi.org/10.1016/j.nbd.2015.04.016>
- Zhang, H., Cicchetti, G., Onda, H., Koon, H. B., Asrican, K., Bajraszewski, N., Vazquez, F., Carpenter, C. L., & Kwiatkowski, D. J. (2003). Loss of Tsc1/Tsc2 activates mTOR and disrupts PI3K-Akt signaling through downregulation of PDGFR. *Journal of Clinical Investigation*, *112*(8), 1223–1233. <https://doi.org/10.1172/jci17222>
- Zhao, J. P., & Yoshii, A. (2019). Hyperexcitability of the local cortical circuit in mouse models of Tuberous Sclerosis Complex. *Molecular Brain*, *12*(1). <https://doi.org/10.1186/s13041-019-0427-6>

- Zhou, J., Shrikhande, G., Xu, J., McKay, R. M., Burns, D. K., Johnson, J. E., & Parada, L. F. (2011). Tsc1 mutant neural stem/progenitor cells exhibit migration deficits and give rise to subependymal lesions in the lateral ventricle. *Genes and Development*, 25(15), 1595–1600. <https://doi.org/10.1101/gad.16750211>
- Zordan, P., Cominelli, M., Cascino, F., Tratta, E., Poliani, P. L., & Galli, R. (2018). Tuberous Sclerosis Complex-associated CNS abnormalities depend on hyperactivation of mTORC1 and Akt. *Journal of Clinical Investigation*, 128(4), 1688–1706. <https://doi.org/10.1172/JCI96342>